Copyright Warning & Restrictions

The copyright law of the United States (Title 17, United States Code) governs the making of photocopies or other reproductions of copyrighted material.

Under certain conditions specified in the law, libraries and archives are authorized to furnish a photocopy or other reproduction. One of these specified conditions is that the photocopy or reproduction is not to be "used for any purpose other than private study, scholarship, or research." If a, user makes a request for, or later uses, a photocopy or reproduction for purposes in excess of "fair use" that user may be liable for copyright infringement,

This institution reserves the right to refuse to accept a copying order if, in its judgment, fulfillment of the order would involve violation of copyright law.

Please Note: The author retains the copyright while the New Jersey Institute of Technology reserves the right to distribute this thesis or dissertation

Printing note: If you do not wish to print this page, then select "Pages from: first page # to: last page #" on the print dialog screen

ABSTRACT

PRESSURE SWING MEMBRANE ABSORPTION PROCESS FOR SEPARATION OF LOW TEMPERATURE POST-SHIFT REACTOR SYNGAS

by
John Chau

This thesis is concerned with a cyclic pressure swing membrane absorption process (PSMAB) for separation of the feed gas mixture containing ~40% CO_2-He balance using pure ionic liquid, 1-butyl-3-methylimidazolium dicyanamide ([bmim][DCA]), and its solution containing poly(amidoamine) (PAMAM) dendrimer Gen 0 primarily with a dry feed gas. An advanced pressure swing membrane absorption process is developed to produce purified He as a surrogate for H_2 at a high pressure from simulated low-temperature shifted syngas for different membrane modules. The PSMAB process also simultaneously produces a highly purified CO_2 stream containing bulk of the CO_2 in the post-shift reactor gas stream and suitable for subsequent sequestration.

The hydrophobized ceramic membrane tubule-based system produces poor quality of products. The hydrophobized poly(ether ether ketone) (PEEK) hollow fiber-based system, on the other hand, provides higher product concentrations due to a much higher contacting area per unit gas volume. Among PEEK modules, the PEEK-L III module provides the highest CO_2 concentration in the CO_2-rich product stream.

Measurements of the solubility and diffusivity of pure carbon dioxide, pure helium, and a feed mixture of ~40% CO_2-He balance are carried out in the ionic liquid, ([bmim][DCA]), and in its solution containing 20 wt% and 30 wt% PAMAM dendrimer

Gen 0 with and without water. Additional solubility studies of pure CO_2 and He are done in polyethylene glycol 400 (PEG 400) and 20 wt% dendrimer in PEG 400.

The solubility of CO_2 decreases with an increase in temperature whereas He solubility increases with an increase in temperature. The CO_2 and He solubilities increase with an increase in feed pressure. Carbon dioxide absorption increases considerably when the amine is added to the ionic liquid and then increases several-fold when moisture is added. Higher CO_2/He solubility selectivity is observed as temperature decreases to as much as 55 at 50 ^oC. Moreover, CO_2 solubilities in PEG 400 and in 20 wt% dendrimer in PEG 400 are somewhat higher than in [bmim][DCA] and 20 wt% dendrimer in [bmim][DCA], respectively.

A mathematical model of the three-valve PSMAB process is developed and verified so that the model may be used to carry out scale up calculations. Such a scale up model can allow determination of the cost of the process of a given CO_2-containing feed gas mixture. The mathematical model is numerically solved to predict the extent of purification of the gas by pure ionic liquid [bmim][DCA] in the three-valve PSMAB device. The decreasing pressures generated by a numerical solution of the model agree well with the experimental runs for ceramic modules during the 900 second absorption step, but are significantly lower for the PEEK hollow fiber modules due to the large dead volumes present in the PEEK modules. There is a 6-10% difference in CO_2 concentration in the two product streams between the predictions and the measured values. The simulation results show that purified (>90%) CO_2 and He can be obtained for two PEEK-L III modules in series using [bmim][DCA] as the absorbent.

PRESSURE SWING MEMBRANE ABSORPTION PROCESS FOR SEPARATION OF LOW TEMPERATURE POST-SHIFT REACTOR SYNGAS

by
John Chau

A Dissertation
Submitted to the Faculty of
New Jersey Institute of Technology
in Partial Fulfillment of the Requirement for the Degree of
Doctor of Philosophy in Chemical Engineering

Department of Chemical, Biological, and Pharmaceutical Engineering

August 2013

APPROVAL PAGE

PRESSURE SWING MEMBRANE ABSORPTION PROCESS FOR SEPARATION OF LOW TEMPERATURE POST-SHIFT REACTOR SYNGAS

John Chau

Dr. Kamalesh K. Sirkar, Dissertation Advisor Date
Distinguished Professor of Chemical, Biological, and Pharmaceutical Engineering, NJIT

Dr. Somenath Mitra, Committee Member Date
Distinguished Professor of Chemistry, NJIT

Dr. Robert Barat, Committee Member Date
Professor of Chemical, Biological, and Pharmaceutical Engineering, NJIT

Dr. Boris Khusid, Committee Member Date
Professor of Chemical, Biological, and Pharmaceutical Engineering, NJIT

Dr. Xianqin Wang, Committee Member Date
Associate Professor of Chemical, Biological, and Pharmaceutical Engineering, NJIT

BIOGRAPHICAL SKETCH

Author: John Chau

Degree: Doctor of Philosophy

Date: August 2013

Undergraduate and Graduate Education:

Doctor of Philosophy in Chemical Engineering,
New Jersey Institute of Technology, Newark, NJ, 2013

Master of Science in Chemical Engineering,
San Jose State University, San Jose, CA, 2006

Bachelor of Science in Chemical Engineering,
University of California-Berkeley, Berkeley, CA, 2003

Major: Chemical Engineering

Presentations and Publications:

Chau, J.; Obuskovic, G.; Jie, X.; Mulukutla, T.; Sirkar, K. K. Solubilities of CO_2 and He in an Ionic Liquid Containing Poly(amidoamine) (PAMAM) Dendrimer Gen 0. *Ind. Eng. Chem. Res.* **2013**, 52, 10484.

Chau, J.; Obuskovic, G.; Jie, X.; Sirkar, K. K. Pressure Swing Membrane Absorption Process for Shifted Syngas Separation: Modeling vs. Experiments. (Manuscript being revised for resubmission).

Jie, X.; Chau, J.; Obuskovic, G.; Sirkar, K. K. Preliminary Studies of CO_2 Removal from Pre-combustion Syngas through Pressure Swing Membrane Absorption Process with Ionic Liquid as Absorbent. *Ind. Eng. Chem. Res.* **2013**, 52, 8783.

Jie, X.; Chau, J.; Obuskovic, G.; Sirkar, K. K. Enhanced Pressure Swing Membrane Absorption Process for CO_2 Removal from Pre-combustion Syngas with Dendrimer-ionic Liquid Mixtures as Absorbent. (Manuscript being submitted).

Chau, J.; Obuskovic, G.; Jie, X.; Sirkar, K. K. Preliminary Studies of CO_2 Removal from Simulated Pre-combustion Syngas Via a Pressure Swing Membrane Absorption Process. **2012** American Institute of Chemical Engineers (AIChE) Annual Meeting, Pittsburgh, PA, November 2nd, 2012.

Chau, J.; Obuskovic, G.; Jie, X.; Sirkar, K. K. Pressure Swing Membrane Absorption Process for CO_2 Removal from Pre-combustion Syngas. **2013** North American Membrane Society (NAMS) Annual Meeting, Boise, ID, June 11th, 2013.

I dedicate this dissertation to my parents,
Châu Hoa Vương and Trịnh Tú Hồng,
who inspired me to start and finish my Ph.D.

(Con xin dành riêng bài luận án này cho Cha Mẹ. Cha Mẹ là người đã dạy dỗ, khuyến khích, và động viên con từ lúc bắt đầu và cho đến lúc kết thúc bằng tiến sĩ của con)

ACKNOWLEDGEMENT

I would like to express my deepest appreciation to my thesis advisor, Professor Kamalesh K. Sirkar for his guidance, support, and valuable suggestions throughout my thesis project. I also would like to thank members of my committee: Dr. Somenath Mitra, Dr. Robert Barat, Dr. Boris Khusid, and Dr. Xianqin Wang, for providing constructive criticism and recommendations.

I would like to thank the Department of Energy (DOE) for funding this project, special thanks to DOE Program Officers for the project: Norman Popkie and Steven R. Markovich. I also would like to thank the Chemical, Biological and Pharmaceutical Engineering department at New Jersey Institute of Technology for the financial support.

This work could not be completed without the help from my colleagues. I would like to thank Dr. Xingming Jie, Dr. Gordana Obuskovic, and everyone in the Membrane Separation and Biotechnology group for their friendship and support.

Special thanks to my family for their support, understanding, and encouragement throughout my years in school.

TABLE OF CONTENTS

TABLE OF CONTENTS
(Continued)

Chapter **Page**

TABLE OF CONTENTS
(Continued)

Chapter **Page**

TABLE OF CONTENTS
(Continued)

LIST OF TABLES

LIST OF TABLES
(Continued)

Table **Page**

LIST OF FIGURES

LIST OF FIGURES
(Continued)

Figure **Page**

LIST OF FIGURES
(Continued)

Figure **Page**

LIST OF FIGURES
(Continued)

Figure **Page**

LIST OF SYMBOLS

©	Copyright
C_{jg}	Concentration of species j in the gas phase, mol/m^3
C_{jl}	Concentration of species j in the liquid phase, mol/m^3
d_i	Inside diameter of a hollow fiber, m
d_o	Outside diameter of a hollow fiber, m
D_{jg}	Diffusion coefficient of species j in the gas phase, m^2/s
D_{jl}	Diffusion coefficient of species j in the liquid phase, m^2/s
H_j	Solubility coefficient of gas species j in a liquid, $mol/(m^3.Pa)$
L	Effective fiber length, m
r	Radial distance, m
r_p	Pore radius, m
r_e	Equivalent radius of free surface, m
R	Universal gas constant, $(m^3Pa)/(mol.K)$
t	Time, s
T	Temperature, K
v_g	Gas velocity in fiber lumen, m/s
z	Longitudinal distance, m
N	Total number of hollow fibers in a module
P_G	Gas pressure, psig
P_{Ab}	Pressure of the absorbent liquid, psig
A	Area, m^2

LIST OF SYMBOLS
(Continued)

V	Volume, m^3
K_C	Equilibrium constant, L/mol or L^4/mol^4
X	Mole fraction
n_j	Mole of species j, mol
MW	Molecular weight, g/mol

Greek Symbols

ε	Void fraction of the fiber bundle
μ	Viscosity, Pa.s
θ	Contact angle
γ	Surface tension of liquid, dyne
π	Pi, 3.14

Superscript and Subscripts

i = interface

g = gas phase

j = component j

l = liquid phase

u = upstream section

CHAPTER 1

INTRODUCTION

Greenhouse gases are believed to be the main cause for global warming which has received a lot of attention in recent years (Berger et al. [1]). When solar energy is transmitted through the earth's atmosphere, it can either be reflected back into space or get absorbed. The earth releases some of the energy back to the atmosphere as heat once the sunlight gets absorbed. Greenhouse gases absorb the energy radiating from the sun, which slows down or in some cases prevents the process of heat release back into space. This causes an increase in the earth's temperature which results in the greenhouse effect. According to Berger et al. [1], the earth's average temperature has increased by only one degree Celsius during the last 150 years, but from 1990 and 2100 it will increase by 1.4 to 5.8 ^{o}C. Rising earth temperature causes the ice to melt, which in turn raises the sea level. The sea level is predicted to go up by 0.09 to 0.88 meters from 1990 to 2100. Furthermore, global warming causes droughts and loss of agriculture productivity and destroys ecosystems.

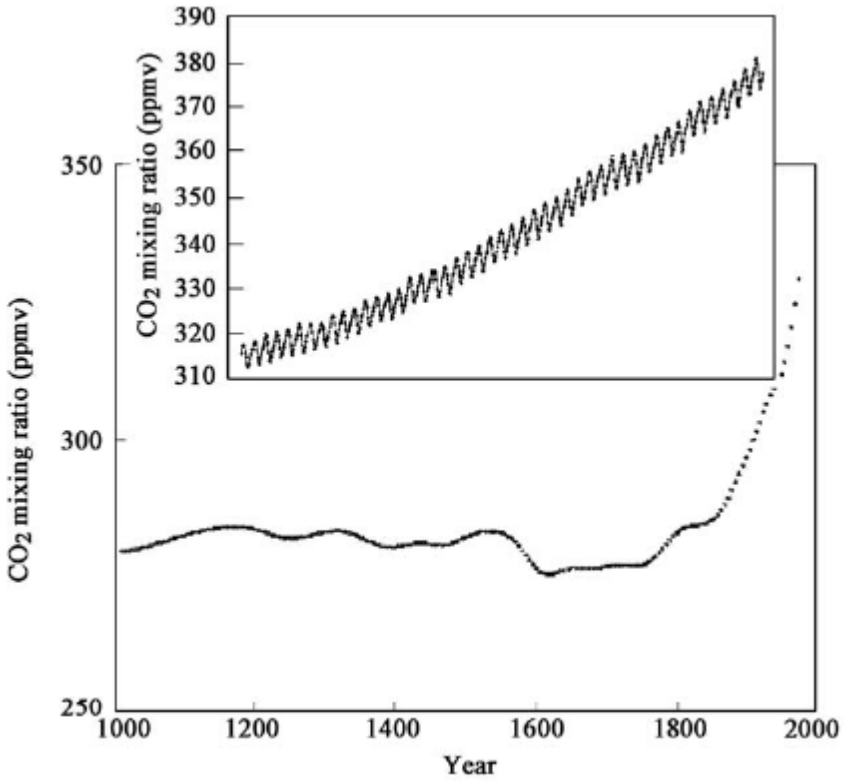

Figure 1.1 Carbon Dioxide Concentration in the Atmosphere from 1000 to 2000.
Source: [2].

Carbon dioxide (CO_2), one of the main greenhouse gases present in the earth's atmosphere, absorbs the sun's infrared radiation and emits back to the earth's surface. As a result, the energy or heat retained in the atmosphere warms up the earth. Even though CO_2 is important for living species, its excess creates environmental problems. The CO_2 concentration in the atmosphere had stayed relatively constant before the Industrial Revolution in the 1800s [2]. However, after the Industrial Revolution, carbon dioxide in the air has risen sharply because the use of coal, oil, and natural gas has increased enormously to accommodate the need of the world's growing population and industrial expansion. According to Rubin et al. [3], doubling the amount of carbon dioxide in the

earth atmosphere leads to an increase in its temperature by 1 to 5 ^{o}C by the middle of this century.

In addition, while fossil fuel burning produces excessive CO_2, there are no economical and clear energy alternatives replacing it yet. Therefore, man-made CO_2 emissions into the atmosphere need to be reduced. Multiple solutions including more efficient energy use, alternative fuels, electrically-driven transportation, electricity from non-CO_2-emitting sources, and carbon sequestration are needed to meet this challenge. Carbon dioxide capture from flue and synthesis gas can be achieved by a number of techniques: chemical and physical absorption, physical adsorption-based pressure swing and temperature swing adsorption, and membrane separation (Rao and Rubin [4]).

1.1 Chemical and Physical Absorption

1.1.1 Chemical Absorption

Chemical absorption is an exothermic process where absorbents are used to separate carbon dioxide from a gas mixture. Amine based processes for capturing carbon dioxide began in the 1970s and the captured CO_2 is used among others to enhance oil recovery [4]. The reaction rates and the equilibrium absorption characteristics for amine based absorption depend on the type of amines used. Alkanolamines are divided into three groups. Group 1 contains primary amines such as monoethanolamine (MEA) and diglycolamine (DGA). Group 2 includes secondary amines such as diethanolamine (DEA) and di-isopropylamine (DIPA). Group 3 consists of tertiary amines triethanolamine (TEA) and methyl-diethanolamine (MDEA) (Robertson et al. [5]). Structures of some of these amines are shown in Figure 1.2.

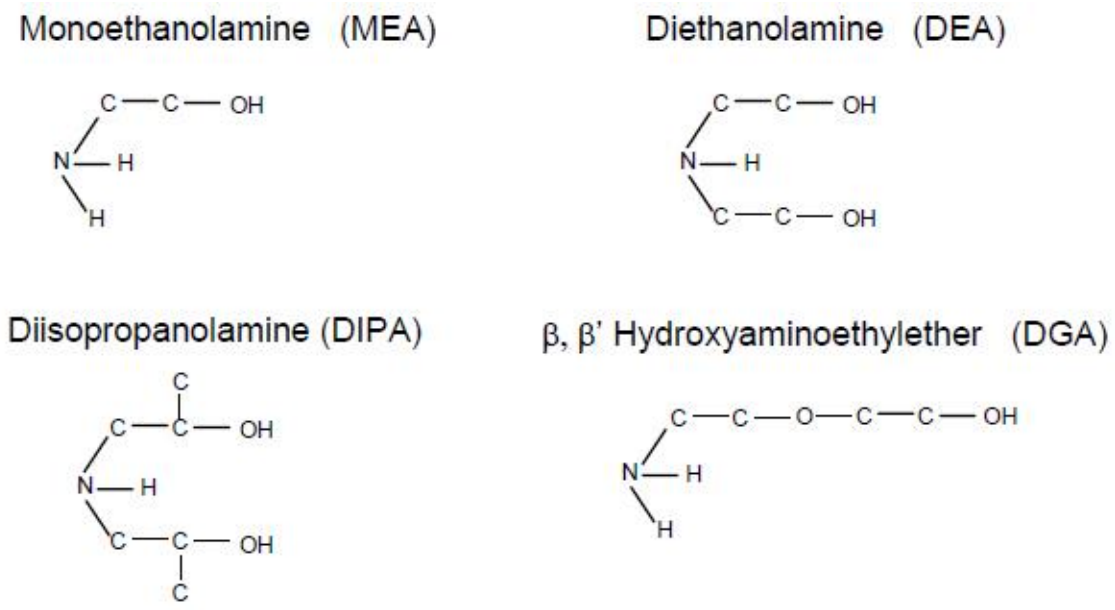

Figure 1.2 Common Alkanolamines.
Source: [5].

Amine based absorption technology involves exposing the gas stream to for example an aqueous solution of a primary amine that reacts with the CO_2 to form a soluble carbamate salt as shown below:

$$2RNH_2 + CO_2 \leftrightarrow RNH_3^+ + RNHCOO^- \quad (1.1)$$

A tertiary amine also reacts with CO_2 in the presence of water, forming a bicarbonate ion:

$$R_3N + CO_2 + H_2O \leftrightarrow R_3NH^+ + HCO_3^- \quad (1.2)$$

Since the reactions are reversible, CO_2 gas can be released by heating the CO_2 enriched amine solution in a separate stripping unit. Monoethanolamine (MEA) is a solvent of choice used for this process since it is the least expensive among the alkanolamines. Furthermore, MEA has the lowest molecular weight which gives it the

ability to possess highest theoretical absorption capacity for carbon dioxide (Wong et al. [6]).

Corrosion is one of the problems associating with amine based absorption processes. Primary amines, such as MEA, react fastest with carbon dioxide. Secondary amines are second fastest while tertiary amines react most slowly with carbon dioxide [5]. Since the dissolved CO_2 is a corroding agent, the corrosion rate is largest for primary amines, then secondary amines and smallest for tertiary amines. Moreover, the faster the reaction between amines and carbon dioxide, the more energy it requires in the solvent regeneration step and the easier the amines are to form degradation products. Shown in Table 1.1 is the heat of reaction among the three amines and carbon dioxide [6].

Table 1.1 Heat of Reaction among Amines and Carbon Dioxide

Amine Type	MEA (primary)	DEA (secondary)	MDEA (tertiary)
ΔH_f for CO_2 (cal/g)	455	360	320
ΔH_f for CO_2 (Btu/lb)	820	650	577

Source: [6].

1.1.2 Physical Absorption

Physical absorption is a temperature and pressure dependent process where carbon dioxide as the solute is absorbed in a solvent according to Henry's law which is shown below.

$$p = H_{CO2}C \tag{1.3}$$

where p is the partial pressure of CO_2 in the gas above the solution, H_{CO2} is Henry's law constant for CO_2, and C is CO_2 concentration.

In physical absorption, the solute concentration increases as pressure increases or temperature decreases. In other words, solute gets absorbed more by the solvent as pressure increases or temperature decreases. As a result, physical absorption method is usually carried out at high partial pressures and low temperatures to ensure that carbon dioxide absorption by solvent is maximum. The solvent can be regenerated by heating or reducing the pressure. Since physical absorption requires high partial pressure of carbon dioxide, it can be used in recovering CO_2 from Integrated Gasification Combined Cycle (IGCC) systems where exhaust CO_2 leaves the system at an elevated pressure. Selexol (dimethylether of polyethylene glycol) and Rectisol (cold methanol) are some of the solvents used in this technique at low temperature (Skinner et al. [7]).

1.2 Physical Adsorption-based Pressure Swing and Temperature Swing Adsorption

1.2.1 Pressure Swing Adsorption (PSA)

Pressure swing adsorption is a technique used to separate a desired gas from a mixture of gases based on the affinity of adsorbents to gases under pressure. Similar to physical absorption, gases get adsorbed onto solid surface of adsorptive materials when pressure is applied and more gases are absorbed by the adsorbents as the pressure increases until saturation is achieved. Some adsorbents for carbon dioxide separation are activated carbon, silica gel, and zeolite. Figure 1.3 shows a single bed PSA process that is used to separate carbon dioxide and hydrogen.

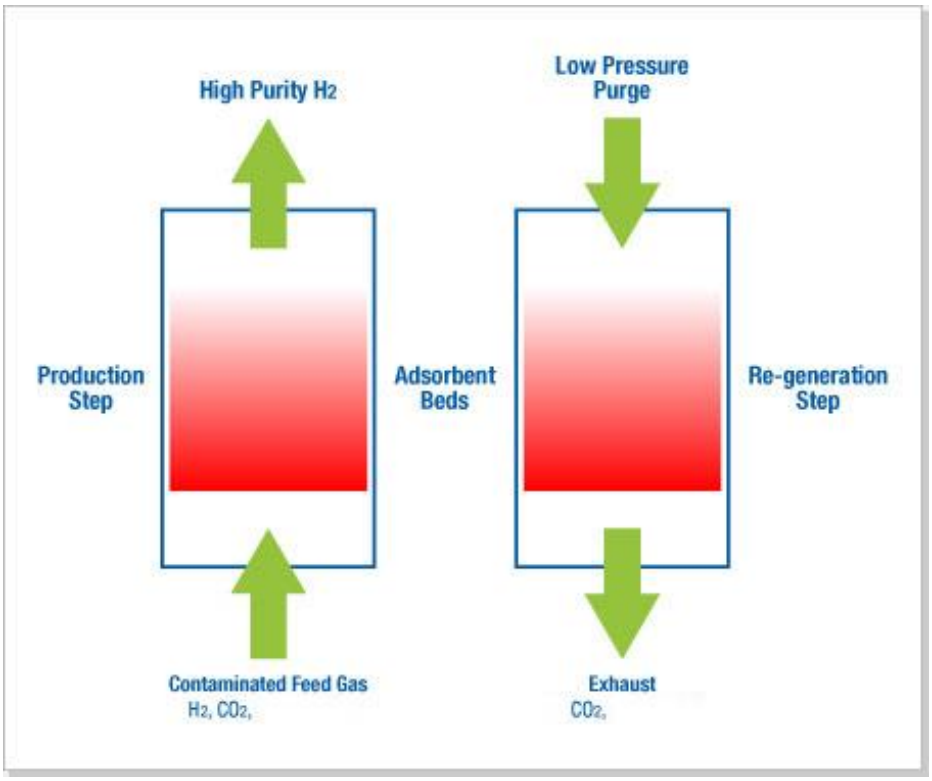

Figure 1.3 Pressure Swing Adsorption Process Schematic.
Source: [8].

In this process, the adsorbent selected such as activated carbon or zeolite has a high selectivity for carbon dioxide over hydrogen. In the production step, the mixture of carbon dioxide and hydrogen enters a column full of adsorbent at high pressure. Since the adsorbent has high selectivity for carbon dioxide, CO_2 is adsorbed onto the surface of the pores in the adsorbent. When hydrogen gas leaves at the other end of the column, carbon dioxide is then desorbed by pressure reduction and removed as a purified product. The adsorbent bed can be regenerated by flushing the column with hydrogen gas [8].

The PSA system is cyclically operated where several adsorbent beds or columns are connected in series or in parallel and undergo successive pressurization and depressurization steps to produce a continuous stream of purified carbon dioxide [7].

Pressure Swing Adsorption is an energy-saving process as it does not require heat to regenerate the absorbents. However, it operates at low temperatures. In addition, it requires carbon dioxide specific adsorbents to capture a reasonable amount of CO_2 [6].

1.2.2 Temperature Swing Adsorption (TSA)

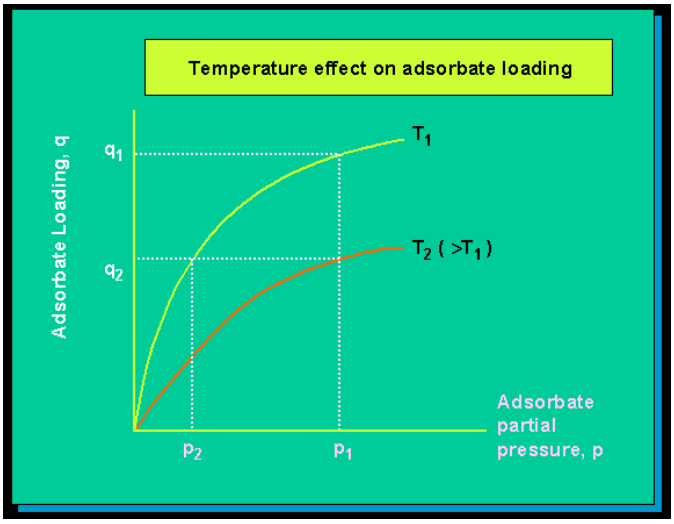

Figure 1.4 Temperature Effect on Solute Solubility.
Source: [9].

Similar to pressure swing adsorption, temperature swing adsorption is used to separate a desired gas from a mixture of gases based on affinity of adsorbents to gases. However, as their names imply, TSA is different from PSA because the process applies temperature instead of pressure on a mixture of gases in the presence of absorbent. In addition, TSA is the method of choice when the desired gas (adsorbate) in the feed stream is dilute [6]. At a given partial pressure of adsorbate in the gas phase, the amount of gas adsorbed decreases with increasing temperature as shown in Figure 1.4. Adsorbent beds are usually

regenerated by increasing the temperature and by purging the beds with a hot less-adsorbed gas/vapor stream.

1.3 Membrane Separation

Membrane separation is based on the principle of selective gas permeation. Gases in the feed stream diffuse through the membrane at different rates depending on their solubility and diffusivity. Different gases have different solubility and diffusivity values for a specific type of membrane. The higher the gas's solubility and diffusivity, the faster it diffuses through that specific membrane. For example, carbon dioxide, water vapor, and hydrogen sulfide are easier to permeate through membrane units whereas methane, ethane, and other hydrocarbons are more difficult to permeate. The driving force of membrane separation process is the partial pressure difference of specific gas component between both sides of membrane [5].

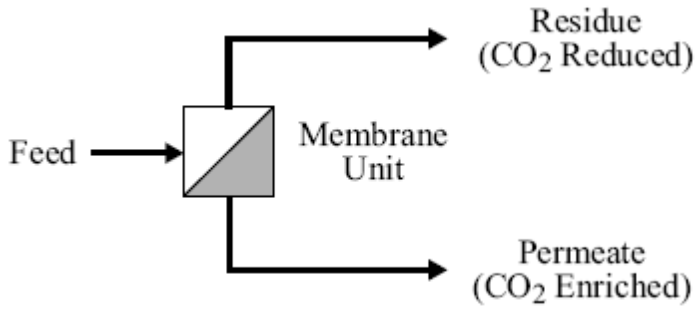

Figure 1.5 Simple Membrane Separation Schematic.
Source: [5].

In addition, membranes can be used to separate carbon dioxide from a feed gas stream based on chemical affinity. Chemical affinity membranes are immobilized with solutions that are selective to carbon dioxide such as amines, ionic liquids, etc. Inorganic, metallic, polymeric, and solid-liquid are some of the forms of membranes used today [10].

Hollow fiber and the spiral-wound modules are the two commonly used modules for membrane separation. A hollow fiber module contains a bundle of cylindrically shaped hollow fibers as shown in Figure 1.6. In the hollow fiber module, the feed gas stream flows through the bores of the membrane tubules. Selective gas such as carbon dioxide diffuses across the fiber wall while other feed gases keep flowing along the wall. CO_2 is then collected as the permeate stream from one side whereas other gases that flow through are collected in the residue stream from another side of the membrane [5].

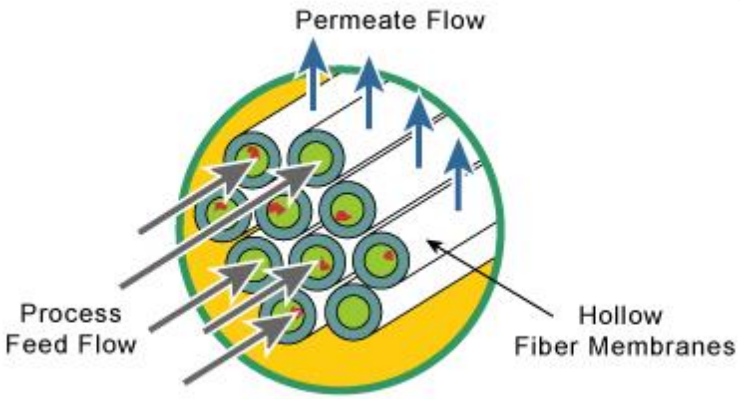

Figure 1.6 Hollow Fiber Membrane.
Source: [5].

In a spiral-wound module shown in Figure 1.7, multiple flat sheets of permeate collection material, membranes, feed channel spacers, and outer wrap are rolled into a

spiral unit. The feed enters the module and flows between membrane sheets. CO_2 gas permeates preferentially through the membrane inward to the central collection tube and exits on one side while other gases exit from the opposite side [5].

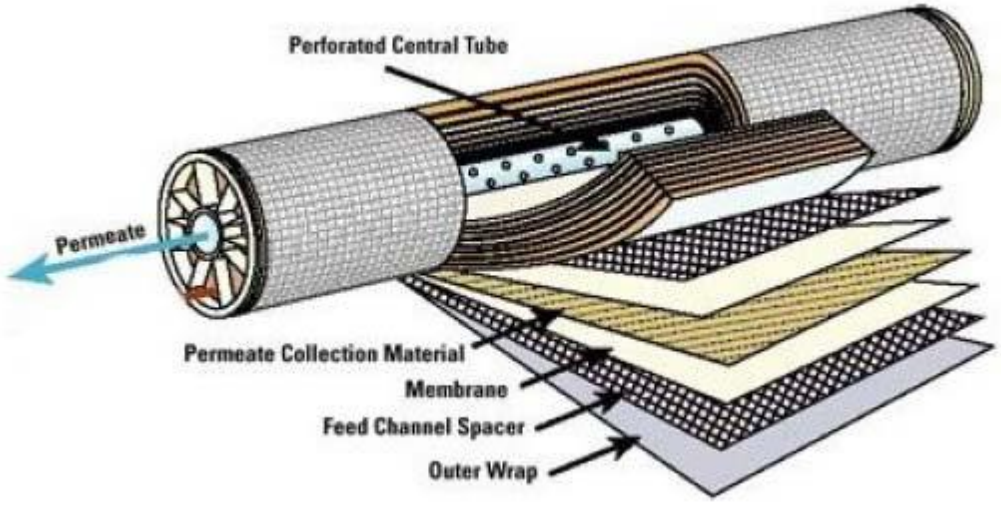

Figure 1.7 Spiral-wound Membrane.
Source: [5].

Membrane units are light and compact which results in much less space and potentially lower equipment cost. Moreover, because membrane systems do not require separating agents, no solvent regeneration step is needed. However, membrane separation cannot produce pure carbon dioxide in a single separation stage. Indeed, it requires multiple membrane units and recycling to achieve high purity and high recovery [5].

Azar et al. [11] and Rubin et al. [12] indicated that carbon dioxide capture and storage (CCS) is considered the most important technique to curtail global climate change at the present time. Carbon dioxide produced from Integrated Gasification Combined Cycle (IGCC) for coal has a much higher partial pressure than CO_2 produced in burning of fossil fuel. As a result, pre-combustion CO_2 capture from post-shift reactor syngas

produced from IGCC is of significant interest. Solvent absorption-based method is a desired and widely used method for CO_2 removal. Since carbon dioxide produced from the low temperature (L-T) water gas shift reactor is at a high temperature around 150-200 ^oC and high pressure, liquid absorbent chosen for CO_2 absorption has to be thermally stable and non-volatile. Furthermore, the chosen absorbent liquid must have a high solubility selectivity of CO_2 over H_2 and CO. Since post L-T water gas shift reactor produces gases with considerable moisture, absorbents having high selectivity of carbon dioxide in the presence of water are also of interest.

Room temperature ionic liquids (RTILs) have been considered green solvents for carbon dioxide capture because of their unique characteristics. RTILs are bulky organic compounds whose cations are organic and anions are either organic or inorganic (Baltus and Moganty [13]). RTILs are in liquid form at room temperature and are generally chemically, thermally stable, and non-volatile. Therefore, they can be used to replace volatile organic solvents as absorbents for carbon dioxide separation (Camper et al. [14]).

Yokozeki and Shiflett [15] reported that carbon dioxide solubility in 1-butyl-3-methylimidazolium hexafluorophosphate [bmim][PF_6] is 30-300 times over that of hydrogen at hydrogen partial pressure of 0.5-3 MPa at room temperature and at lower temperatures. Myers et al. [16] succeeded in synthesizing task specific ionic liquids (TSILs) that have functional groups which can form complexes with carbon dioxide, and used them as facilitated supported liquid membrane (FSLM). Facilitated supported ionic liquid membrane has been used in the separation of carbon dioxide from hydrogen at higher temperatures; the selectivity of CO_2 over H_2 in FSLM is reported to be 10-20 at ~85 ^oC [16]. Yegani et al. [17] reported that CO_2/H_2 solubility selectivity of polymeric

membranes containing amine moieties dropped sharply as the feed gas moisture content decreased. Meindersma et al. [18] reviewed the application of task-specific ionic liquids for CO_2 separation and suggested that 1-butyl-3-methylimidazolium dicyanamide ([bmim][DCA]) could be a good choice as CO_2 liquid absorbent.

Primary and tertiary amines or compounds containing those amines can be used as carbon dioxide absorbents. Effective CO_2 absorption however requires significant amount of moisture in systems containing tertiary amines. Previous studies have shown that a pure liquid membrane of PAMAM dendrimer Gen 0 with humidified gas streams had a very high selectivity of CO_2 over N_2/O_2 in the range of 15,000-18,000 (Kovvali et al. [19,20]). This amine molecule with a molecular weight of 517 contains four primary amines and two tertiary amines. Additional supported liquid membrane studies using pure PAMAM dendrimer Gen 0 for CO_2 separation have been carried out (Duan et al. [21,22], Taniguchi et al. [23]). This dendrimer Gen 0 has also been used as a reactive absorbent in an aqueous solution in a hollow fiber membrane contactor at room temperature (Kosaraju et al. [24]). In addition, Rolker et al. [25] have succeeded in achieving high CO_2/N_2 solubility selectivity in nonvolatile hyper-branched oligomeric liquid absorbents.

Membrane-based gas-liquid contacting can avoid the shortcomings present in PSA or dispersive contacting-based absorption process. This thesis is concerned with the pressure swing membrane absorption process (PSMAB). This PSMAB process combines the specific advantages of a number of basic separation techniques: highly selective absorption of CO_2 in a nonvolatile liquid/oligomeric absorbent at temperatures and pressures characteristics of the feed stream under consideration; pressure swing absorption (PSAB) process simulating a PSA process (which however uses adsorbent

particles); hollow microporous tubules/fibers providing per unit device volume a very large surface area of non-dispersive contact between the post-shift reactor synthesis gas stream flowing through the fiber lumen and the liquid absorbent present as a thin stagnant absorbent liquid layer in between the microporous tubules/hollow fibers on the shell side of the separation device.

Jie et al. [26] have developed a pressure swing membrane absorption (PSMAB) process to simultaneously obtain purified helium and carbon dioxide from lower temperature (L-T) post shift reactor synthesis gas which will be available at around 150 ^{o}C and pressure in the range of 200-300 psig. The highest temperature and pressure range of operation is 100 ^{o}C and 250 psig. The feed gas mixture consists of 40% CO_2, 60% He. In this process a porous hydrophobic membrane is used primarily as a membrane contactor to facilitate non-dispersive contacting of the gas phase and the absorbent liquid phase at the membrane pore mouths via a rapid pressure swing absorption technique developed earlier by Bhaumik et al. [27].

Evaluation of the potential of such a process requires a careful and detailed analysis of the PSMAB technique. It is necessary to determine the properties of the absorbent before one can model the PSMAB process. A mathematical model of this process needs to be developed and verified so that the model may be used to carry out scale up calculations. Such a scale up model can allow determination of the cost of the process of a given CO_2-containing feed gas mixture. Therefore, the objectives of this thesis follow in the next subsection.

1.4 Objectives of This Thesis

1. Conduct studies on solubility of carbon dioxide and helium in absorbent liquid such as 1-butyl-3-methylimidazolium dicyanamide ([bmim][DCA]), polyethylene glycol 400 (PEG 400), and their solutions with poly(amidoamine) dendrimer Gen 0.

2. Develop a mathematical model to predict the behavior of a pressure swing membrane absorption (PSMAB) process and compare the predictions with the results of experimental runs over a range of temperatures from room 23 to 100 ^{o}C.

3. Advance the study of pressure swing membrane absorption process for a five-valve system in a polyether ether ketone (PEEK) hollow fiber-based modified membrane module.

Extensive measurements of the solubilities of pure carbon dioxide, pure helium, and a feed mixture of ~40% CO_2-He balance were carried out in the ionic liquid, ([bmim][DCA]), and in its solution containing 20 wt% and 30 wt% poly(amidoamine) (PAMAM) dendrimer Gen 0 with and without water. Additional solubility measurements for pure CO_2 and pure He in PEG 400 and 20 wt% dendrimer in PEG 400 were also performed.

A mathematical model was developed to predict the extent of purification of the gas by pure ionic liquid [bmim][DCA] in the 3-valve PSMAB device. It is assumed that the analysis for a single fiber can be extended to the whole device and the free surface model is valid. This model assumes a cylindrical fluid envelope surrounding each hollow fiber. As a result, there exists two concentric cylinders: the inner cylinder consists of one hollow fiber and the outer cylinder consists of the absorbent liquid with a free surface across which there is no mass transfer. All assumptions used to develop the mathematical model for the PSMAB system using non-reactive absorbent are reported in Chapter 3. Information on Henry's law constants and diffusion coefficients for CO_2 and He in the

ionic liquid is determined from the solubility studies, which is used in the model to numerically predict the performance of the PSMAB process.

Additional runs of the five-valve PSMAB system were performed in an advanced PEEK module at different feed pressures and temperatures using pure [bmim][DCA] and 20 wt% dendrimer in [bmim][DCA] to achieve >90% CO_2 in CO_2-rich product stream since Jie et al. [26] could only achieve up to a maximum of 85% CO_2 in the CO_2-rich product stream using PEEK-L II module with PTFE balls to reduce dead volume.

CHAPTER 2

SOLUBILITIES OF CO_2 AND HELIUM IN AN IONIC LIQUID WITH OR WITHOUT POLY(AMIDOAMINE) DENDRIMER GEN 0

2.1 Introduction

Greenhouse gases are believed to be the main contributors for global warming which has caused an increase in the earth's temperature and an increase in severe climate disturbances [1]. Among the greenhouse gasses, carbon dioxide accounts for 80% of greenhouse emissions [2]. Carbon dioxide capture and storage (CCS) is considered the most important technique to curtail global climate change at the present time [11,12]. Pre-combustion CO_2 capture from post-shift reactor syngas produced from IGCC is of significant interest since carbon dioxide produced from Integrated Gasification Combined Cycle (IGCC) for coal has a much higher partial pressure than CO_2 produced in burning of fossil fuel. The composition of the syngas from a low temperature post shift reactor consists of 38% H_2, 29% CO_2, 33% H_2O, and 0.15% CO (Laan et al. [28]). At present, solvent absorption-based method is a desired and widely used method for CO_2 removal. Since carbon dioxide produced from the low temperature water gas shift reactor is at a high temperature and high pressure, CO_2 liquid absorbent chosen not only has to be thermally stable and non-volatile but also must have a high solubility selectivity of CO_2 over H_2 and CO. Post L-T water gas shift reactor produces gases with considerable moisture; therefore, absorbents having high selectivity of carbon dioxide in the presence of water are also of interest.

Room temperature ionic liquids (RTILs) are generally chemically, thermally stable, and non-volatile, so they can be used to replace volatile organic solvents as

absorbents for carbon dioxide separation [14]. Yokozeki and Shiflett [15] reported that solubility selectivity of CO_2/He in 1-butyl-3-methylimidazolium hexafluorophosphate ([bmim][PF_6]) is 30-300 times at hydrogen partial pressure of 0.5-3 MPa and at room temperature. Meindersma et al. [18] reviewed the application of task-specific ionic liquids for CO_2 separation and suggested that 1-butyl-3-methylimidazolium dicyanamide ([bmim][DCA]) could be a good choice as CO_2 liquid absorbent.

Primary and tertiary amines or compounds containing those amines can be used as carbon dioxide absorbents. Effective CO_2 absorption however requires significant amount of moisture in systems containing tertiary amines. Previous studies have shown that a pure liquid membrane of PAMAM dendrimer Gen 0 with humidified gas streams had a very high selectivity of CO_2 over N_2/O_2 in the range of 15,000-18,000 [19,20].

The cost of purified analytical grade PAMAM dendrimer Gen 0 per Aldrich Catalog is quite high of the order of $3000/kg. However, the manufacturer of this chemical proposes to supply industrial grade of this compound in large scale at ~ $10-20/lb (Kaiser [29]). This price is quite reasonable when compared with other specialized amines being studied e.g. piperazine whose bulk price is around $9/lb. The industrial grade dendrimer may have small amounts of impurities all of which are going to be amines highly capable of CO_2 absorption. Further, reactions of this dendrimer amine with CO_2 are completely reversible as was observed with runs of thousands of cycles of absorption and desorption every day in the research in laboratory [26].

Solubilities of many gases in ionic liquids have been studied and published by utilizing a number of different techniques that include a gravimetric method (Muldoon et al. [30], Shiflett et al. [31,32,33], Anthony et al. [34]), a pressure decay method

(equilibrium pressure and volume techniques) (Blanchard et al. [35], Kamps et al. [36]), a quartz crystal microbalance method (Baltus et al. [37]), and gas uptake into a thin ionic liquid film technique (Hou and Baltus [38], Hou [39], Moganty [40]). This study utilizes the pressure decay method to find solubilities of pure carbon dioxide and pure helium in [bmim][DCA]. It has been already indicated that this ionic liquid is a good absorbent for CO_2; more importantly it has been found that it has a very good solubility for PAMAM dendrimer Gen 0 unlike some others. Solutions of PAMAM dendrimer Gen 0 in [bmim][DCA] having 20 wt% dendrimer and 30 wt% dendrimer with and without moisture have also been investigated at different feed gas pressures up to 1.38 MPa (200 psig) and at 323, 353, 363, and 373K. Solubilities from a CO_2-He feed gas mixture (40% CO_2, He balance) have also been obtained.

The apparent reaction equilibrium constants for reactions with primary amine functional groups in dendrimer have been determined for dry gas systems subject to particular assumptions. The range of reaction possibilities include only one primary amine consumed to all primary amines consumed since PAMAM contains a total of four primary amines. Most studies of CO_2 absorption with amines in a liquid absorbent employ an amine or two having a single amine functionality, primary, secondary, or tertiary. The dendrimer of this study has multiple amine functionalities, four primary and two tertiary amines. Therefore, the analysis of the data to determine the reaction equilibrium constant is complicated with a considerable uncertainty.

2.2 Experimental Procedure

2.2.1 Materials

The ionic liquids [bmim][DCA] and [emim][Tf_2N] were purchased from EMD Chemicals, Philadelphia, PA. Poly(amidoamine) (PAMAM) dendrimer Gen 0 in methanol was purchased from Dendritech Inc., Midland, MI. Polyethylene glycol having a molecular weight of 400 (PEG 400) was purchased from Chemicals Direct, Roswell, GA. Ultrahigh purity grade carbon dioxide, helium, and simulated pre-combustion syngas containing 40.67% CO_2, helium balance were obtained from Air Gas, Piscataway, NJ.

2.2.2 Solubility of Dendrimer in Absorbent Liquids

Before [bmim][DCA] was chosen as the absorbent liquid of choice, solubility of dendrimer Gen 0 in the following liquids, [emim][Tf_2N], [bmim][DCA], PEG 400, and glycerol carbonate, was studied. The solubility of dendrimer in these liquids is summarized in Table 2.1.

Table 2.1 Solubility of Dendrimer in Absorbent Liquids

% Dendrimer in solution (%)	[emim][Tf_2N]	[bmim][DCA]	PEG 400	Glycerol Carbonate
1	Soluble	Soluble	Soluble	Soluble
5	Not Soluble	Soluble	Soluble	Soluble
10	Not Soluble	Soluble	Soluble	Soluble
15	Not Soluble	Soluble	Soluble	Soluble
20	Not Soluble	Soluble	Soluble	Soluble
25	Not Soluble	Soluble	Soluble	Soluble
30	Not Soluble	Soluble	Soluble	Soluble
35	Not Soluble	Soluble	Soluble	Soluble
40	Not Soluble	Soluble	Soluble	Partially Soluble
45	Not Soluble	Soluble	Soluble	Partially Soluble
50	Not Soluble	Soluble	Soluble	Partially Soluble

Table 2.1 shows that dendrimer is not soluble in [emim][Tf_2N] except at 1% concentration; however, the dendrimer is very soluble in [bmim][DCA] as well as in PEG 400. Dendrimer is soluble in glycerol carbonate at lower concentration (35% or less) but becomes partially soluble at higher concentration.

2.2.3 Apparatus and Measurements

The gas solubility measurements were made using a pressure decay method. The schematic of the apparatus is shown in Figure 2.1.

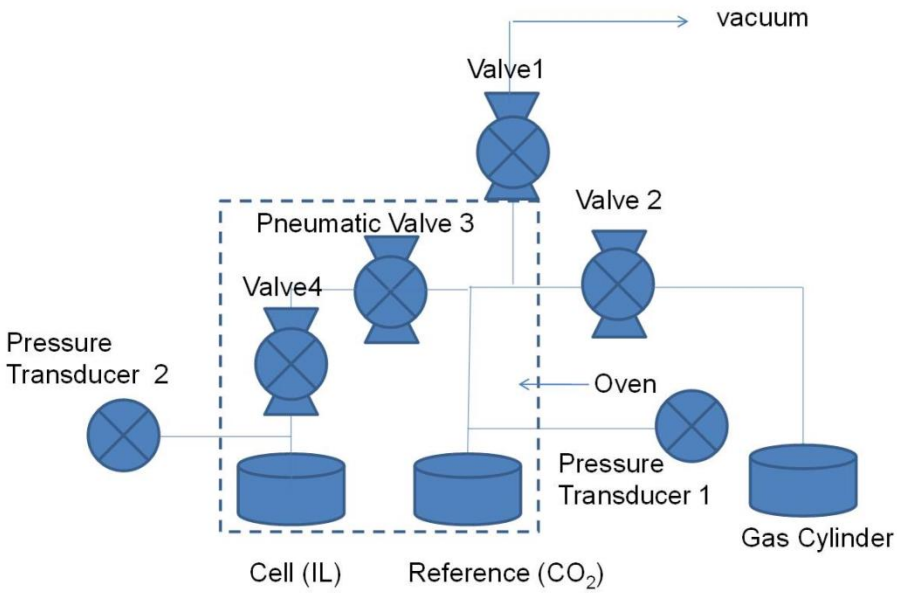

Figure 2.1 Apparatus for Measuring Gas Solubility.

The gas solubility measurement system mainly contains a cell volume, a reference volume, a programmable temperature oven (Model PH-202, ESPEC North America Inc.,

Hudsonville, MI), and a gas cylinder. A volume of 10 mL of liquid absorbent was measured, weighed, and added to the cell. The whole system was then degassed for about 5 hours using a vacuum pump (KNF, model UN 726.3 FTP, Trenton, NJ) with all valves (R.S. Crum & Company, product # SS-2P4T-BK, Mountainside, NJ) opened.

For the solubility measurement involving moisture, a predetermined amount of water was weighed and added along with the absorbent liquids to make up to 10 mL in a graduated cylinder. The solution was then transferred into the cell (stainless steel cylinder). After the connection to the cell cylinder was closed with an open/closed valve 4, the system was degassed for 3 hours without the cell cylinder to prevent water being evacuated during the degassing process. Then the cell cylinder was attached onto the system and was degassed for 15 minutes. The same process was repeated for the case of gas mixtures.

After the degassing process, the desired gas (CO_2 or He or a mixture of both) was loaded into the reference stainless steel cell cylinder (R.S. Crum & Company, product # 304L-05SF4-150, Mountainside, NJ) with valves 1, 3, and 4 closed to a pre-determined pressure while valve 2 was opened. The oven was turned on to allow temperature of the gas to reach a desired temperature in the reference volume after opening valve 4. Then, valve 3 was opened and controlled by a pneumatic controlling unit (PneuMagnetic, Quakertown, PA) while valves 1 and 2 were closed. The pneumatic controlling unit allows any user to open and close valve 3 with a toggle switch that is easily accessible and positioned outside the oven. Valve 3 can be opened for up to 99 hours which is long enough to ensure that equilibrium is fully established between both cylinders. The final

pressure difference was used to calculate the number of moles of gas absorbed by the absorbent liquid.

Changes in pressure versus time were also read and recorded by pressure transducer units in both cell and reference cylinders. The rate of change of the pressure indicates the rate of absorption of CO_2; from such data one can calculate the diffusion coefficient using the assumption that the depth of the liquid in the test cell is infinite [38,39]. Such calculations are reported in Chapter 3 since they are part of a transport modeling and separation research for the PSMAB process. The pressure transducer units include two pressure transducers (Model PX32B1-250GV), two assembly cables (Model CA-6TE24-010-PX32), and two universal input Ethernets (Model DP41-B-EI) purchased from Omegadyne Inc., Sunbury, OH. The pressure in the transducers ranges from zero to 1.72 MPa (~250 psig) with 0.25% linearity accuracy. The transducers can withstand a temperature of up to 115 ^{o}C (388K). This provided an upper limit to the measurements.

For CO_2/He gas mixture, the equilibrium gas mixture composition was determined by a gas chromatograph (Shimadzu Scientific Instruments, Inc., Model GC-2014, Somerset, NJ). A CarboxenTM-1010 PLOT Capillary (Sigma-Aldrich Inc., product #: 25467, Saint Louis, MO) was used in the analysis of the gas mixture at equilibrium. Nitrogen was used as the carrier gas; column and TCD temperatures were kept at 180 ^{o}C and 230 ^{o}C respectively. The temperature of the split injector was kept at 200 ^{o}C with a linear velocity flow control and a split ratio of 5. The run time for the analysis was set at ten minutes.

2.2.4 Pressure Transducer Calibration

Pressure transducers for cell (IL) and reference (gas) cylinders record the pressures in both cell and reference cylinders in term of milli-direct voltage (mdV). As a result, calibration curves for the pressure transducers for CO_2 and He gases used in the study were established and are shown in Figures 2.2 to 2.7.

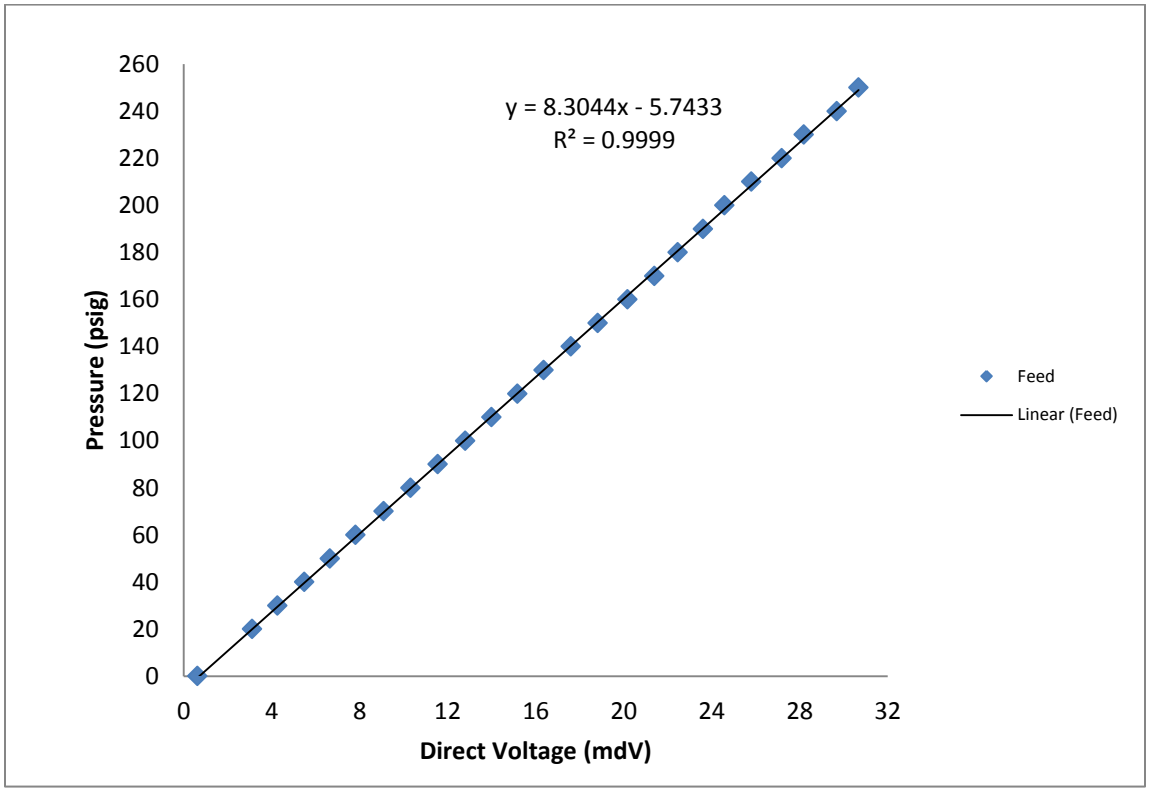

Figure 2.2 Pressure Transducer Calibration of Reference Cylinder for CO_2.

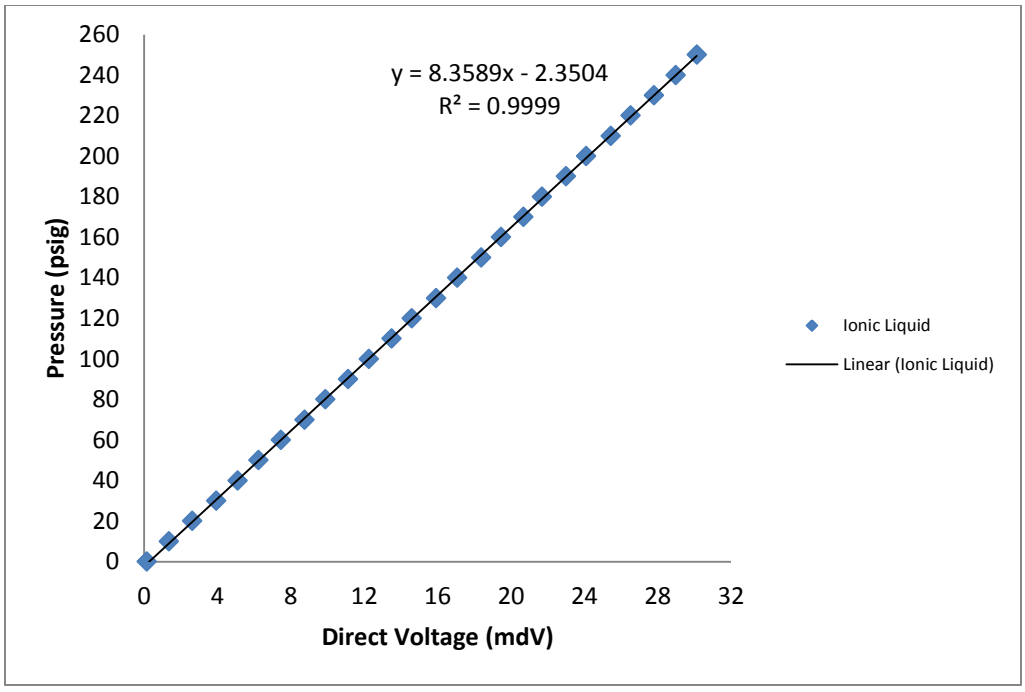

Figure 2.3 Pressure Transducer Calibration of Cell Cylinder for CO_2.

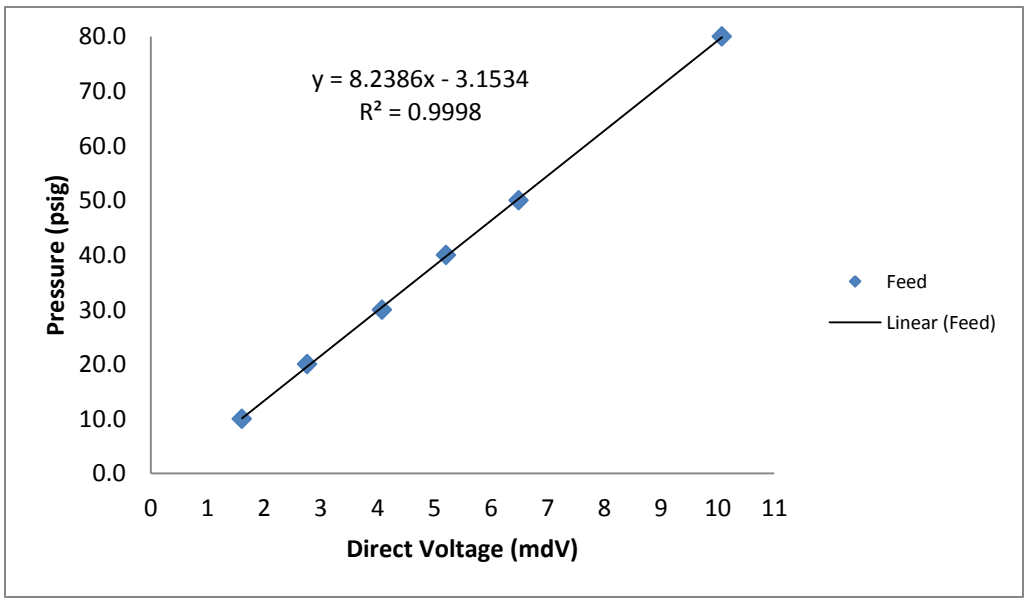

Figure 2.4 Pressure Transducer Calibration of Reference Cylinder for He at Low Feed Pressure.

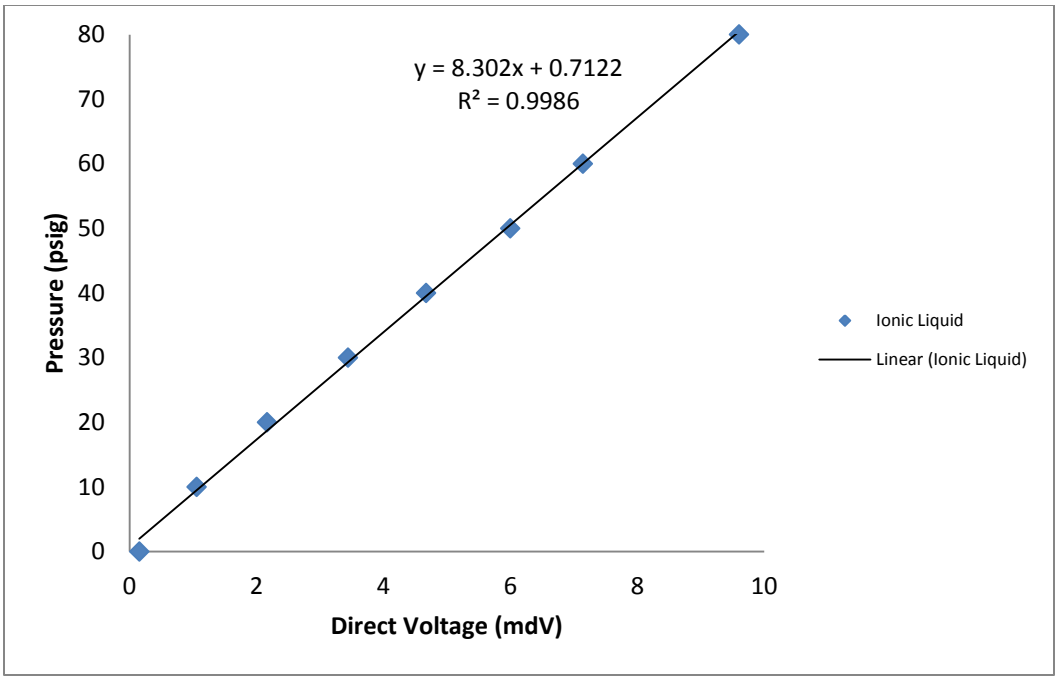

Figure 2.5 Pressure Transducer Calibration of Cell Cylinder for He at Low Feed Pressure.

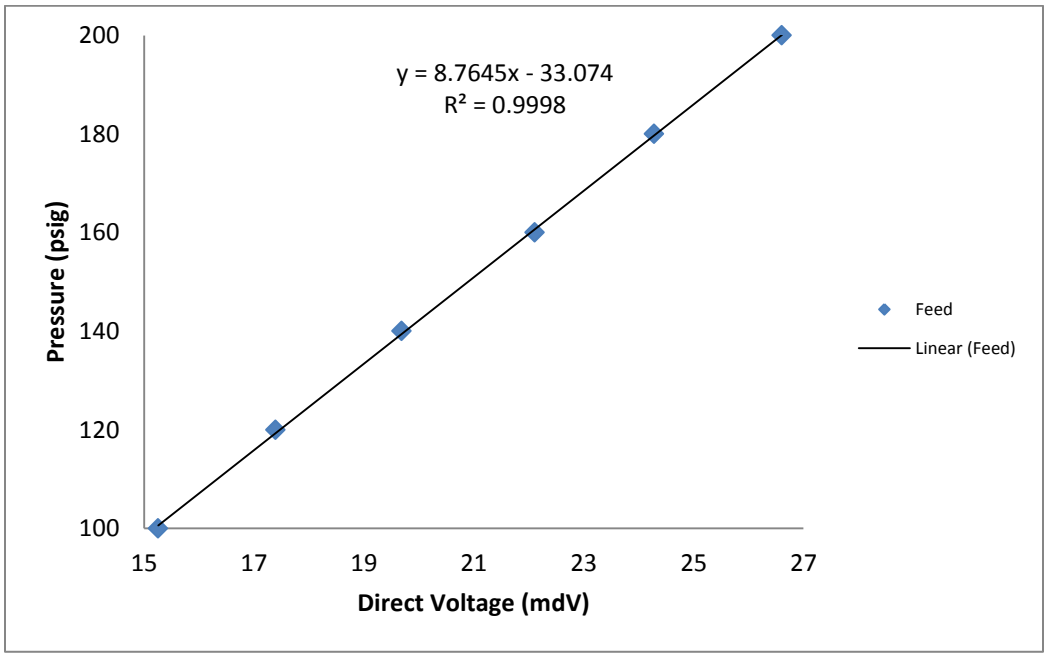

Figure 2.6 Pressure Transducer Calibration of Reference Cylinder for He at High Feed Pressure.

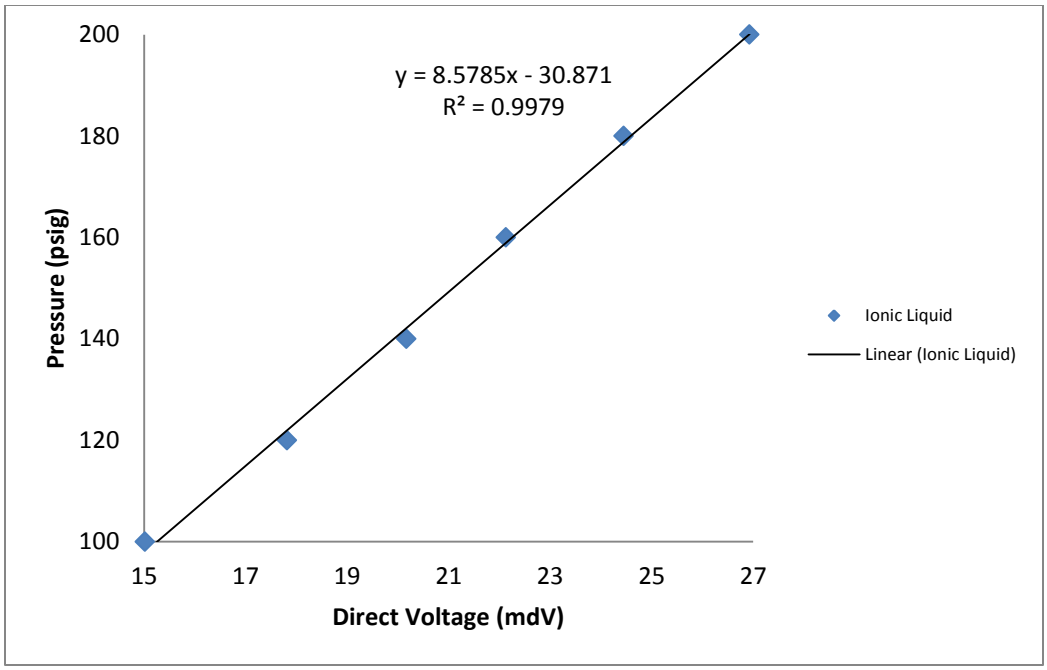

Figure 2.7 Pressure Transducer Calibration of Cell Cylinder for He at High Feed Pressure.

2.3 Results and Discussions

2.3.1 Data Analysis for Pure Ionic Liquid

Solubilities of pure carbon dioxide and pure helium as well as their mixtures were determined in various absorbents at different temperatures and pressures up to 1.38 MPa. The gas mole fractions in absorbent liquids were calculated from the differences in the values of the initial and final pressures. The general equation of state based on the compressibility factor was used to calculate the number of moles of gas. The total number of initial moles of the desired gas at pressure P_1 is given by

$$n_T = \frac{P_1 V_{ref}}{Z_i RT} \tag{2.1}$$

The number of moles in cell and reference volumes after equilibrium is reached at a pressure P_2 is given by:

$$n_1 = \frac{P_2 (V_{ref} + V_{cell} - V_{IL})}{Z_f RT} \tag{2.2}$$

The moles of gas absorbed is:

$$n_2 = n_T - n_1 \tag{2.3}$$

Here P_1 is the initial feed pressure of the desired gas in the reference cylinder; P_2 is the final equilibrium pressure; V_{ref} and V_{cell} are volumes of reference and cell cylinders, respectively; V_{IL} is the volume of absorbent added in cell cylinder; Z_i and Z_f are compressibility factors at pressures P_1 and P_2. The compressibility factor value at a temperature and a pressure point can be found in IUPAC handbooks (Angus et al. [41,42]).

Henry's law constants for pure CO_2 and pure He were calculated by extrapolating the solubility data of each pure gas to zero pressure and are shown in Table 2.2 for the ionic liquid [bmim][DCA] at 50, 80, 90, and 100 ^oC. The value of a Pseudo Henry's law constant for each gas was also determined for the case where there was a gas mixture. Since Henry's law constant is defined for a pure component only, the result determined is being called a Pseudo Henry's law constant when a gas mixture is used. Table 2.3 lists these values and they will be deliberated on later.

Table 2.2 Henry's Law Constants of Pure CO_2 and Pure He in [bmim][DCA] at Different Temperatures

Absorbent liquid	Temperature (K)	Henry's law constant (bar)		Reference H_{CO2} [44] (bar)
		H_{CO2}	H_{He}	
[bmim][DCA]	323	74.4±0.5	751.8±5.1	60.3±1.6 @303K
	353	104.2±2.5	521.1±7.2	94.4±3.5@333K
	363	114.3±3.0	440.8±6.4	111.4±4.8 @344K
	373	129.8 ±1.1	365.1±3.0	

Table 2.3 Pseudo Henry's Law Constants of CO_2 and He Mixture in [bmim][DCA] at Different Temperatures

Absorbent liquid	Temperature (K)	Pseudo Henry's law constant (bar)	
		H_{CO2}	H_{He}
[bmim][DCA]	323	78.2±1.7	761.5±3.9
	353	116.9±2.0	537.4±3.1
	363	120.5±3.1	450.3±3.4
	373	135.3±3.3	368.9±3.1

2.3.2 Solubilities of Pure Gases at Various Temperatures

Table 2.2 shows that as the temperature increased the solubility of CO_2 decreased in the pure ionic liquid which is represented by an increase in Henry's law constant. The temperature-solubility trend observed agrees with literature results for CO_2 (Husson-Borg et al. [43]). Henry's law constants of CO_2 in [bmim][DCA] at 30, 60, and 71 ^{o}C reported by Sanchez [44] are 60.3, 94.4, and 111.4 bar, respectively. Although the measurement conditions in the present study are somewhat different from these conditions, the literature values are in the expected range of the values obtained here. The solubility of helium in the studied absorbent, on the other hand, increased with increasing temperature. This trend can be explained based on thermodynamic relationships.

For helium, increasing temperature corresponds to a positive change in the enthalpy of absorption and the entropy of absorption leading to higher solubility in liquid absorbents (Finotello et al. [45]). For CO_2 increasing temperature results in a negative change in the enthalpy of absorption and the entropy of absorption which leads to lower solubility [45]. In other words, for low-solubility gases (N_2, He, H_2, etc.), the solubility increases when the temperature increases. The reverse trend is observed for the high-solubility gases such as CO_2 [45]. The same temperature-solubility trends, in terms of

mole fractions, for carbon dioxide and helium in the ionic liquid [bmim][DCA] are shown in Figure 2.8 for a variety of pressures and four temperatures.

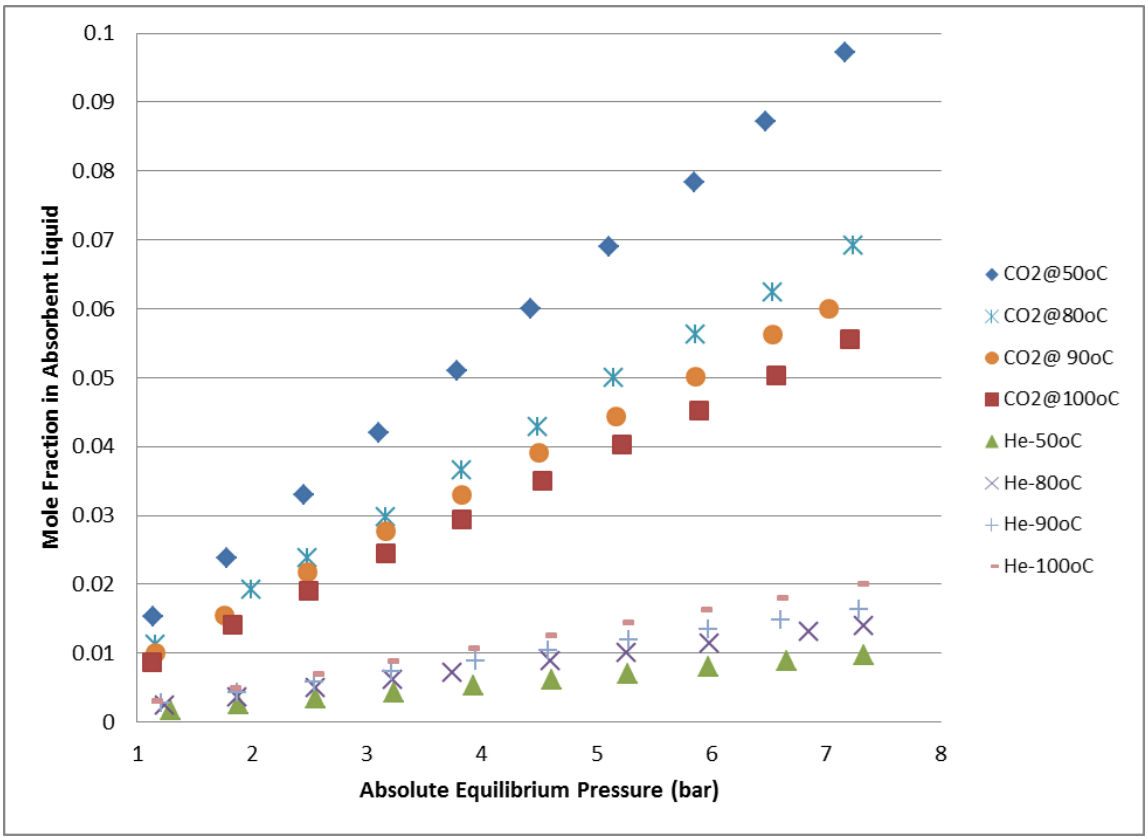

Figure 2.8 Influence of Temperature on Solubilities of Pure CO_2 and He in [bmim][DCA].

2.3.3 Solubilities of Pure Gases as a Function of Pressure

The solubilities of carbon dioxide and helium in [bmim][DCA] at the same temperatures increased with increasing pressure as shown in Figures 2.9 to 2.16 (for four temperatures 50, 80, 90, and 100 ^{o}C).

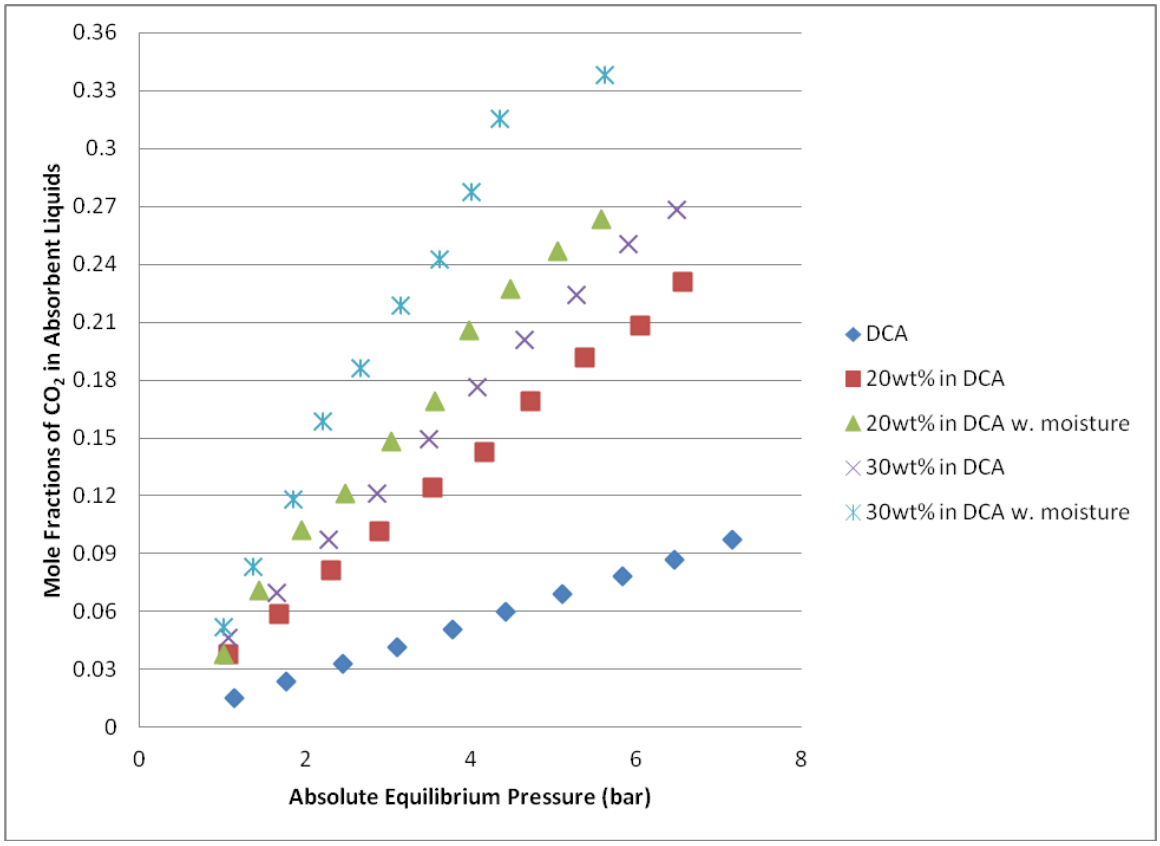

Figure 2.9 Solubilities of Pure CO_2 in Different Absorbent Liquids* at 50 ^{o}C.
*DCA used here is short for pure [bmim][DCA]

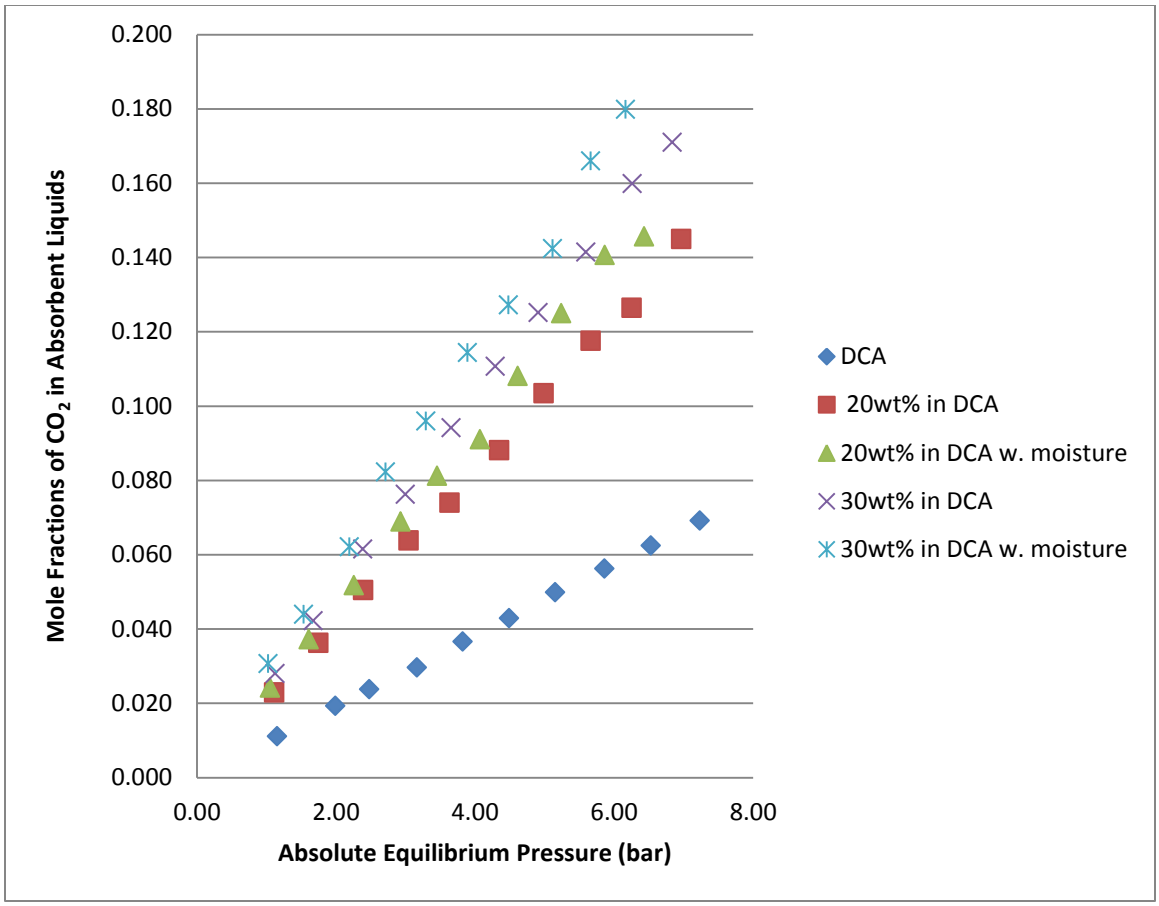

Figure 2.10 Solubilities of Pure CO_2 in Different Absorbent Liquids at 80 ^{o}C.

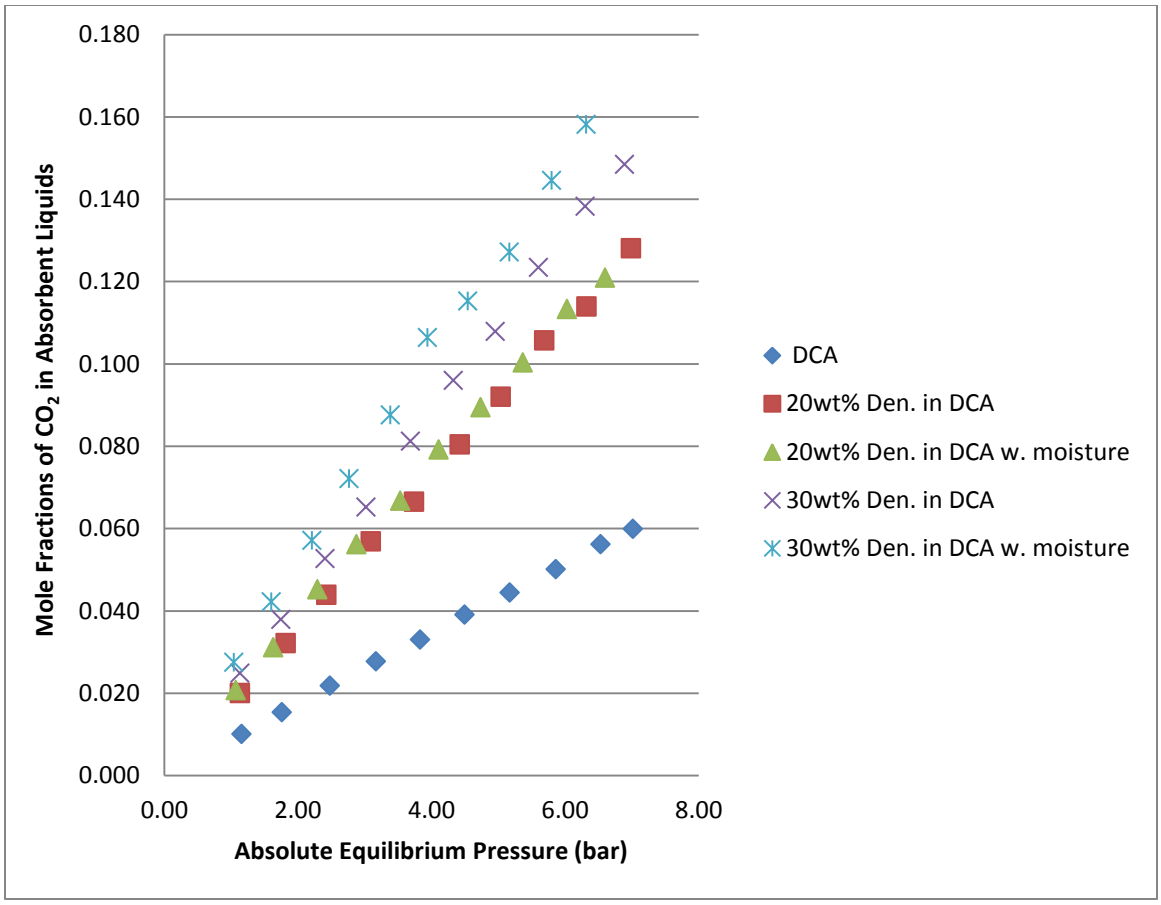

Figure 2.11 Solubilities of Pure CO_2 in Different Absorbent Liquids at 90 ^{o}C.

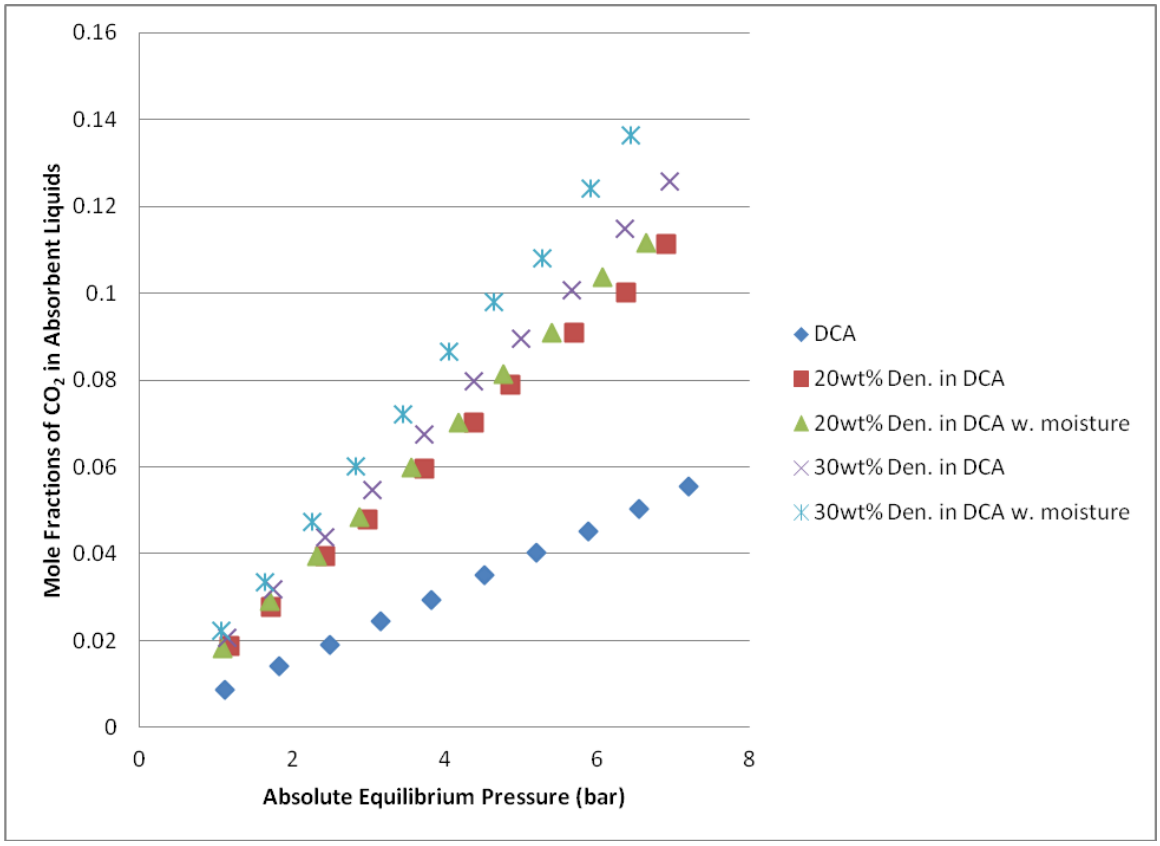

Figure 2.12 Solubilities of Pure CO_2 in Different Absorbent Liquids at 100 ^{o}C.

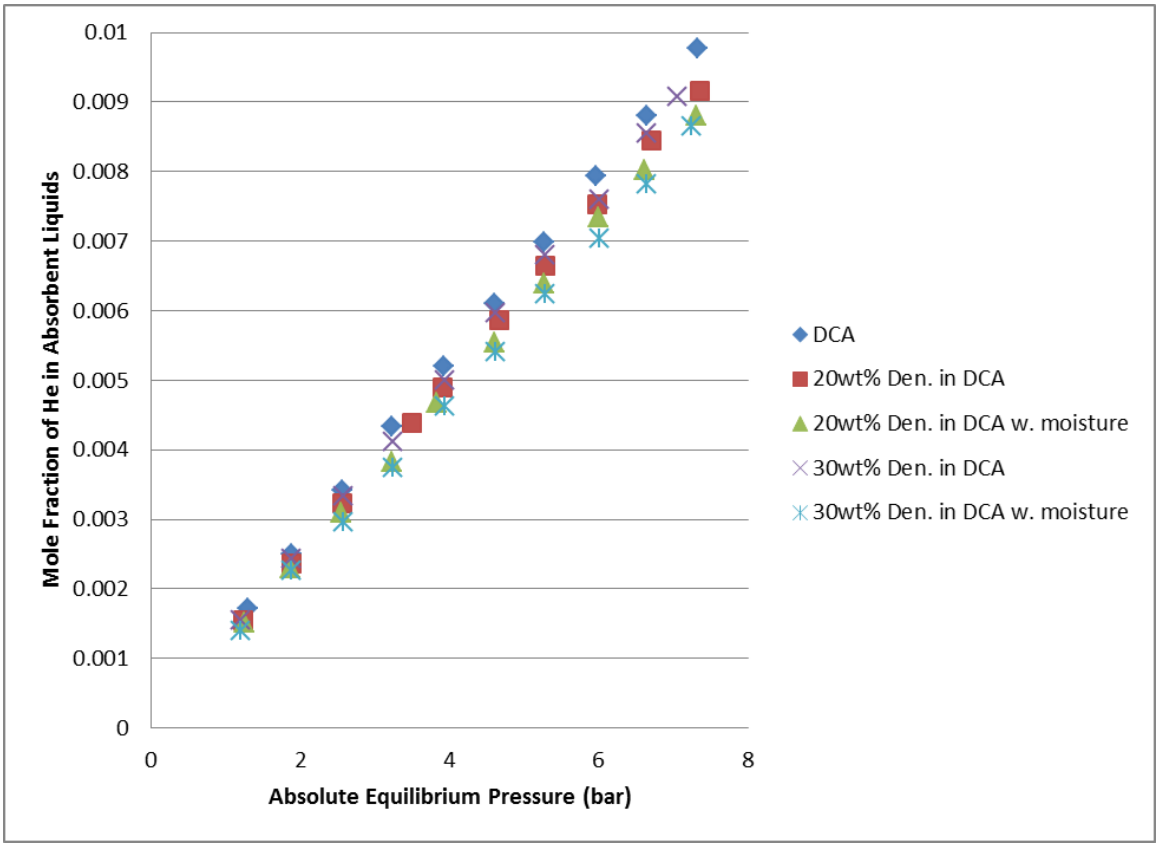

Figure 2.13 Solubilities of Pure He in Different Absorbent Liquids at 50 ^{o}C.

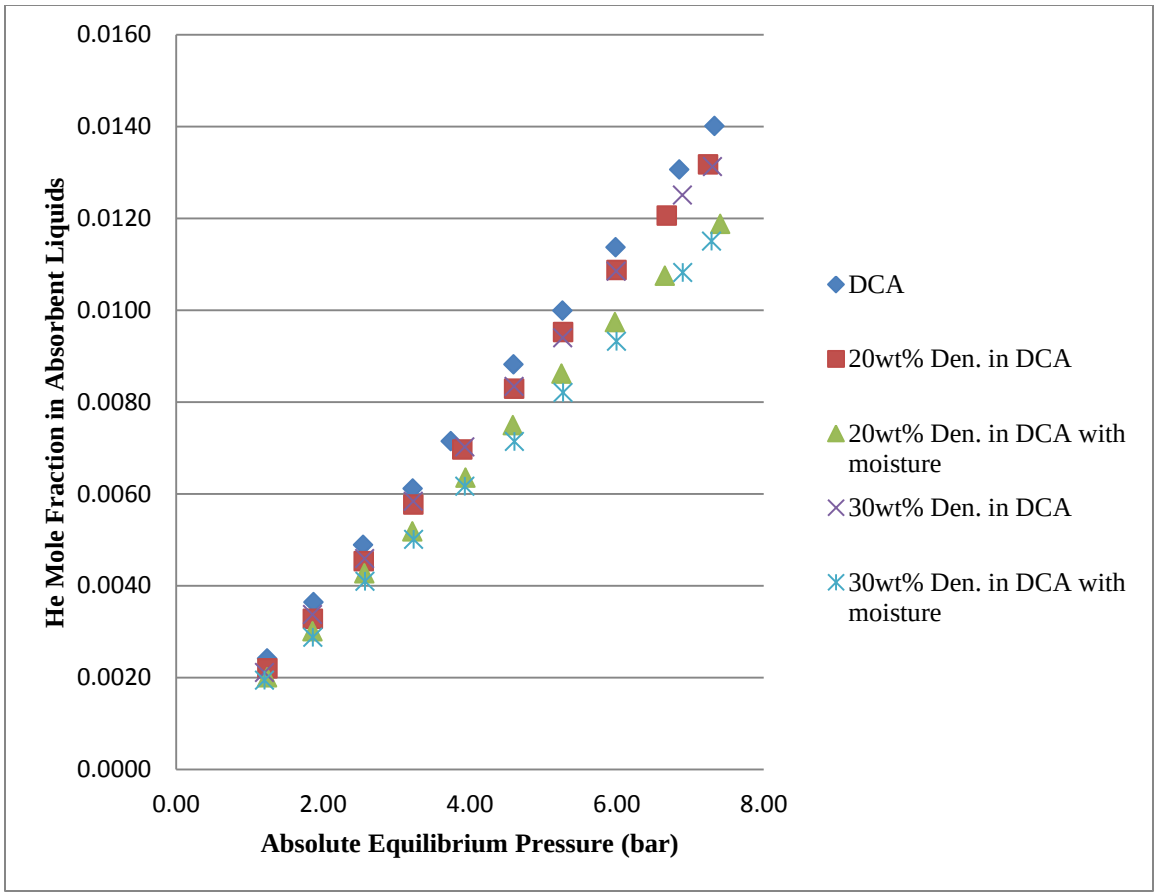

Figure 2.14 Solubilities of Pure He in Different Absorbent Liquids at 80 ^{o}C.

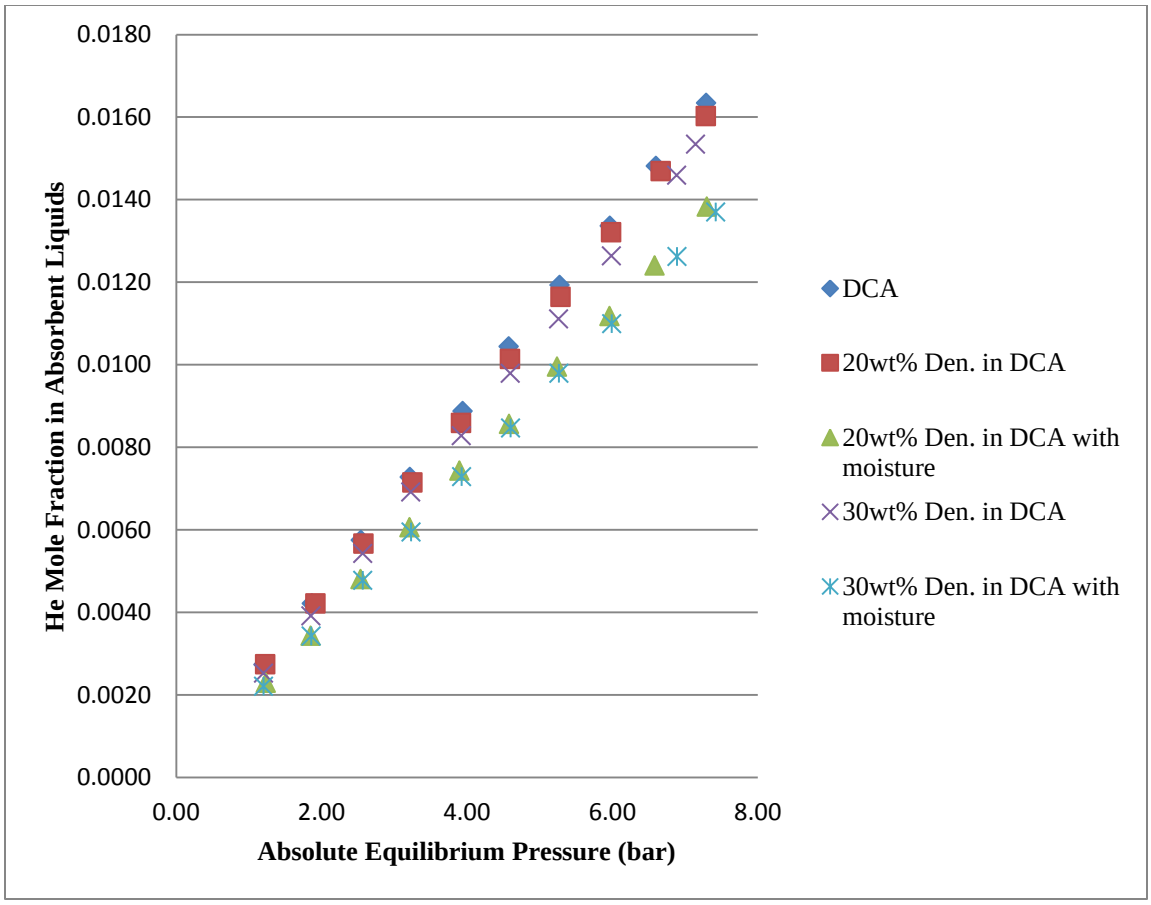

Figure 2.15 Solubilities of Pure He in Different Absorbent Liquids at 90 ^{o}C.

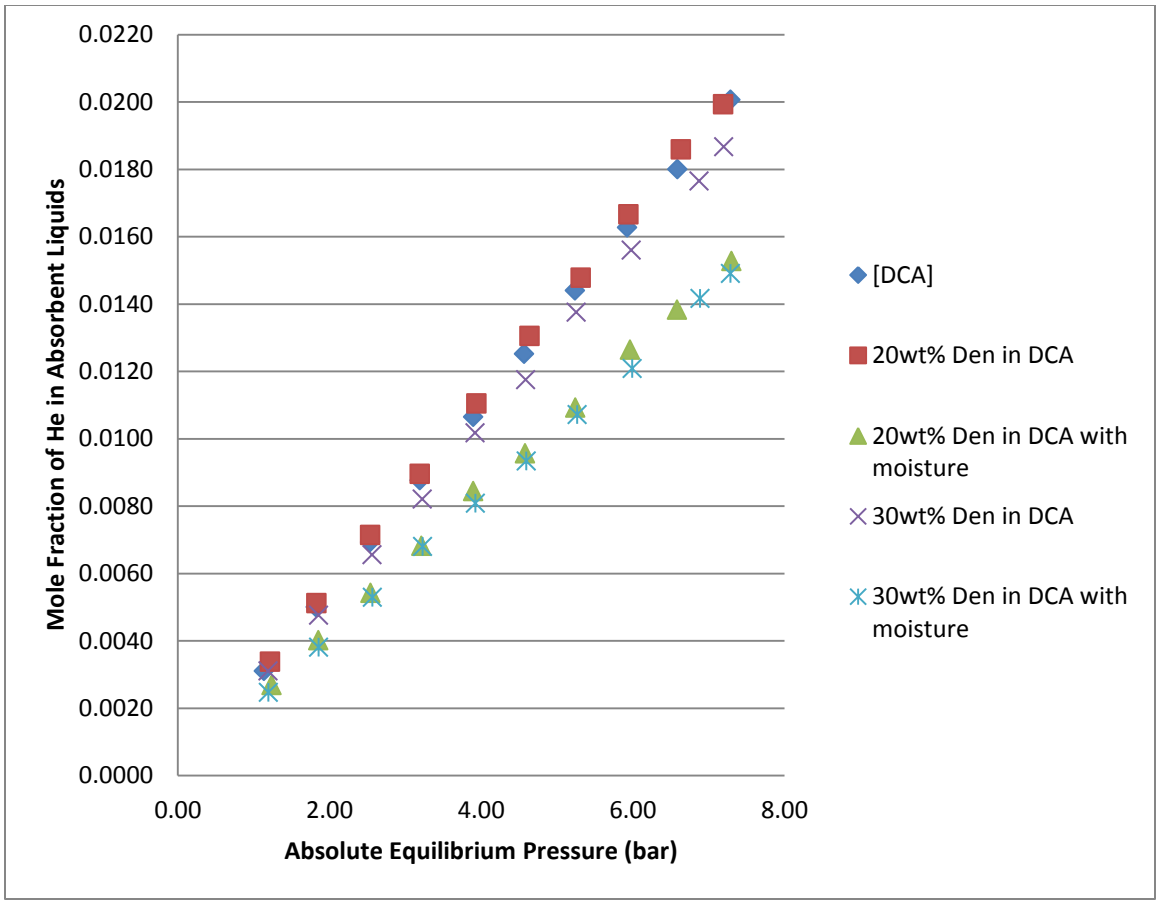

Figure 2.16 Solubilities of Pure He in Different Absorbent Liquids at 100 ^{o}C.

Table 2.4 shows the mole fraction values of carbon dioxide in [bmim][DCA] at 30 ^{o}C for various pressures reported by Sanchez [44]. In this study, the lowest temperature of solubility measurement was 50 ^{o}C except for two additional runs carried out at room temperature. The data obtained from additional runs at room temperatures were used to determine diffusion coefficients and Henry's law constant at room temperature, which are used in the mathematical model in Chapter 3. For general comparison purpose, the mole fraction values of CO_2 in the same ionic liquid at 50 ^{o}C for similar pressures, also shown in Table 2.4, show trends similar to those of Sanchez's at 30 ^{o}C, namely the solubility increased with increasing pressure and further the values are in the same range.

Table 2.4 CO_2 Mole Fractions in [bmim][DCA] for Different Pressures at 30 ^oC and 50 ^oC

	Pressure (bar)	CO_2 mole fraction
Sanchez [44] at 30 ^oC	2	0.035
	4	0.068
	5	0.08
	7	0.11
	9	0.13
Experimental data at 50 ^oC (This work)	1.14	0.015
	1.78	0.024
	2.45	0.033
	3.11	0.042
	3.78	0.051
	4.42	0.060
	5.11	0.069
	5.85	0.078
	6.48	0.087
	7.17	0.097

Table 2.5 (Table A15 in Appendix A provides a complete data set) shows the values of CO_2 mole fraction in [bmim][DCA] at various feed pressures and temperatures. The data show that carbon dioxide mole fraction values are directly proportional to the feed pressures. In addition, for the same feed pressure, the mole fraction ratio (= the ratio

of mole fractions at the two pressures) at different temperatures is the same. The same trend could also be observed for other liquid absorbents in this study.

Table 2.5 CO_2 Mole Fractions in [bmim][DCA] at Various Feed Pressures and Temperatures

Temperature (^oC)	Pressure (bar)	CO_2 mole fraction	Pressure Ratio	Mole Fraction Ratio
50	2.43	0.015	1.00	1.00
	7.92	0.051	3.26	3.33
	14.77	0.097	6.08	6.35
80	2.43	0.015	1.00	1.00
	7.92	0.051	3.24	3.28
	14.77	0.097	6.07	6.21
90	2.43	0.015	1.00	1.00
	7.92	0.051	3.28	3.26
	14.77	0.097	6.15	5.92
100	2.43	0.015	1.00	1.00
	7.92	0.051	3.39	3.39
	14.77	0.097	6.32	6.42

2.3.4 Solubilities of Pure Gases in Different Liquid Absorbents

Solubilities of carbon dioxide in various absorbents other than pure [bmim][DCA] at 50, 80, 90, and 100 ^oC have been shown in Figures 2.9 to 2.12, respectively. Among these different liquid absorbents, carbon dioxide was least absorbed in pure [bmim][DCA].

CO_2 solubility in the absorbent increased with increasing dendrimer concentration in the absorbent solutions since a PAMAM dendrimer (generation 0) molecule contains four primary amine groups and two tertiary amine groups (Figure 2.17), which helps increase the reactive absorption of carbon dioxide.

Solubilities of He in various absorbents other than pure [bmim][DCA] at 50, 80, 90, and 100 ^{o}C are shown in Figures 2.13 to 2.16, respectively. Unlike carbon dioxide, He was most absorbed in pure [bmim][DCA]. He solubility in the absorbent somewhat decreased with increasing dendrimer concentration in the absorbent solutions. The possible reason was due to the influence by the presence of other electrolytes/compounds such as dendrimer that affected the physical solubility of He in the IL.

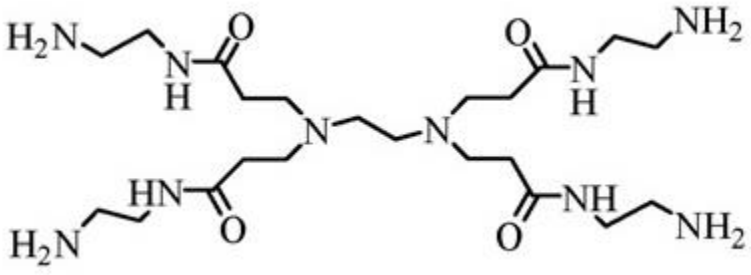

Figure 2.17 PAMAM Dendrimer of Generation 0.
Source: [20].

Only primary and secondary amine groups can react with carbon dioxide without any water present. The reaction between primary amine groups in a dendrimer molecule with CO_2 has been shown in Equation (2.4):

$$2\ R(NH_2)_4 + 4\ CO_2 \leftrightarrow R(NHCOO^-)_4 + R(NH_3^+)_4 \qquad (2.4)$$

There is spectroscopic evidence (FTIR) shown in Figure 2.18 indicating the presence of carbamate species in the dendrimer Gen 0 system with ionic liquid exposed to CO_2. Figure 2.19 shows that pure [bmim][DCA] did not have any band at around 1655 cm^{-1} on the IR spectra while 20 wt% dendrimer Gen 0 in [bmim][DCA] without any exposure to CO_2 had the band at 1655 cm^{-1} due to the presence of the amines in the solution. Figure 2.18 shows that the band at the wavenumber of 1651 cm^{-1} decreased in intensity while the bands at 1567 and 1170 cm^{-1} increased in intensity after CO_2 was introduced to the 20 wt% dendrimer Gen 0 in [bmim][DCA]. This indicates that CO_2 reacted with the primary amine groups to form carbamate species. The bands at approximately 1550 and 1100 cm^{-1} correspond to the C=O asymmetric and symmetric stretching bands of NH_2COO^- (Park et al. [46], Krevelen et al. [47]).

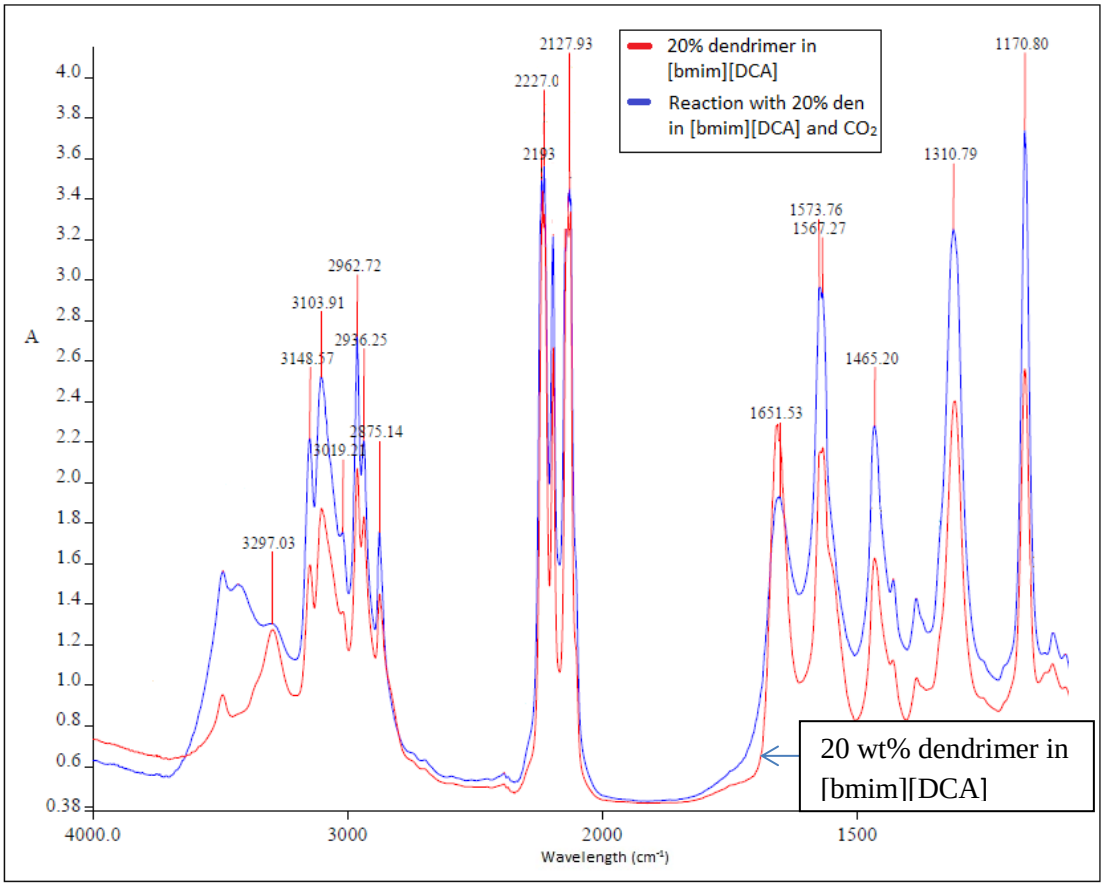

Figure 2.18 IR Spectra of 20wt% Dendrimer in [bmim][DCA] and Other Species in the Solution Exposed to CO_2 (Borrowed from T. Mulukutla's Ph.D. Thesis under Preparation).

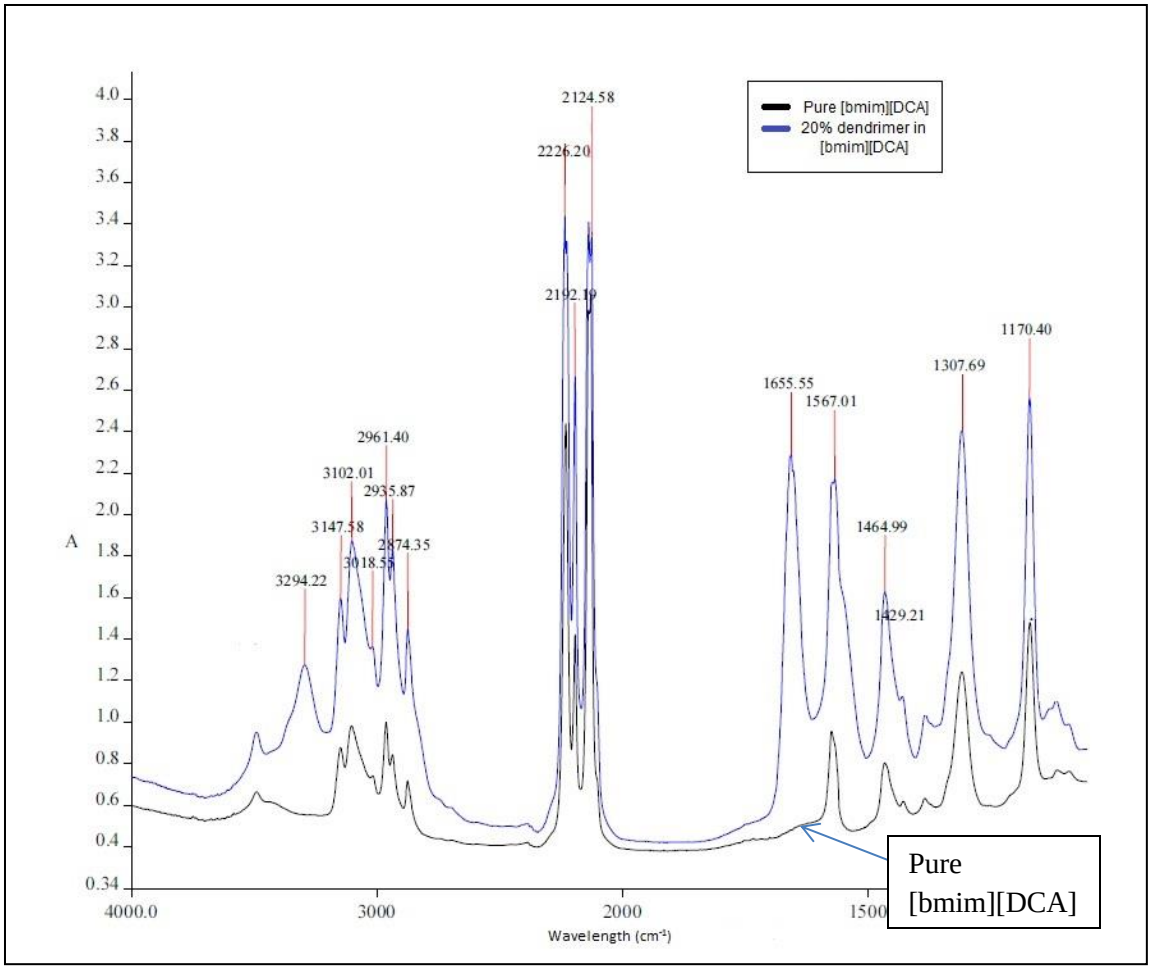

Figure 2.19 IR Spectra of Pure [bmim][DCA] and 20wt% of Dendrimer Gen 0 in [bmim][DCA] not Exposed to CO_2 (Borrowed from T. Mulukutla's Ph.D. Thesis under Preparation).

In addition, CO_2 solubility increased significantly when moisture was added to the dendrimer-ionic liquid solution due to the contribution of the tertiary amine groups contained in dendrimer besides the primary amine groups. Equation (2.5) shows the reaction of tertiary amine groups in the presence of water with carbon dioxide [20]:

$$2\ CO_2 + R_2\text{-}N\text{-}R\text{-}N\text{-}R_2 + 2H_2O \leftrightarrow 2HCO_3^- + R_2\text{-}NH^+\text{-}R\text{-}NH^+\text{-}R_2 \qquad (2.5)$$

The effect of water in [bmim][DCA] containing dendrimer on CO_2 solubility was largest at 50 ^oC, as shown in Figure 2.9. Some water evaporated at the higher

temperature; as a result, the presence of water in [bmim][DCA] containing dendrimer solutions was less effective, corresponding to a smaller increase in CO_2 solubility.

In aqueous systems, the physical solubility of CO_2 is affected by the presence of various ions. When reactive absorption of CO_2 takes place it is difficult to know what the concentration of free CO_2 is. A method followed in literature [46,47] involves determining the change in solubility of an inert gas due to the presence of various ions. The ratio of this change in solubility of this inert gas due to various ions is used to correct the free CO_2 concentration by the same factor. Normally N_2O is used (Versteeg et al. [48], Blauwhoff et al. [49]); here, the solubility ratio of inert He has been used to correct the concentration of free CO_2 in the reactive absorbent liquid:

$$H_{CO2T} = H_{CO2} \frac{H_{HeT}}{H_{He}} = \frac{P_f}{x} \tag{2.6}$$

where H_{CO2T}: Henry's law constant of CO_2 due to physical absorption in the IL containing dendrimer.

H_{CO2}: Henry's law constant of CO_2 in pure IL

H_{HeT}: Henry's law constant of He in the IL containing dendrimer

H_{He}: Henry's law constant of He in pure IL

x: mole fraction of free CO_2.

Due to the radically different charge climate in an ionic liquid as opposed to water (for example), the effect is expected to be minor. This correction has been found to be around 2-8%, which is shown in Table A18 in Appendix A.

2.3.5 Solubilities of Gases in a Mixture

Table 2.3 summarizes the Pseudo Henry's law constants for an initial feed gas mixture containing 40% CO_2, He balance for different absorbent liquids and at different temperatures. Here Pseudo Henry's law constant has been defined as the value of the slope of the curve of the gas partial pressure vs. mole fraction of species in liquid as this mole fraction tends to zero. The Pseudo Henry's law constants for each of CO_2 and He in the gas mixture were slightly higher than Henry's law constants of pure CO_2 and He. The Henry's law constants for pure CO_2 and He in pure [bmim][DCA] at 50 ^oC are 74.4 and 751.8 bar respectively whereas the Pseudo Henry's law constants for CO_2 and He in the gas mixture at 50 ^oC are respectively 78.2 and 761.5 bar. The differences between those values are within 5%. In addition, all the solubility trends with temperature, pressure, and absorbent liquids observed with the pure gases were also observed here. This was also a way to verify that the results are consistent and reproducible.

2.3.6 CO_2-He Solubility Selectivity

Solubility selectivity of CO_2 over He is defined in this study as the ratio of Henry's law constant of pure helium to that of pure carbon dioxide at a given temperature for [bmim][DCA]. For other reactive absorbents the solubility selectivity is defined as the ratio:

$$\text{Solubility selectivity } (CO_2/He) = \frac{\text{Pseudo Henry's law constant for He}}{\text{Pseudo Henry's law constant for } CO_2} \qquad (2.7)$$

Here as before the Pseudo Henry's law constant has been defined as the value of the slope of the curve of the gas partial pressure vs. mole fraction of species in liquid as this mole fraction tends to zero. When there is a reactive absorbent, Henry's law constant

defined for physical absorption in the limit of zero mole fraction in the liquid phase is misleading. However, in all four dendrimer-containing absorbents studied (Figures 2.9-2.16), there is essentially a linear behavior over almost the whole range of pressures and certainly as the pressure is lowered.

Figure 2.20 shows the solubility selectivity of CO_2 over He in a number of liquid absorbents at four temperatures. The solubility selectivity decreased with increasing temperature for all liquid absorbents. The highest selectivities were observed at 50 ^{o}C. Solubility selectivity of carbon dioxide over helium in pure [bmim][DCA] decreased from ~10 at 50 ^{o}C to ~2.8 at 100 ^{o}C. A solution of 30 wt% dendrimer in [bmim][DCA] with moisture gave the highest CO_2/He solubility selectivity among the three studied absorbents based on the IL[bmim][DCA] and five systems: a value of 55 at 50 ^{o}C and 10 at 100 ^{o}C.

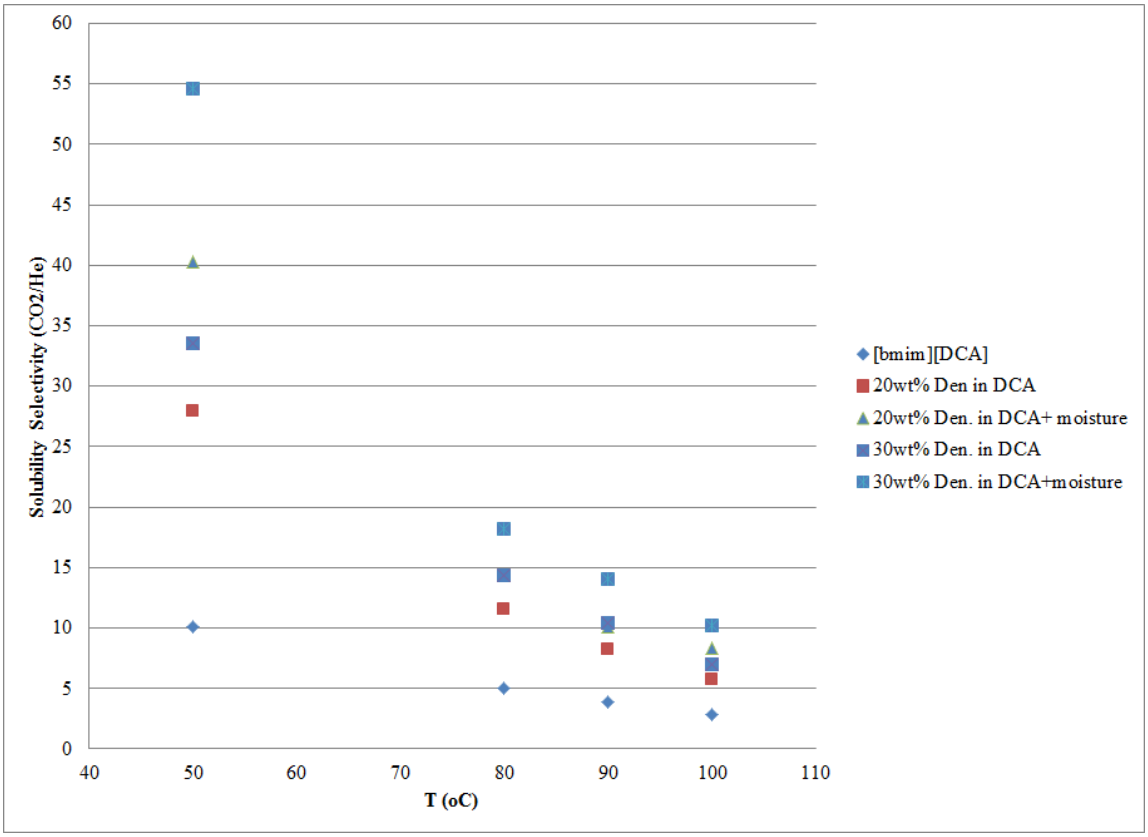

Figure 2.20 Solubility Selectivity of CO_2/He in Absorbent Liquids at Different Temperatures.

2.3.7 Apparent Equilibrium Constant for the Reaction in Reactive Absorption

The PAMAM Gen 0 molecule has four primary amines and two tertiary amines (Figure 2.17). For a dry system, one needs to focus only on primary amines. The reaction scenario is complicated by the fact that under conditions of excess CO_2, one can have all four primary amines in a molecule consumed. However, if one has a limited amount of CO_2, one can envisage a scenario where only one primary amine in a molecule has been consumed (In reality there will be a variety of intermediate conditions). Here appropriate equations will be developed for these two extreme cases so that one can extract values of

the corresponding apparent equilibrium constants. First focus on the situation where all four primary amines in a PAMAM Gen 0 have been consumed:

$$2\ R(NH_2)_4 + 4\ CO_2 \leftrightarrow R(NHCOO^-)_4 + R(NH_3^+)_4 \quad (2.8)$$

The approach for determining the equilibrium constant from the measured data is as follows. For 20 wt% dendrimer in [bmim][DCA] with a known mass (m) and volume of 0.01L (V_{IL}), the number of moles of dendrimer and [bmim][DCA] are, respectively

$$n_{den} = \frac{0.2m}{517.0} \quad (2.9)$$

$$n_{IL} = \frac{0.8m}{205.26} \quad (2.10)$$

The number of moles of CO_2 absorbed in the IL containing dendrimer, n_2, was calculated from the experimental data via Equation (2.3). The Henry's law constants for CO_2 due to physical absorption in the IL containing dendrimer are calculated via equation (2.6).

This approach is adopted since the physical solubility of CO_2 in the IL will be influenced by the presence of other electrolytes/compounds such as dendrimer. The effect of these compounds on the solubility of He will provide some guidance on the correction needed for CO_2 solubility. If N_2O was used instead of He, the correction may have been more accurate [48,49]. However, as mentioned earlier due to the radically different charge climate in an ionic liquid as opposed to water (for example), the effect is expected to be minor.

Mole fraction of free CO_2 in the liquid, x, is calculated below:

$$x = \frac{n}{n + n_{IL} + n_{den}} = \frac{P_f}{H_{CO2T}} \quad (2.11)$$

Therefore,

$$n = \frac{x(n_{IL} + n_{den})}{1-x} = \text{moles of free } CO_2 \text{ in solution} \qquad (2.12)$$

Now, n_{CO2r}, the moles of CO_2 reacted with primary amines present in dendrimer, is equal to

$$n_{CO2,r} = n_2 - n \qquad (2.13)$$

From Equation (2.4), the apparent reaction equilibrium constant, K_C, may be written as:

$$K_C = \frac{\frac{n_{R(NHCOO^-)_4}}{V_{IL}} \frac{n_{R(NH_3^+)_4}}{V_{IL}}}{\left(\frac{n_{CO_2|free}}{V_{IL}}\right)^4 \left(\frac{n_{R(NH_2)_4}}{V_{IL}}\right)^2} \qquad (2.14)$$

where we have assumed that any dendrimer molecule has all four primary amine groups reacting with CO_2 per Equation (2.4). Obviously

$$n_{R(NHCOO^-)_4} = \frac{n_{CO2,r}}{4} = n_{R(NH3^+)_4} \qquad (2.15)$$

Also the unreacted dendrimer molecules, $n_{R(NH_2)_4}$ are related to

$$n_{R(NH_2)_4} = n_{den} - \frac{n_{CO_2,r}}{4} - \frac{n_{CO_2,r}}{4} = n_{den} - \frac{n_{CO_2,r}}{2} \qquad (2.16)$$

Substituting relations (2.12), (2.15), and (2.16) in (2.14), one gets

$$K_C = \frac{\left(\frac{n_{CO_2,r}}{4}\right)^2}{n^4 \left(n_{den} - \frac{n_{CO_2,r}}{2}\right)^2} V_{IL}^{\ 4} \qquad (2.17)$$

Since all of the quantities on the right hand side are known, K_C can be determined.

In the other limit, only one primary amine of each dendrimer molecule may be reacting with CO_2. In reality, there will be a variety of scenarios. However, one can calculate the K_C value in the limit where only one primary amine of each dendrimer reacts with CO_2:

$$CO_2 + 2\ R(NH_2)_4 \leftrightarrow R(NH_2)_3HNCOO^- + R(NH_2)_3NH_3^+ \tag{2.18}$$

Similar to the case where all four primary amines reacting with carbon dioxide, for 20wt% dendrimer in [bmim][DCA] with a known mass (m) and volume of 0.01L (V_{IL}), the number of moles of carbon dioxide reacting with only primary amine, $n_{CO2,r}$, is calculated using Equations (2.9) to (2.13).

From Equation (2.18), the reaction equilibrium constant, K_C, may be written as:

$$K_C = \frac{\dfrac{n_{R(NH2)_3\ HNCOO^-}}{V_{IL}}\dfrac{n_{R(NH2)_3\ NH_3^+}}{V_{IL}}}{\left(\dfrac{n_{CO_2|free}}{V_{IL}}\right)\left(\dfrac{n_{R(NH_2)_4}}{V_{IL}}\right)^2} \tag{2.19}$$

where assuming only one primary amine group in any dendrimer molecule is reacting with CO_2 per Equation (2.18). Obviously

$$n_{R(NH2)_3\ HNCOO^-} = n_{CO2,r} = n_{R(NH2)_3NH_3^+} \tag{2.20}$$

Also the unreacted dendrimer molecules, $n_{R(NH_2)_4}$ are related to

$$n_{R(NH_2)_4} = n_{den} - n_{CO_2,r} - n_{CO_2,r} = n_{den} - 2n_{CO_2,r} \tag{2.21}$$

Substituting relations (2.20), and (2.21) into (2.19), we get

$$K_C = \frac{\left(n_{CO_2,r}\right)^2}{n\left(n_{den} - 2n_{CO_2,r}\right)^2} V_{IL} \tag{2.22}$$

The apparent reaction equilibrium constant, K_C, in this case could be expressed as:

$$K_C = \frac{\left(n_{CO_2,r}\right)^2}{n\left(n_{den} - 2n_{CO_2,r}\right)^2} V_{IL} \tag{2.23}$$

One can calculate the theoretical capacity of CO_2 absorption by PAMAM dendrimer molecules under dry conditions as well as under wet conditions. This value has been calculated for dry conditions for a certain concentration of PAMAM in the ionic liquid. By taking into account the total CO_2 absorbed minus the amount due to CO_2 solubility in the ionic liquid under the selected condition, one can then find out what fraction of this theoretical absorption capacity has been consumed under this particular condition. If one is very close to the theoretical capacity, one can argue that Equation (2.8) describes the situation. On the other hand, if the results very far away from the theoretical capacity, the case for reaction (2.18) improves.

In Table 2.6 (For a complete table which includes many pressures at any temperature, refer to Table A16 in Appendix A), the percent theoretical capacity consumed has been provided for a few pressures for a given temperature for 20 wt% dendrimer in the ionic liquid.

Table 2.6 Percent Theoretical Capacity* of Primary Amines Consumed Under Different Pressures and Its Corresponding Apparent Equilibrium Constant of Primary Amine Reaction with CO_2 for 20 wt% Dendrimer in [bmim][DCA] at Different Temperatures**

Tempearature (^oC)	P_{feed} (bar)	% Saturation (%)	K_C
50	2.43	10.56	6100 L/mol
	14.66	97.69	29972 L^4/mol^4
80	2.39	5.51	2804 L/mol
90	2.41	4.13	2227 L/mol
100	2.47	3.84	1790 L/mol

*Theoretical capacity is the theoretical moles of carbon dioxide absorbed due to reacting with primary amines in dendrimer based on the Equation (2.8)
**Dry system

At 14.66 bar, one finds that the absorption amount is 97.69% of the theoretical capacity at 50^{o}C. Therefore, Equation (2.17) may be used to estimate the apparent equilibrium constant K_C; the value is 29972 L^4/mol^4. At 2.41 bar, the absorption amount is 10.56% of the theoretical capacity at 50 ^{o}C. One may therefore use Equation (2.23) to estimate K_C; the value is 6100 L/mol. In addition, at 80, 90, and 100 ^{o}C, Equation (2.23) is used to calculate the apparent equilibrium constants due to the small percent amine saturation. The K_C values for 20 wt% dendrimer in [bmim][DCA] at 80, 90, and 100 ^{o}C are 2804, 2227, and 1790 L/mol, respectively.

One can carry out similar calculations for the 30 wt% dendrimer in the ionic liquid at different temperatures and pressures; the results are shown in Table 2.7 (for a complete table, refer to Table A17 in Appendix A). Since the percent amine saturation for most cases at all the temperatures studied is small, Equation (2.23) is used to calculate the

apparent equilibrium constants at different temperatures. The K_C values for 30 wt% dendrimer in [bmim][DCA] at 50, 80, 90, and 100^oC are 6659, 3061, 2431, and 1954 L/mol respectively. At 50 ^oC and 14.66 bar, the % saturation is 69.58%. Therefore, Equation (2.17) may be used to calculate K_C: the value is 10329 L^4/mol^4. Due to lower % saturation this value is quite different from 29972 L^4/mol^4 calculated for 20 wt% case with 97.69% saturation at 50 ^oC.

Table 2.7 Percent Theoretical Capacity* of Primary Amines Consumed under Different Pressures and Its Corresponding Apparent Equilibrium Constant of Primary Amine Reaction with CO_2 for 30 wt% Dendrimer in [bmim][DCA] at Different Temperatures*

Tempearature (^oC)	P_{feed} (bar)	% Saturation (%)	K_C
50	2.41	9.29	6659 L/mol
	14.66	69.58	10329 L^4/mol^4
80	2.43	4.49	3061 L/mol
90	2.43	3.93	2431 L/mol
100	2.43	2.98	1954 L/mol

*Theoretical capacity is the theoretical moles of carbon dioxide absorbed due to reacting with primary amines in dendrimer based on the Equation (2.8)
**Dry system

What one observes is as follows: the apparent reaction equilibrium constants decreased as the temperature was increased. Further the value of K_C for the case of only one primary amine being consumed is likely to be independent of the dendrimer concentration at all four temperatures.

2.3.8 Solubilities of Pure CO_2 and Pure He in PEG 400 and 20 wt% Dendrimer in PEG 400

PEG 400 and 20 wt% dendrimer in PEG 400 solution were also used as absorbents to study the solubility of carbon dioxide and helium. Solubilities of pure CO_2 and pure He in PEG 400 and 20 wt% dendrimer in PEG 400 are presented in terms of Henry's law constant and pseudo Henry's law constant and shown in Tables 2.8 and 2.9. Figures 2.21 to 2.28 show the solubilities of carbon dioxide and helium in pure PEG 400 and in 20 wt% dendrimer in PEG 400 at four temperatures. The figures show the same solubility trends are observed. Increasing feed pressure increases the number of moles of carbon dioxide and helium absorbed in the studied liquids. In addition, increasing temperature decreases the number of moles of carbon dioxide absorbed but increases the number of moles of helium absorbed in the liquids.

Table 2.8 shows the Henry's law constants of carbon dioxide obtained in the study are comparable to the ones obtained by Li et al. [50] especially at 323 K. Moreover, Tables 2.2 and 2.8 indicate that carbon dioxide gets absorbed more in pure PEG 400 than in pure [bmim][DCA] as the Henry's law constants for CO_2 in PEG 400 are less than those in [bmim][DCA] at the same temperature. Similarly, Table 2.9 shows that 20 wt% dendrimer in PEG 400 absorbs more carbon dioxide than 20 wt% dendrimer in [bmim][DCA]. As a result, the solubility selectivities of CO_2/He in pure PEG 400 and in 20 wt% dendrimer in PEG 400 are higher than the solubility selectivities of CO_2/He in pure [bmim][DCA] and in 20 wt% dendrimer in [bmim][DCA], which is shown in Figure 2.29.

Table 2.8 Henry's Law Constants of Pure CO_2 and Pure He in PEG 400 at Different Temperatures

Absorbent liquid	Temperature (K)	Henry's law constant (bar)		Reference H_{CO2} [50] (bar)
		H_{CO2}	H_{He}	
PEG 400	323	65.0±3.4	791.0±6.5	56.6±1.2 @313K
	353	91.1±2.3	565.6±10.2	65.4±0.7@323K
	363	101.5±2.0	463.2±8.6	70.9±1.2 @333K
	373	110.2±4.6	361.4±4.7	

Table 2.9 Pseudo Henry's Law Constants of Pure CO_2 and Pure He for 20 wt% Dendrimer in PEG 400 and [bmim][DCA] at Different Temperatures

Absorbent liquids	Temperature (K)	Pseudo Henry's law constant (bar)	
		H_{CO2}	H_{He}
20 wt% dendrimer in PEG 400	323	25.4±2.3	800.0±12.1
	353	40.9±2.0	574.8±12.5
	363	48.3±2.7	473.1±8.4
	373	56.0±2.3	375.7±7.3
20 wt% dendrimer in [bmim][DCA]	323	28.5±1.0	796.7±5.8
	353	48.1±1.3	555.8±10.4
	363	55.3±1.2	453.3±3.3
	373	62.1±1.5	360.2±5.1

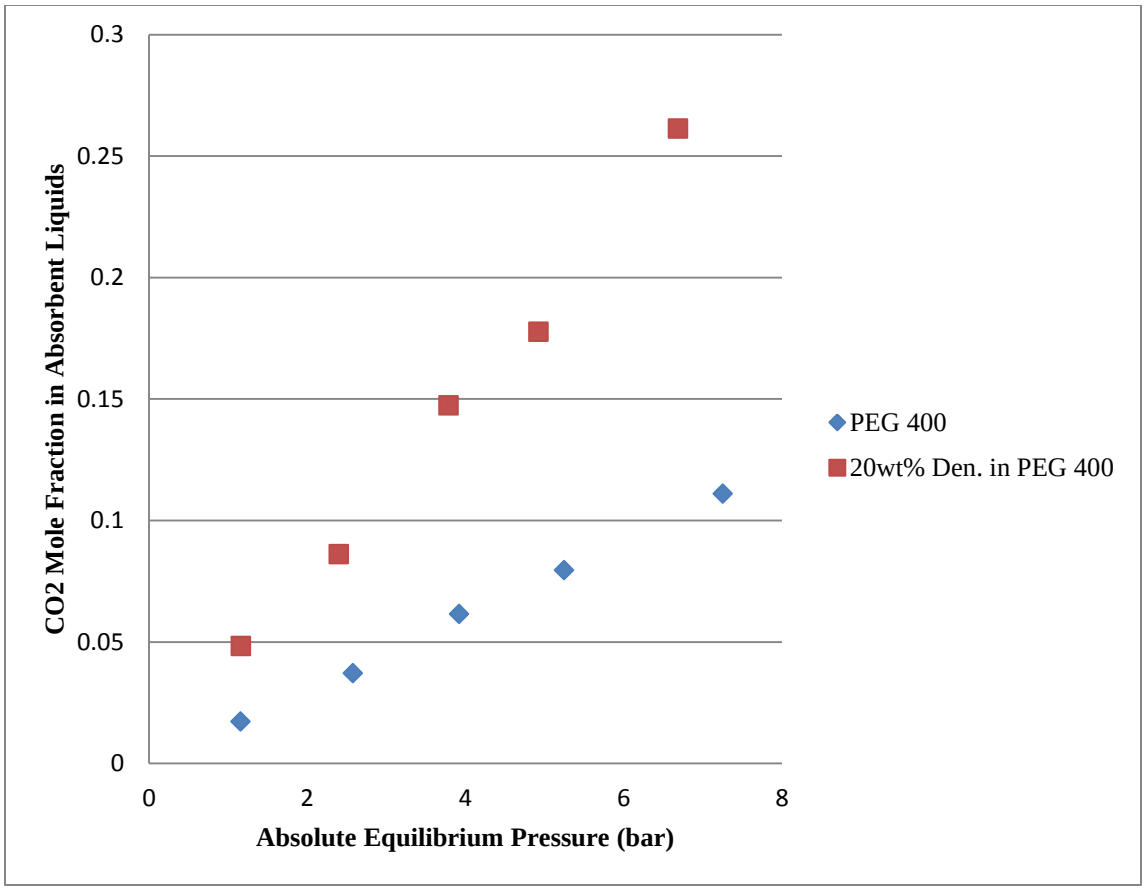

Figure 2.21 Solubilities of Pure CO_2 in Different Absorbent Liquids Based on PEG 400 at 50 ^{o}C.

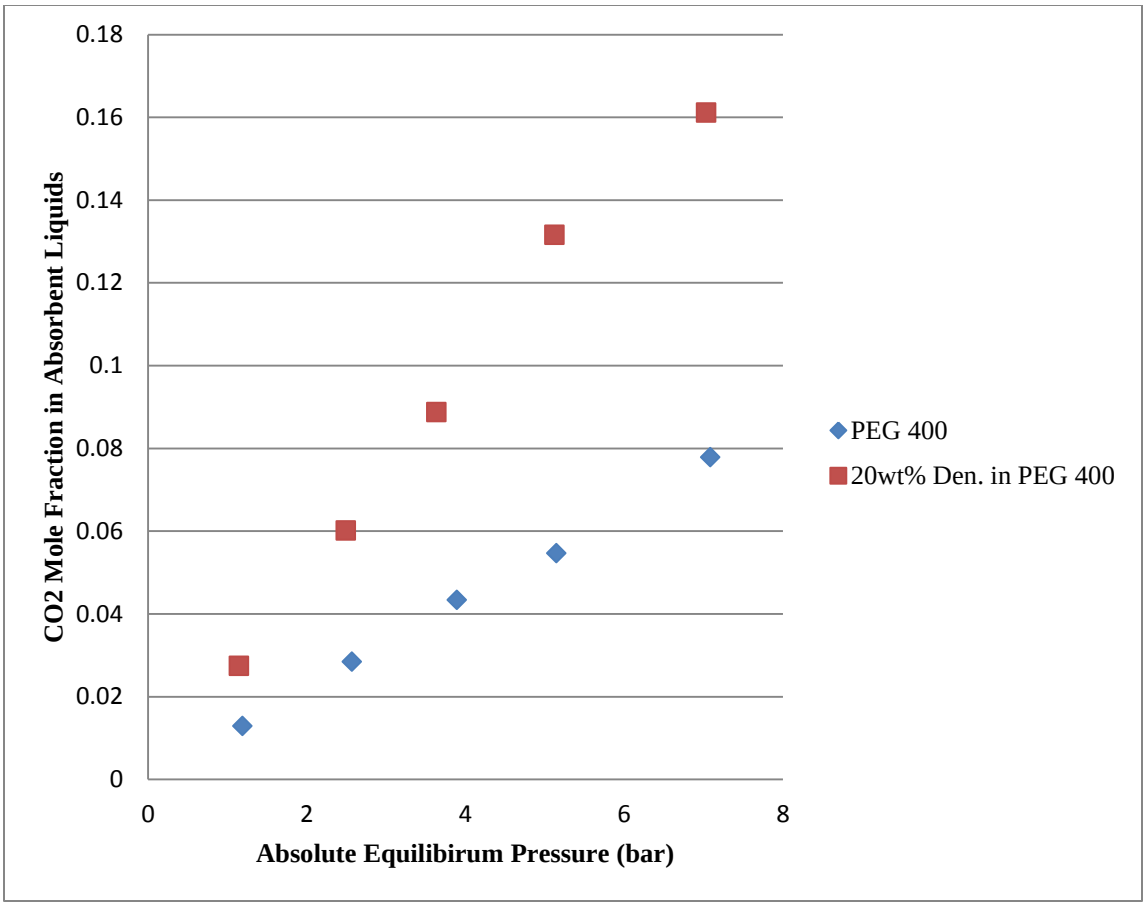

Figure 2.22 Solubilities of Pure CO_2 in Different Absorbent Liquids Based on PEG 400 at 80 ^{o}C.

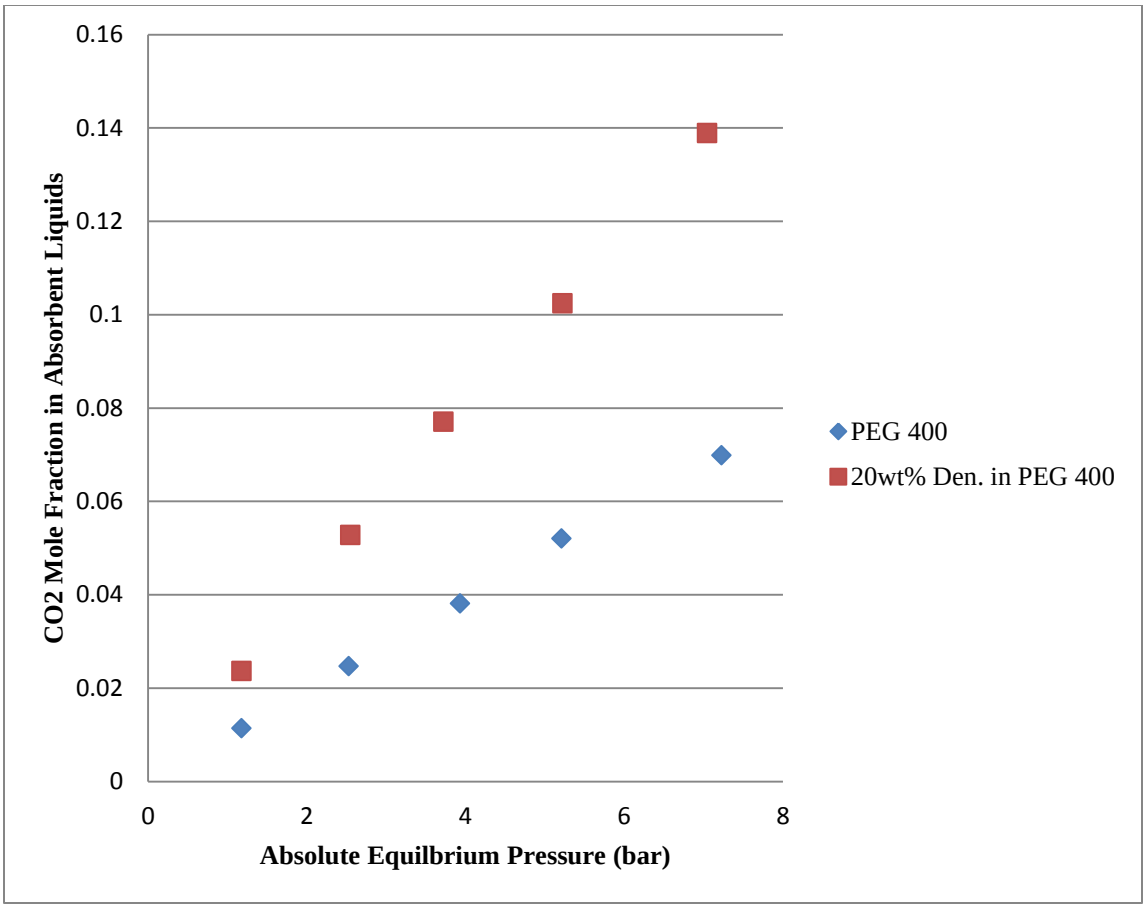

Figure 2.23 Solubilities of Pure CO_2 in Different Absorbent Liquids Based on PEG 400 at 90 ^{o}C.

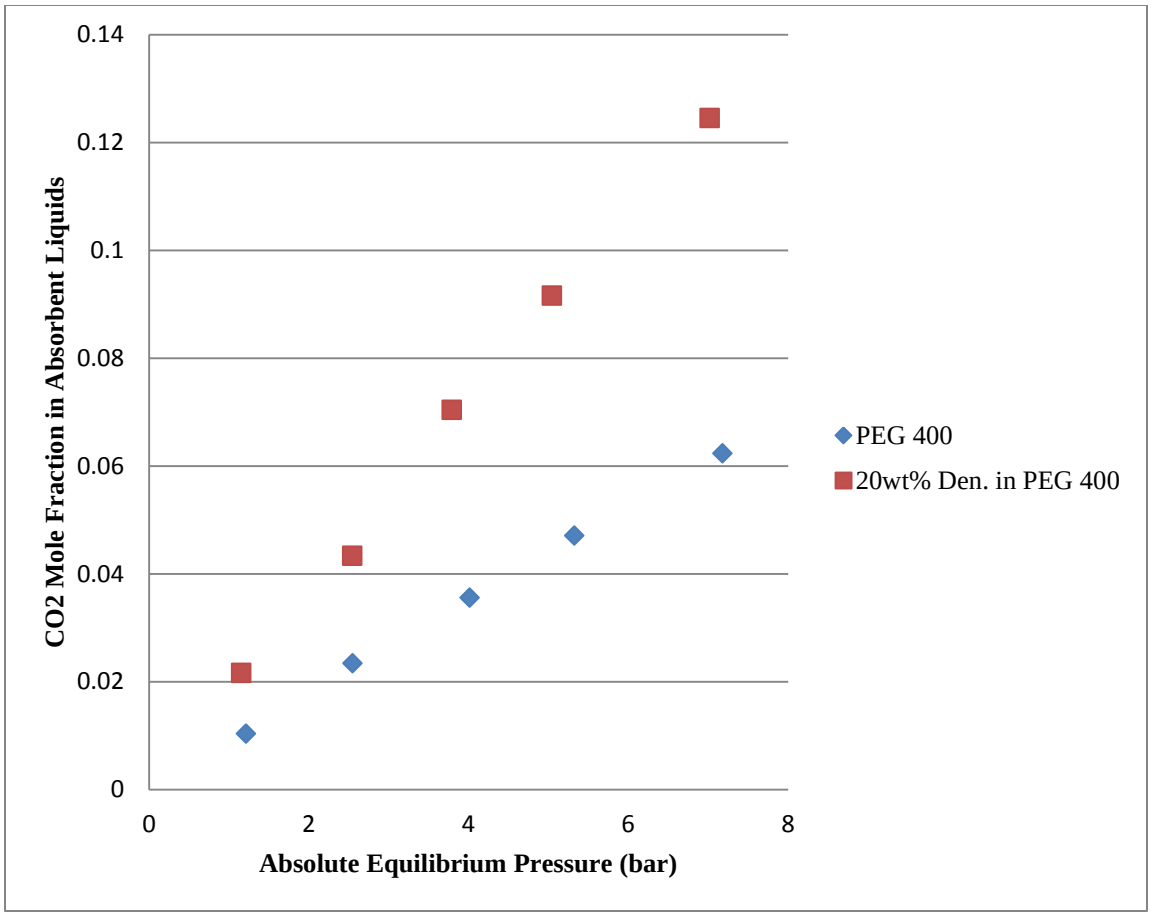

Figure 2.24 Solubilities of Pure CO_2 in Different Absorbent Liquids Based on PEG 400 at 100 ^{o}C.

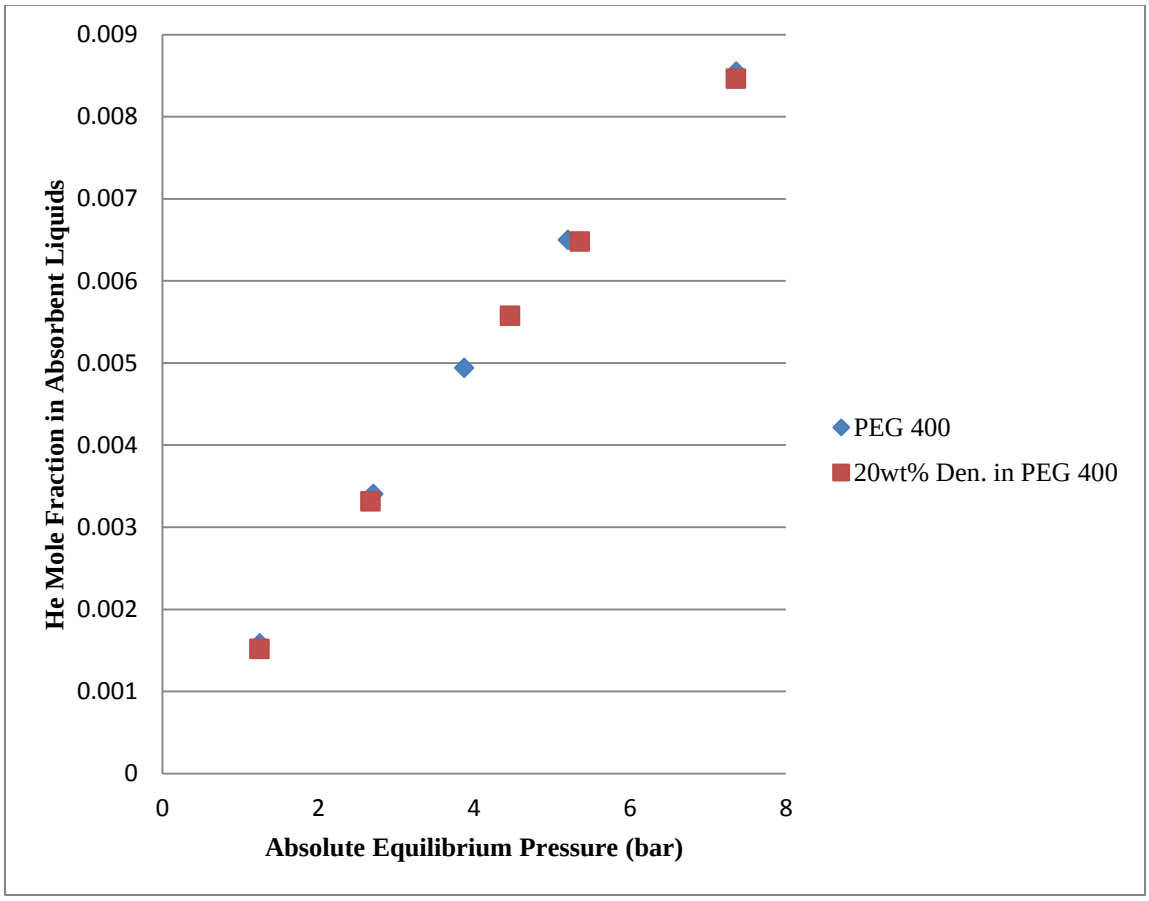

Figure 2.25 Solubilities of Pure He in Different Absorbent Liquids Based on PEG 400 at 50 ^{o}C.

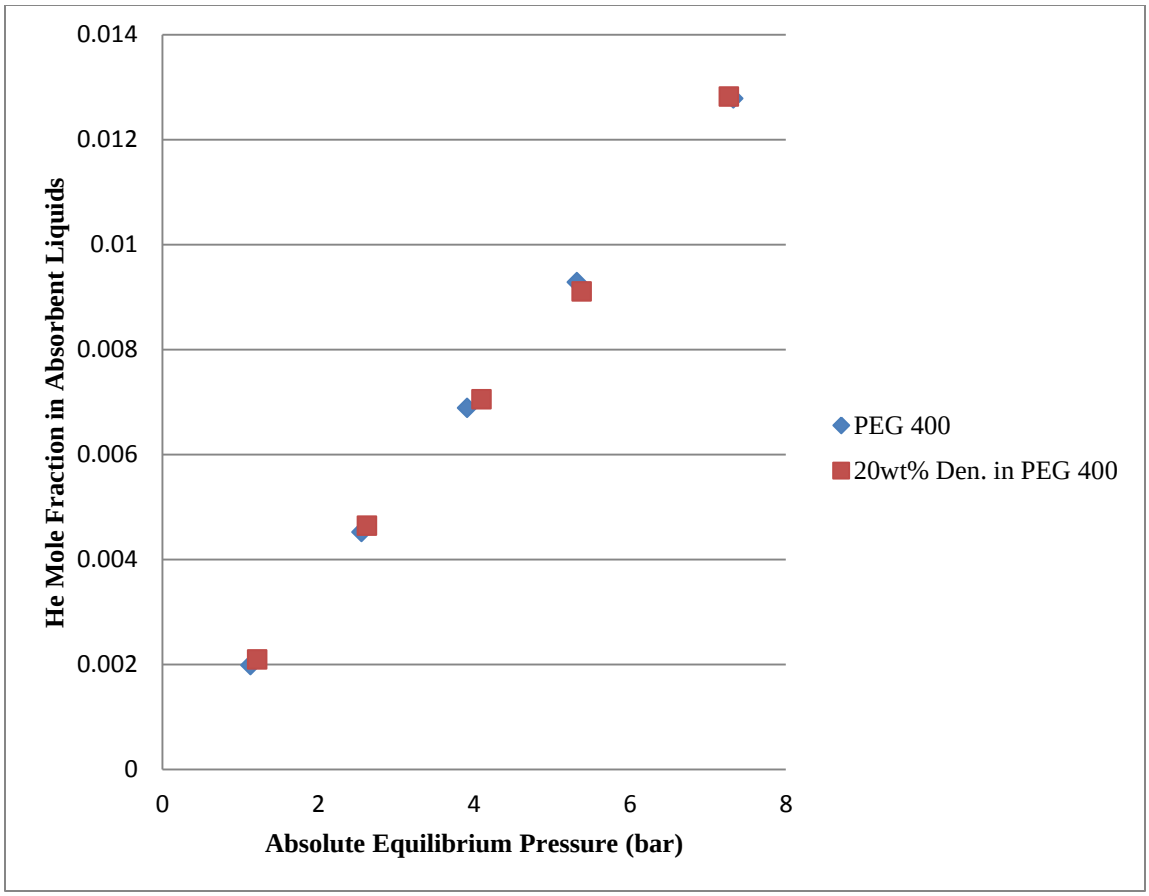

Figure 2.26 Solubilities of Pure He in Different Absorbent Liquids Based on PEG 400 at 80 ^{o}C.

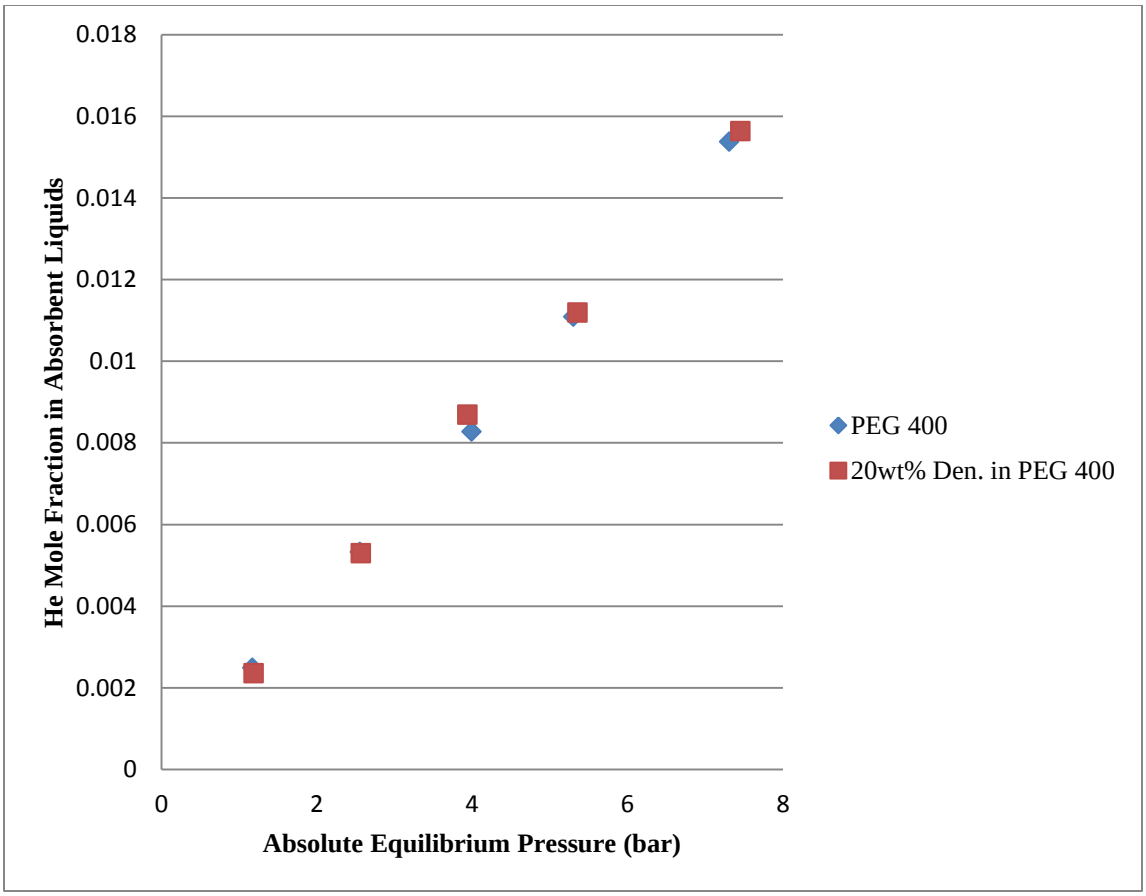

Figure 2.27 Solubilities of Pure He in Different Absorbent Liquids Based on PEG 400 at 90 ^{o}C.

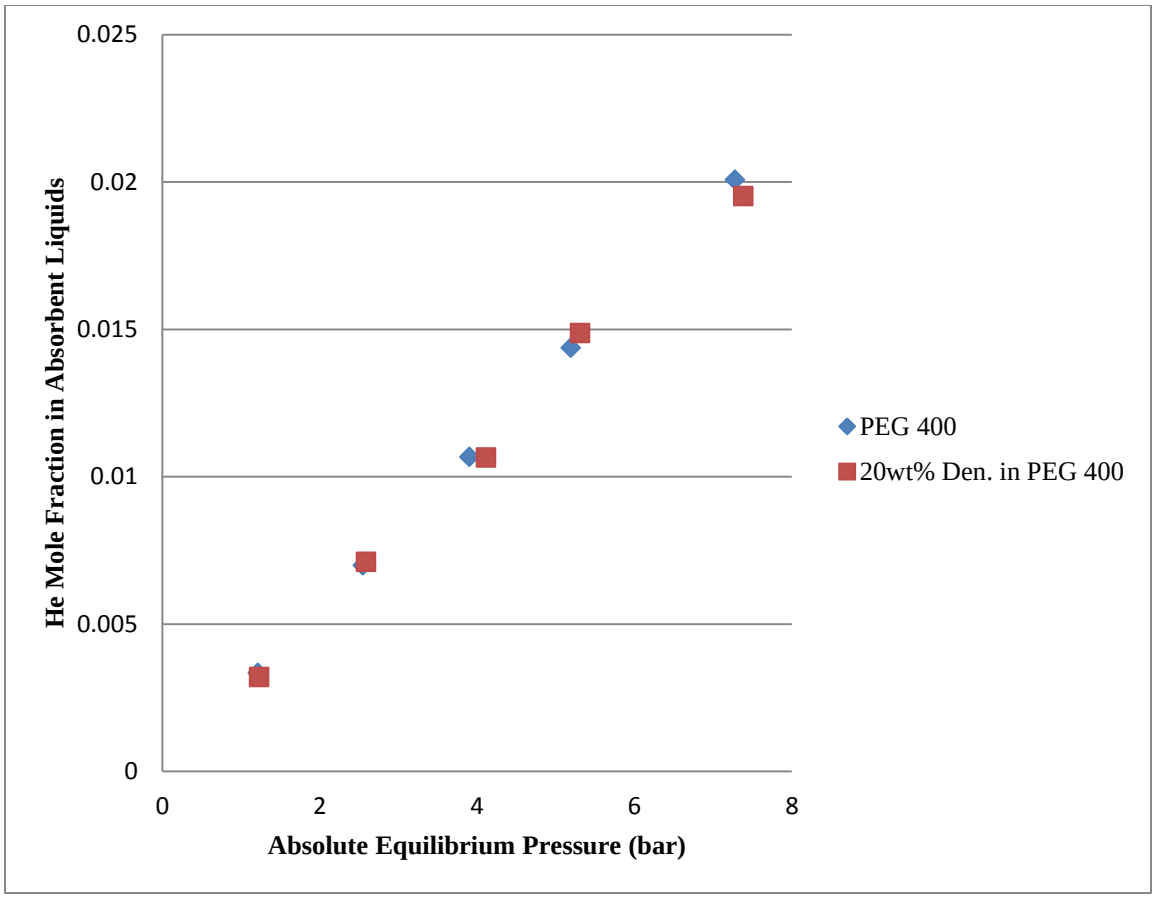

Figure 2.28 Solubilities of Pure He in Different Absorbent Liquids Based on PEG 400 at 100 ^{o}C.

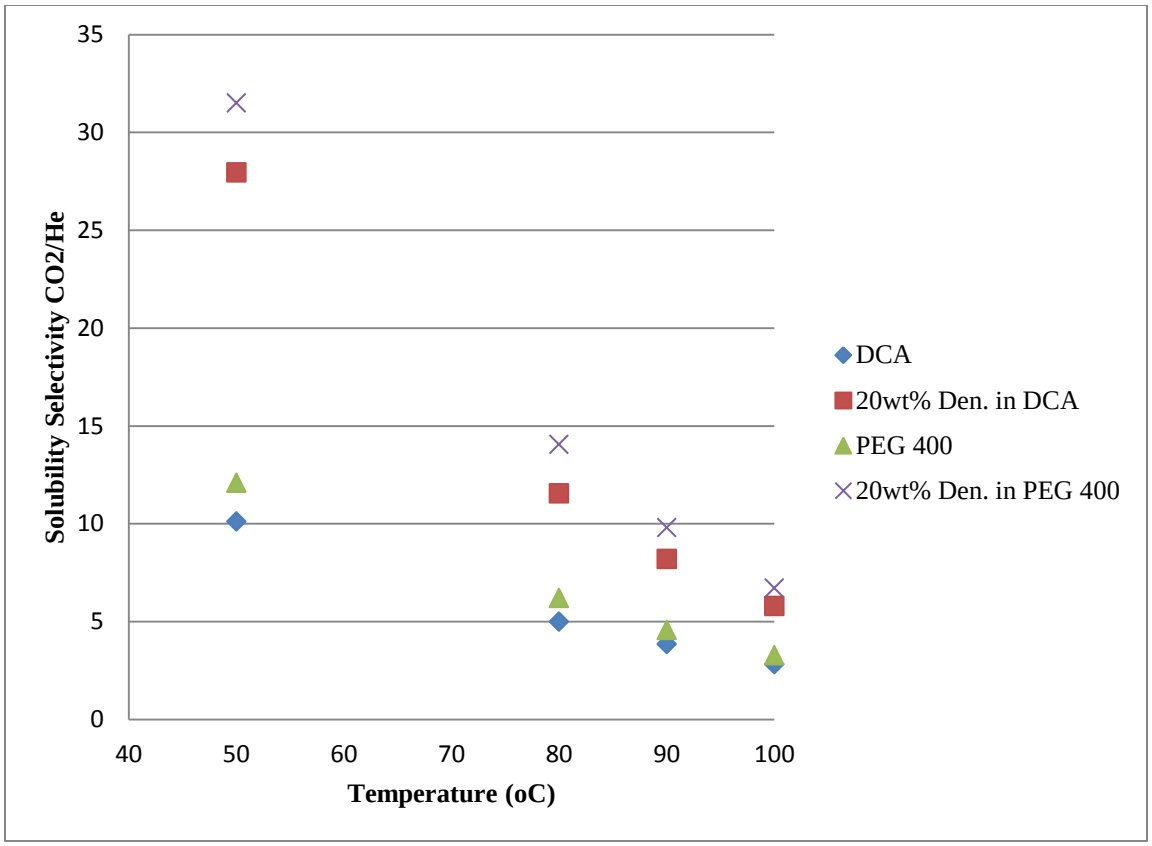

Figure 2.29 Solubility Selectivity of CO_2/He in [bmim][DCA], PEG 400, and 20 wt% Dendrimer in [bmim][DCA] and PEG 400.

2.4 Concluding Remarks

This chapter focused on finding out the CO_2 absorption characteristics and CO_2-He selectivity of an ionic liquid with or without a nonvolatile PAMAM dendrimer Gen 0 CO_2 for use in the pressure swing membrane absorption process [26]. A gas solubility apparatus was successfully setup to measure the solubility of pure CO_2, pure He and a CO_2-He mixture at temperatures of 50, 80, 90, and 100 ^oC and at pressures up to 1.38 MPa (~200 psig). Gas solubility measurements were made using a pressure decay method. Here, CO_2 solubility decreased with an increase in temperature whereas He solubility increased with an increase in temperature. The CO_2 and He solubilities

increased with an increase in pressure. An increase in the PAMAM dendrimer concentration led to a substantial increase in CO_2 solubility in a liquid absorbent due to reactions with the primary amine groups in the dendrimer molecule. An increase in dendrimer concentration led to a decrease in He solubility in the liquid absorbent. The presence of water in the ionic liquid containing dendrimer led to a considerable increase in CO_2 absorption in the liquid absorbent due to the reactivity of the tertiary amine groups. Among the studied absorbent liquids, 30 wt% dendrimer in [bmim][DCA] with moisture gave the highest CO_2 solubility at all temperatures studied. Higher CO_2/He solubility selectivity was observed as temperature decreased. A solution of 30 wt% dendrimer in [bmim][DCA] with moisture gave the highest CO_2/He solubility selectivity: a value of 55 at 50 ^oC and 10 at 100 ^oC. The solubilities of gases in a mixture are consistent with those of pure gases. In addition, carbon dioxide gets absorbed more in PEG 400 and 20 wt% dendrimer in PEG 400 than in [bmim][DCA] and 20 w% dendrimer in [bmim][DCA], respectively. That results in a higher solubility selectivities of CO_2/He in PEG 400 and 20 wt% dendrimer in PEG 400 than in pure [bmim][DCA] and 20 wt% dendrimer in [bmim][DCA].

Estimates of apparent reaction equilibrium constant (K_C) for a dry environment were also developed for two cases: all primary amines consumed; only one primary amine consumed. The values of K_C for the case of only one primary amine consumed were almost independent of dendrimer concentration at all four temperatures.

CHAPTER 3

PRESSURE SWING MEMBRANE ABSORPTION PROCESS FOR SHIFTED SYNGAS SEPARATION: MODELING vs. EXPERIMENTS

3.1 Introduction

Large-scale gas separation processes such as physical and/or reactive absorption of gases, pressure swing adsorption on solid adsorbents, cryogenic, and selective permeation through a membrane, all have advantages and disadvantages. Pressure swing adsorption (PSA) process is efficient to remove small impurities. However, the process is generally bulky and becomes costly when the impurity concentration increases (Yang [51]). Gas absorption involving reactive or non-reactive systems requires large contactors, which leads to high capital costs due to limited contacting area per unit device volume. In addition, it not only requires a tremendous amount of energy for the heating and cooling involved in the process, but also is prone to flooding, foaming, weeping, corrosion, and degradation (Qi and Cussler [52], Spilman [53]). Membrane-based gas-liquid contacting can avoid the shortcomings present in PSA or dispersive contacting-based absorption process. It uses a microporous hollow fiber membrane module providing high interfacial area per unit volume.

Solvent absorption-based method is a desired and widely used method for CO_2 removal. Since carbon dioxide produced from the low temperature (L-T) water gas shift reactor is at a high temperature around 150-200 ^{o}C and high pressure, CO_2 liquid absorbent chosen has to be thermally stable and non-volatile. Furthermore, the chosen absorbent liquid must have a high solubility selectivity of CO_2 over H_2 and CO. Since

post L-T water gas shift reactor produces gases with considerable moisture, absorbents having high selectivity of carbon dioxide in the presence of water are also of interest.

In this study, a pressure swing membrane absorption (PSMAB) process originally proposed by Bhaumik et al. [27], and later developed further by Jie et al. [26] was utilized to separate a feed gas mixture containing 40% CO_2-He balance. The process uses a microporous hydrophobic hollow fiber-based gas-liquid contactor with the absorbent liquid being stationary on the shell side and the feed gas mixture flowing through the tube side. The feed gas mixture was introduced into the membrane module through the tube side for five seconds. There, for a short period of time (30 seconds) the feed gas comes into contact with the stagnant and pressurized liquid absorbent on the fiber outer diameter (Shown in Figure 3.1) where carbon dioxide gets absorbed. During the rest of the cycle, two different product streams are withdrawn from two different ends of the tube side. He-rich product is withdrawn for two seconds while the CO_2-rich product is desorbed for 30 seconds. The absorbent liquid used is pure [bmim][DCA]. A mathematical model has been developed to predict the behavior of such a process and compare the predictions with the results of experimental runs over a range of temperatures from 23 to 100 ^{o}C.

3.2 Experimental Procedure

3.2.1 Materials

The ionic liquid [bmim][DCA] was purchased from EMD Chemicals, Philadelphia, PA. Simulated pre-combustion syngas containing 40.67% CO_2- He balance was obtained from Air Gas, Piscataway, NJ.

Ceramic membrane modules were purchased from Media and Process Technology, Pittsburgh, PA. One module contains a single ceramic tubule in a stainless steel housing. The ceramic tubule has a γ-alumina coating on an α-alumina substrate with all surfaces hydrophobized with nonafluorohexylsilane coating; the outside surface has a pore size ~5 nm.

Teflon membrane modules were purchased from Applied Membrane Technology Inc., Minnetonka, MN. The surface of the Teflon tube was completely hydrophobized by a nanoporous fluorosilicone coating to reduce the pore size to ≤0.01μm.

Three types of hydrophobized polyether ether ketone (PEEK) membrane modules were obtained from Porogen, Woburn, MA. One type is a small PEEK module (identified as PEEK-S). It contains a certain number of straight microporous hydrophobized PEEK hollow fibers in a cylindrical stainless steel housing with additional 1 to 1.5 inch (2.54 to 3.81 cm) on each open end of the fibers for stainless steel fittings. The second type (identified as PEEK-L II) has exactly the same type but much longer fibers helically wound in stainless steel housing. The third type (PEEK-L III) has fibers of similar length as in PEEK-L II; however, the membrane surface area was almost doubled for the same shell side volume. Therefore, the gas volume in the fiber I.D. region would be almost twice of that in PEEK-L II and correspondingly the effect of the tube-side header dead volume will be reduced in so far as product quality is concerned. Details of all membrane modules are listed in Table 3.1.

Table 3.1 Dimensional Characteristics of the Membrane Absorption Modules

Module[1]	OD/ID; cm	L; cm	Pore Size[5]; Å	VVF	Fiber Number	Surface area[2]; cm^2	A/V; cm^{-1}
Ceramic	0.57/0.37	44.0	~50	0.35~0.4	1	78.75	4.3
Teflon	0.108/0.053	58.0	<100	NA	28	570	27.2
PEEK-L II [3,4]	0.0452/0.029	41.0	~20	~0.4	568	3420	54.7
PEEK-L III	0.047/0.0272	41.0	~20	~0.4	908	5500	57.4

[1] OD: outer diameter of fiber; ID: inner diameter of fiber; L: effective fiber length; VVF: void volume fraction; [2] Based on outer diameter of fibers; [3] PEEK-L II module has a packing density around 21.8% that was defined as the ratio between total fiber volume and the real volume they occupied (total fiber volume plus space between the fibers in the fiber strands wound helically in the module); [4] PEEK-L module with PTFE bead-filled tube-side headers in the module; [5] Pore size of the outside surface.

One eighth inch diameter PTFE balls (Engineering Laboratories, Inc., Oakland, NJ) were put in the tube side headers of the PEEK-L II module to reduce the dead volume in tube-side headers; however, there were no PTFE balls in the tube-side headers of PEEK-L III. PEEK-S modules were not studied. Teflon modules were also not studied due to their low breakthrough pressures.

3.2.2 Breakthrough Pressure Test for Membrane Modules

Before the membrane modules were used in the pressure swing membrane absorption process system, breakthrough pressure tests on these modules were performed using different absorbent liquids since this determined how high a feed gas pressure for PSMAB studies could be used. Breakthrough pressure is determined mainly by two factors: pore size of membrane fibers at the liquid-gas interface on the shell side and the surface tension of the absorbent, namely, the IL. Breakthrough pressure for a non-wetted pore size of radius, r_p, is described by the Young-Laplace equation:

$$\Delta P_{breakthrough} \cong \frac{2\gamma \cos\theta}{r_p} \tag{3.1}$$

where γ is the surface tension of the liquid.

During the test, the module shell side was filled with [bmim][DCA]. One port of the membrane module shell side was connected to a small cylinder containing the IL while the other port was closed. The IL cylinder was also connected to a N_2 cylinder to develop the desired pressure. The membrane module tube side had a low flow of nitrogen gas to bring any possible breakthrough of IL out when the pressure was gradually increased. When leaked IL could be detected from tube side, the test pressure was defined as the breakthrough pressure. Liquids other than ILs were also tested. Some modules were tested up to 300 psig and all the breakthrough pressure tests were performed at room temperature. Table 3.2 summarizes the breakthrough pressures of all membrane modules tested.

Table 3.2 Breakthrough Pressure Results

Module type	Water	[bmim][DCA]	[emim][Tf_2N]	PEG 400	20% Dendrimer in PEG 400	20% Dendrimer in [bmim][DCA]
Ceramic I	210 psig	*No leakage up to 300 psig	N/A	N/A	300 psi	N/A
Ceramic II	*No leakage up to 300 psig	*No leakage up to 300 psig	180 psig	*No leakage up to 300 psig	N/A	N/A
Ceramic III	*No leakage up to 300 psig	*No leakage up to 300 psig	*No leakage up to 300 psig	N/A	N/A	N/A
Ceramic IV	*No leakage up to 300 psig	*No leakage up to 300 psig	*No leakage up to 300 psig	N/A	N/A	N/A
Teflon I (S/N: 1004)	*No leakage up to 100 psig	100 psig	N/A	80 psig	N/A	100 psig
Teflon II (S/N: 1005)	140 psig	40 psig	N/A	80 psig	N/A	40 psig
Teflon III (S/N: 1006)	*No leakage up to 140 psig	60 psig	N/A	80 psig	N/A	60 psig
PEEK 2PG295	*No leakage up to 200 psig	*No leakage up to 200 psig	*No leakage up to 200 psig	*No leakage up to 200 psig	N/A	N/A
PEEK 2PG296	*No leakage up to 260 psig	*No leakage up to 260 psig	N/A	*No leakage up to 260 psig	N/A	N/A
PEEK 2PG261	N/A	*No leakage up to 250 psi	N/A	N/A	N/A	N/A
PEEK (S/N:30-105-20)	*No leakage up to 200 psig	40 psig	N/A	140 psig	N/A	N/A
PEEK (S/N:30-105-21)	*No leakage up to 200 psig	*No leakage up to 140 psig	80 psi	180 psig	N/A	N/A
PEEK-L I	>260 psig	>260 psig	N/A	>260 psig	N/A	N/A
PEEK-L II	>300 psig	>250 psig	N/A	>250 psig	N/A	N/A
PEEK-L III	>250 psig	>250 psig	N/A	N/A	N/A	N/A

3.2.3 Pressure Swing Membrane Absorption (PSMAB) Process

Figure 3.1 shows the concentration profile of the absorbed gas species in the gas and the liquid phases in a membrane absorber.

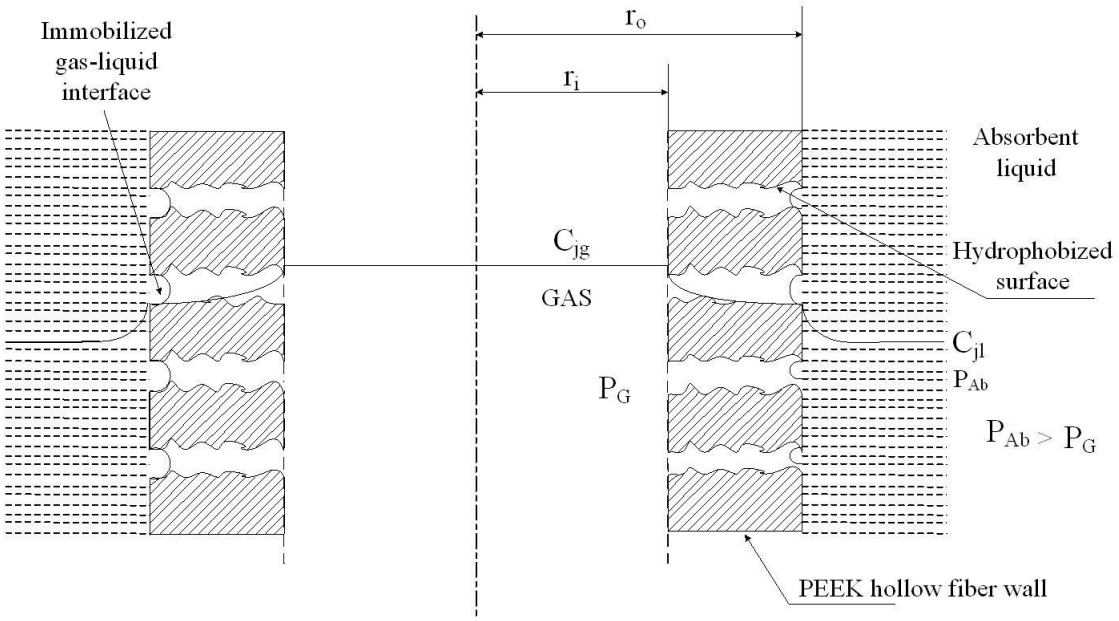

Figure 3.1 Concentration Profile for Absorbed Species in Gas and Liquid Phases in a Porous Membrane Gas-Liquid Contactor.

Pressure swing membrane absorption process of a gas mixture was usually carried out in a hollow fiber membrane module shown in Figure 3.2.

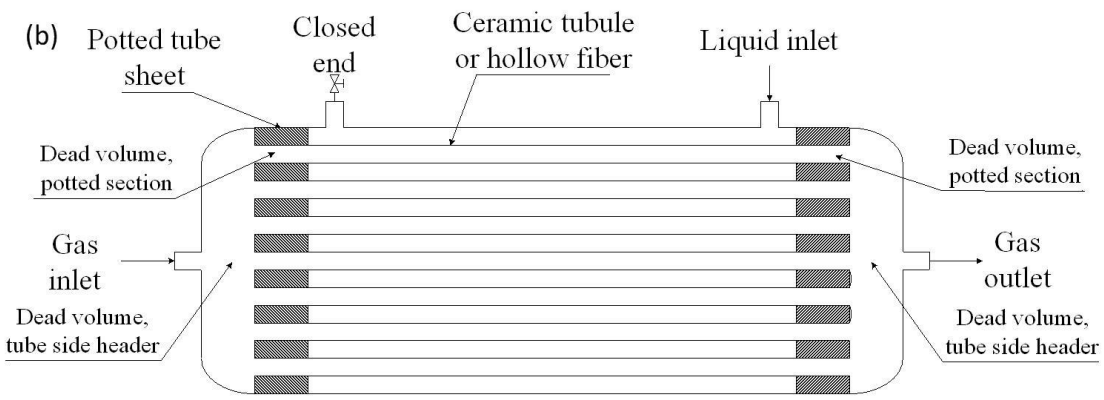

Figure 3.2 Schematic of the Membrane Containing Ceramic Tubules or Hollow Fibers.

Figure 3.3 shows a schematic diagram of the pressure swing membrane absorption experimental setup employing three valves.

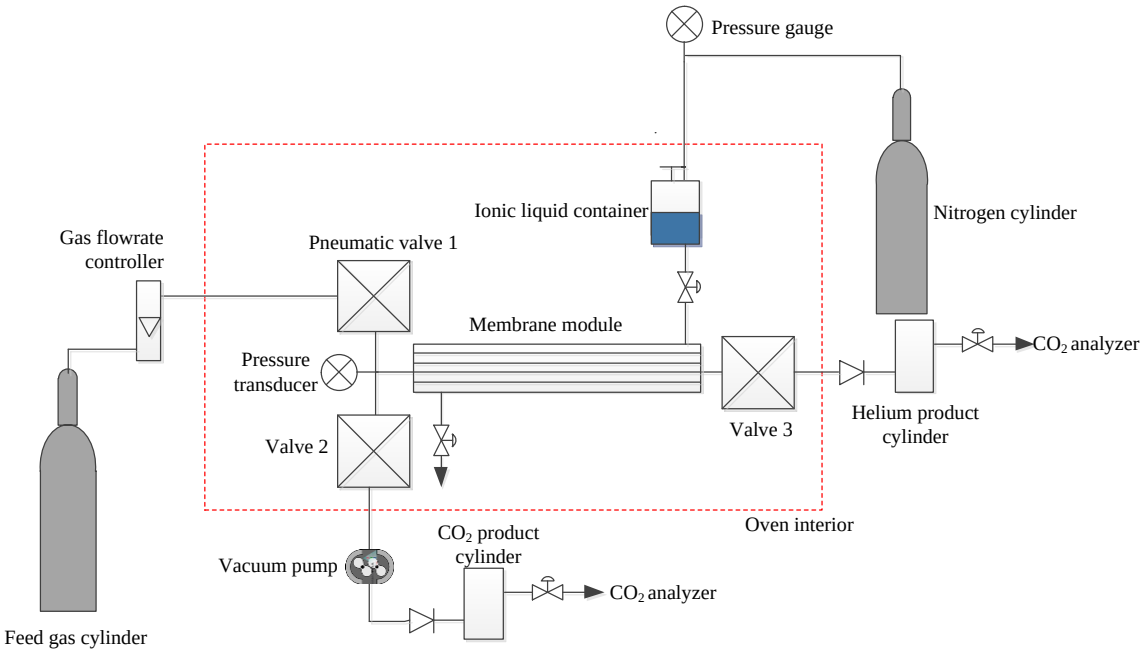

Figure 3.3 Schematic Diagram of the Pressure Swing Membrane Absorption Setup.

The membrane module was put inside a temperature controlled oven (Model PV-222, ESPEC North America Inc., Hudsonville, MI) so that the exact temperature could be set and controlled. The shell side of the module was filled with a certain absorbent such as ionic liquid supplied from the absorbent container connected to a nitrogen cylinder to maintain the desired pressure. Feed gas mixture was introduced into the membrane bore side where the gases contacted the absorbent through the micropores and got absorbed. The absorbent pressure in the shell side was always kept about 138 kPag (20 psig) higher than the highest feed gas pressure in tube side to avoid any possible gas bubbling into the liquid absorbent. The CO_2 product side was connected to a vacuum pump to supply driving force for product withdrawal; three pneumatic valves were used to control exactly the time period for different steps in one absorption cycle (Three-valve system). This valve control system was realized via a Programmable Logic Controller (PLC) scheme installed by PneuMagnetic, Quakertown, PA.

Both He-rich and CO_2-rich product streams were analyzed by an IR-based CO_2 analyzer (Model 906, Quantek Inc., Grafton, MA), which allowed estimation of real time CO_2 concentration fluctuations in the two product gas streams.

A pressure transducer unit was installed inside the oven and directly connected to the tube side of the membrane module to record detailed pressure changes with time during the absorption process. Changes in pressure versus time were read and recorded by a pressure transducer unit. The pressure transducer unit included one pressure transducer (Model PX32B1-300GV), one assembly cable (Model CA-6TE24-010-PX32), and one universal input Ethernet (Model DP41-B-EI) purchased from Omegadyne Inc., Sunbury, OH.

3.2.4 Experimental Procedure

In a typical pressure swing membrane absorption process usually a 3-valve control system is applied as shown in Figure 3.4; there will be four steps in each cycle [26,27]:

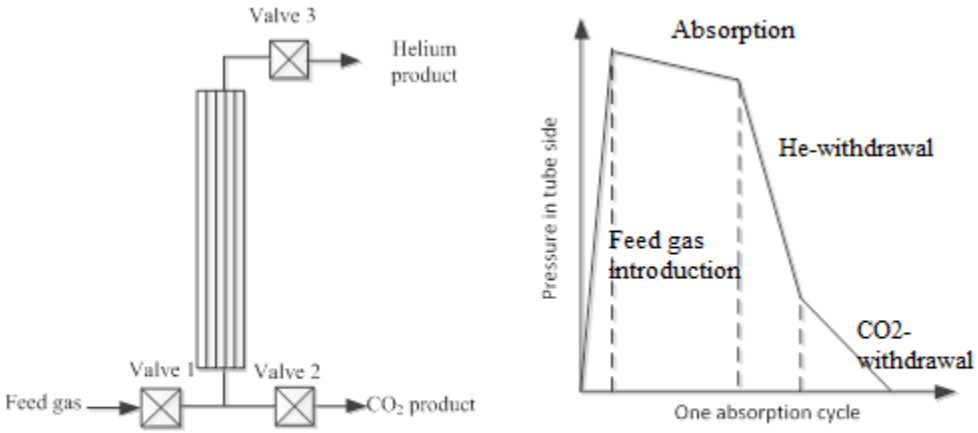

Figure 3.4 Schematic Diagram of a Three-valve Pressure Swing Membrane Absorption Process.

Feed gas introduction: Feed gas was introduced through valve 1 into the tube side of the membrane module for five seconds to develop a desired feed gas pressure (a sharp pressure increase in the tube side).

Absorption (all valves closed): Feed gas in tube side gets absorbed by the absorbent liquid in the shell side at the interface of micro-pores for 30 seconds (pressure in the tube side decreases gradually in this step due to gas absorption).

He-Product withdrawal: Valve 3 opened for two seconds to withdraw the He-rich product present in the tube side of the membrane module (a sharp pressure decrease takes place in the tube side because of He-rich product withdrawal) from the end opposite to the feed gas introduction end.

CO_2-Product withdrawal: Valve 3 is closed. Valve 2 is opened for 30 seconds for CO_2 to desorb (pressure decreases further) and to be removed.

3.2.5 Mathematical Model for a Three-valve PSMAB Process

A mathematical model has been developed that describes the three-valve PSMAB process in terms of the pressure drop in the absorption step and in terms of the concentrations of the two product gas streams. In the model, hollow fibers are assumed to be arranged in a regular pitch and the analysis based on a single fiber can be extended to the whole module. The numerical model utilized the Happel free surface model (Happel [54]), shown in Figure 3.5 (Karoor and Sirkar [55]).

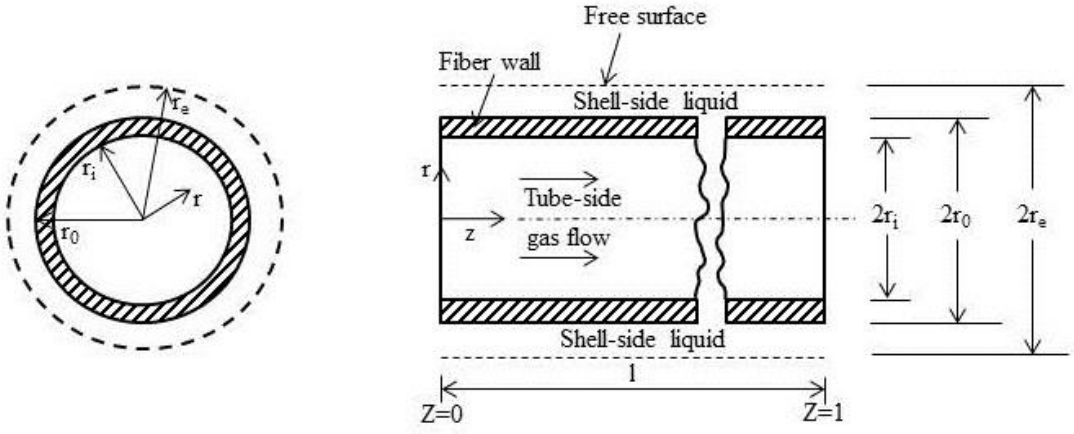

Figure 3.5 Schematic Representation of Happel's Free Surface Model for Gas Absorption by a Hollow Fiber.
Source: [55].

Figure 3.5 shows two concentric cylinders: the inner cylinder consists of one hollow fiber and the outer cylinder consists of the absorbent liquid with a free surface

across which there is no mass transfer. The following assumptions are introduced to develop a mathematical model for the PSMAB system using a non-reactive absorbent (Bhaumik et al. [56]).

1. Ideal gas law is valid.
2. The absorption process is isothermal.
3. Diffusion coefficient and solubility coefficient are constant and independent of concentration.
4. No reaction takes place between the liquid and any gas component.
5. The components of the gas phase are in equilibrium with the absorbed components at the gas-liquid interface and Henry's law is valid.
6. The flow pattern within the fiber bore can be described by the model of plug flow with axial diffusion.
7. The mass transfer mechanism from the bulk gas phase to the outside surface of the fiber where the gas-liquid interface is located may be described by a first order model based upon a constant mass transfer coefficient and a concentration difference between the two locations.
8. The pressure drop in the fiber lumen is governed by Hagen-Poiseuille equation for the compressible fluid without any effect of radial absorption.
9. The deformation of the fibers due to the higher external pressure of the liquid is negligible so that the fiber size and the void fraction remain unchanged.
10. End effects are negligible.
11. Volume of gas in the pores is negligible compared to that in the fiber lumen.
12. Feed gas species concentrations do not change during the very rapid first step of the cyclic PSMAB process.

The void fraction of the fiber bundle containing N hollow fibers, ε, is defined as follows:

$$\varepsilon = 1 - \frac{\textit{shell side cross sectional area occupied by the hollow fibers } (N\pi r_0^{\,2})}{\textit{total cross sectional area of the shell side } (\pi r_S^{\,2})} \qquad (3.2)$$

Then the equivalent radius, r_e, can be calculated:

$$r_e = \left(\frac{1}{1-\varepsilon}\right)^{1/2} r_0 \tag{3.3}$$

When the gas pressure drop in the fiber lumen is not negligible, the governing balance equations and boundary conditions for any species j (He, CO_2) in a single hollow fiber can be written as [56]:

Gas Phase:

$$\frac{\partial C_{jg}}{\partial t} = D_{jg}\frac{\partial^2 C_{jg}}{\partial z^2} - \frac{\partial}{\partial z}\left(v_g C_{jg}\right) - \frac{4K_{jg}d_0}{d_i^{\,2}}\left(C_{jg} - C_{jg}^{\,i}\right) \tag{3.4}$$

where

$$v_g = -\frac{RTd_i^{\,2}}{32\mu_{mix}}\sum_{j=1}^{n}\frac{\partial C_{jg}}{\partial z} \tag{3.5}$$

$$C_{jg}^{\,i} = \frac{C_{jl}\big|_{r=r_0}}{H_j RT} \tag{3.6}$$

Initial condition:

$$\text{at } t = 0, C_{jg} = 0 \ (0 \le z \le L) \tag{3.7}$$

Boundary conditions:

$$v_g C_{jg}\big|_u = v_g C_{jg}\big|_{z=0} - D_{jg}\left.\frac{\partial C_{jg}}{\partial z}\right|_{z=0} \tag{3.8}$$

$$D_{jg}\left.\frac{\partial C_{jg}}{\partial z}\right|_{z=L} = 0 \tag{3.9}$$

The corresponding governing balance equation and boundary conditions for the liquid phase for species j are:

$$\frac{\partial C_{jl}}{\partial t} = D_{jl}\left(\frac{\partial^2 C_{jl}}{\partial r^2} - \frac{1}{r}\frac{\partial C_{jl}}{\partial r}\right) \tag{3.10}$$

Initial condition:

$$\text{at } t = 0, C_{jl} = 0 \; (0 \le z \le L \; and \; r_0 < r < r_e) \tag{3.11}$$

Boundary conditions:

$$-D_{jl} \left. \frac{\partial C_{jl}}{\partial r} \right|_{r=r_0} = K_{jg} \left(C_{jg} - \frac{C_{jl}\big|_{r=r_0}}{H_j RT} \right) \tag{3.12}$$

$$\left. \frac{\partial C_{jl}}{\partial r} \right|_{r=r_e} = 0 \tag{3.13}$$

These equations in dimensionless forms were numerically solved using the method of lines technique and programs developed using MATLAB. The method of lines technique was used to discretize the spatial component of the partial differential equations (PEDs), hence, reducing the system of PDEs to a coupled system of ordinary differential equations (ODEs) (Brian III et al. [57]). For the three different steps, the initial and boundary conditions are identified below:

For Absorption:

Initial condition:

$$\text{at } t = 0, C_{jg} = C_{jg\ feed} \tag{3.14}$$

Boundary conditions:

$$\left. \frac{\partial C_{jg}}{\partial z} \right|_{z=0} = 0 \tag{3.15}$$

$$\left. \frac{\partial C_{jg}}{\partial z} \right|_{z=L} = 0 \tag{3.16}$$

For He-withdrawal:

Initial condition:

$$\text{at } t = 0, C_{jg} = C_{jg\ in\ tubeside after absorbtior} \tag{3.17}$$

Boundary conditions:

$$\left.\frac{\partial C_{jg}}{\partial z}\right|_{z=0} = 0 \tag{3.18}$$

$$v_g C_{jg}\Big| = v_g C_{jg}\Big|_{z=L} - D_{jg}\left.\frac{\partial C_{jg}}{\partial z}\right|_{z=L} \tag{3.19}$$

For CO_2-withdrawal:

Initial condition:

$$\text{at } t = 0, C_{jg} = C_{jl\ in\ \text{shell}\ side after absorbtion} \tag{3.20}$$

Boundary conditions:

$$v_g C_{jg}\Big|_u = v_g C_{jg}\Big|_{z=0} - D_{jg}\left.\frac{\partial C_{jg}}{\partial z}\right|_{z=0} \tag{3.21}$$

$$\left.\frac{\partial C_{jg}}{\partial z}\right|_{z=L} = 0 \tag{3.22}$$

One needs information on CO_2 solubility and diffusivity in the ionic liquid to numerically predict the performance of the PSMAB process. Measurements of the solubilities of pure carbon dioxide, pure helium, and a feed mixture of 40% CO_2-He balance carried out in the [bmim][DCA] (and in its solution containing 20 wt% and 30 wt% poly(amidoamine) (PAMAM) dendrimer Gen 0 with and without water) are described in Chapter 2. From the pressure changes versus time collected in these solubility studies, the diffusion coefficients of CO_2 and He in pure [bmim][DCA] can also be found via Equation (3.23) shown below [38]:

$$\ln\left(\frac{P}{P_0}\right)=\left(\frac{k}{H_{CO2}}\right)\sum_{n=0}^{\infty}\frac{1}{(2n+1)^2}\left\{\exp\left[-\frac{(2n+1)^2\pi^2 D_{CO2}t}{4L^2}\right]-1\right\} \tag{3.23}$$

where

$$k=\frac{8RTV_{IL}\rho_{IL}}{\pi^2 V(MW)_{IL}} \tag{3.24}$$

P_0: initial feed gas pressure

V: volume of gas

ρ_{IL}: density of ionic liquid

V_{IL}: volume of ionic liquid

L: height of ionic liquid

$(MW)_{IL}$: molecular weight of ionic liquid

These equations have two unknowns: H_{CO2} and D_{CO2}. Fitting Equation (3.23) above to the experimental P vs. time data in MATLAB, the unknowns are determined. The unit for k and H_{CO2} in Equation (3.23) is atm. The unit for H_{CO2} and H_{He} used in the numerical model is mol/atm*m^3. From the solubility measurement data, Henry's law constants of CO_2 and He in the unit of mol/atm*m^3 can be calculated using Equations (3.25) and (3.26) below:

$$H_{CO2}=\frac{moles\ of\ CO_2\ absorbed\ in\ the\ IL}{V_{IL}(P_f)} \tag{3.25}$$

$$H_{He}=\frac{moles\ of\ He\ absorbed\ in\ the\ IL}{V_{IL}(P_f)} \tag{3.26}$$

where P_f: equilibrium pressure obtained in the solubility measurement, and V_{IL}: volume of ionic liquid.

3.3 Results and Discussions

3.3.1 Optimal Absorption Duration for PSMAB Cycle

Absorption is an important step in this process; it directly determines how long the feed gas will be in contact with the ionic liquid in the shell side and will undergo gas absorption. To find out the optimal absorption time, at first the absorption time in one cycle was set as long as 900 seconds to examine the pressure drop caused by gas absorption into pure [bmim][DCA] in the shell side of the membrane module during this step. The experimental pressure drop during the absorption will be compared with that generated by the numerical model. Jie et al. [26] have determined the optimal absorption duration for different membrane modules. Due to the very high surface area per unit volume of the PEEK-L system, much more rapid absorption takes place into the surrounding liquid compared to that in the ceramic tubule system. In the PSMAB process, rapid initial absorption is important.

3.3.2 Diffusion Coefficients and Henry's Law Constants of CO_2 and He in Pure [bmim][DCA]

As mentioned earlier, Equation (3.23) has two unknowns: H_{CO2} and D_{CO2}. Fitting this equation to the experimental pressure vs. time data in MATLAB, the unknowns are determined. Similarly, H_{He} and D_{He} can also be determined. Henry's law constant for pure carbon dioxide and pure helium were also experimentally determined from the solubility measurement illustrated in Chapter 2 (Two solubility measurement runs for He and CO_2 were carried at room temperature, so they could be used to determine the diffusion coefficients and Henry's law constants). These can be used to compare and check the Henry's law constants generated by the MATLAB program to ensure that they

are comparable. Table 3.3 summarizes the diffusion coefficients and Henry's Law constants (Calculated using Equations (3.25) and (3.26)) in [bmim][DCA] for CO_2 and He at room temperature, 50 ^oC, and 100 ^oC. The carbon dioxide diffusion coefficients in [bmim][DCA] at room temperature and at 50 ^oC are in range with the diffusion coefficients for CO_2 in [emim][Tf_2N] reported by Camper et al. [58]. The Henry's law constants reported in Table 3.3 were calculated based on the solubility measurement data obtained in Chapter 2.

Table 3.3 Diffusion Coefficients and Henry's Law Constants of CO_2 and He in [bmim][DCA] at Different Temperatures

	Diffusion Coefficients (m^2/s)		Henry's Law Constant ($gmol/m^3*atm$)	
Temperature (^oC)	D_{CO2}	D_{He}	H_{CO2}	H_{He}
23	$3.54x10^{-10}$	$7.64x10^{-10}$	93.32	2.81
50	$6.55x10^{-10}$	$9.64x10^{-10}$	74.75	6.89
100	$9.52x10^{-10}$	$1.14x10^{-9}$	41.47	14.37

3.3.3 Pressure Drop during the Absorption Step

3.3.3.1 Ceramic Membrane Modules

Three ceramic membrane modules were connected in series and were employed with pure ionic liquid [bmim][DCA] as the liquid absorbent. The absolute pressure changes in the tube side tests during the 900-second absorption step were measured at 23 ^oC, 50 ^oC, and 100 ^oC for a fixed initial feed gas pressure of 1034 kPag (150 psig). The decreasing pressures measured from the experimental runs and predicted by the mathematical model are shown in Figures 3.6, 3.7, and 3.8, respectively. The total pressure in simulation is the sum of the partial pressures of all species in the gas mixture (e.g. He and CO_2).

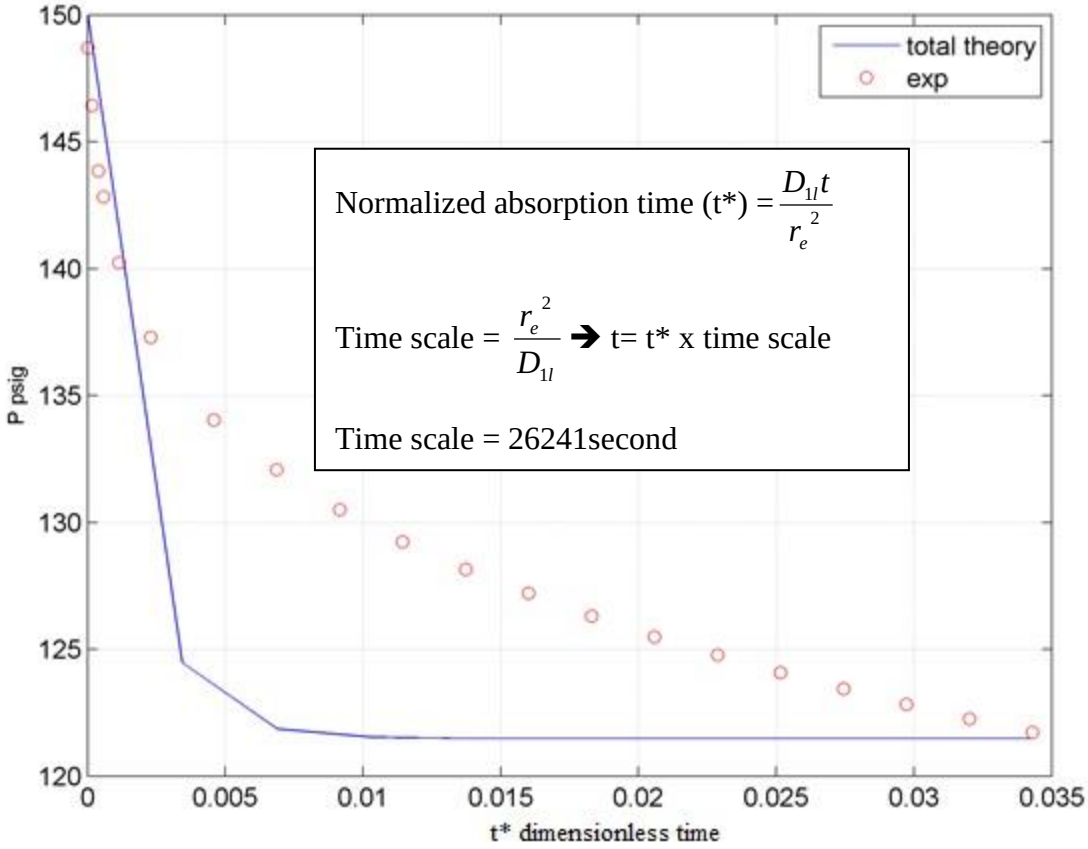

Figure 3.6 Pressure of Gas Phase as a Function of Time during the Absorption Step in Three Ceramic Modules in Series at 23 ^{o}C, 1034 kPag (150 psig), and r_e= 0.00368 m*.
*For ceramic module, ε=0.4 and r_0 = 0.285 cm

$$r_e = \left(\frac{1}{1-\varepsilon}\right)^{1/2} r_0 = \left(\frac{1}{1-0.4}\right)^{1/2} 0.285 = 0.368\ cm$$

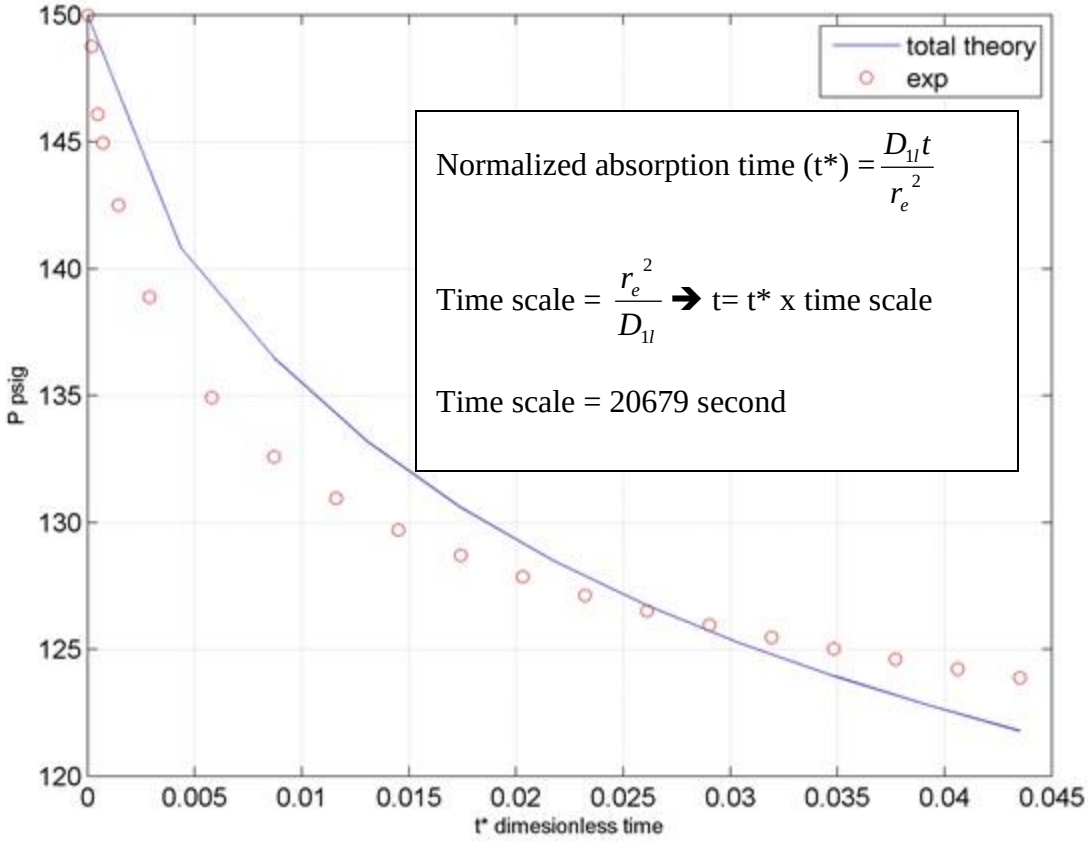

Figure 3.7 Pressure of Gas Phase as a Function of Time during the Absorption Step in Three Ceramic Modules in Series at 50 ^{o}C, 1034 kPag (150 psig), and r_e= 0.00368 m.

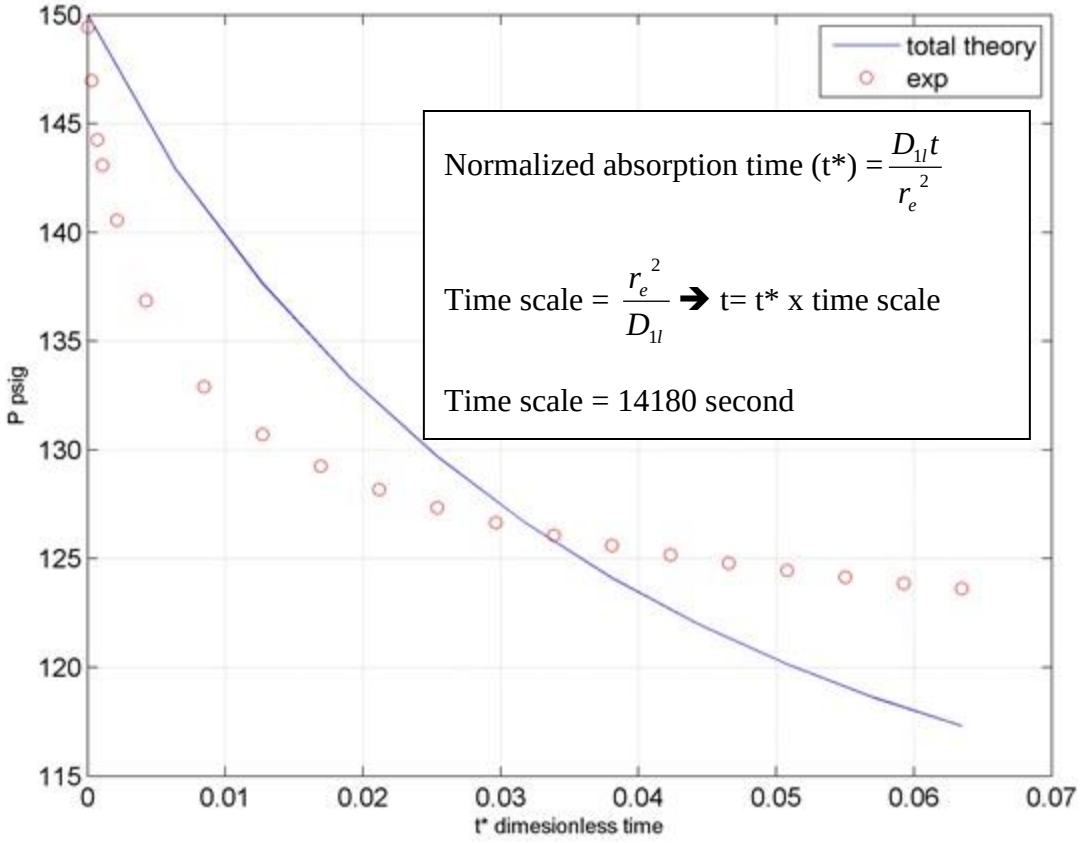

Figure 3.8 Pressure of Gas Phase as a Function of Time during the Absorption Step in Three Ceramic Modules in Series at 100 ^{o}C, 1034 kPag (150 psig), and r_e= 0.00368 m.

The decreasing pressure in the absorption step was plotted against the normalized (dimensionless) absorption time ($\frac{D_{1l}t}{r_e^2}$). The decreasing pressures generated by the numerical model are reasonably close to those measured in the experimental runs at all temperatures. One will later find out that there are two reasons for it vis-à-vis the behavior in PEEK hollow fiber modules. First, there is no ambiguity about the value of r_e, the free surface radius. The second reason for this agreement is that the ceramic

membrane modules had much less dead volume compared to those in the PEEK membrane module vis-à-vis the feed gas volume (as will be discussed later).

3.3.3.2 PEEK-L II Membrane Module

One large PEEK membrane module (PEEK-L II) was used with pure [bmim][DCA] as the liquid absorbent for the absorption test. The experiments were carried out at 689 kPag (100 psig) and 1379 kPag (200 psig) feed gas pressures and at room temperature. The decreasing pressure was plotted against the dimensionless time and the results are shown in Figures 3.9 and 3.10

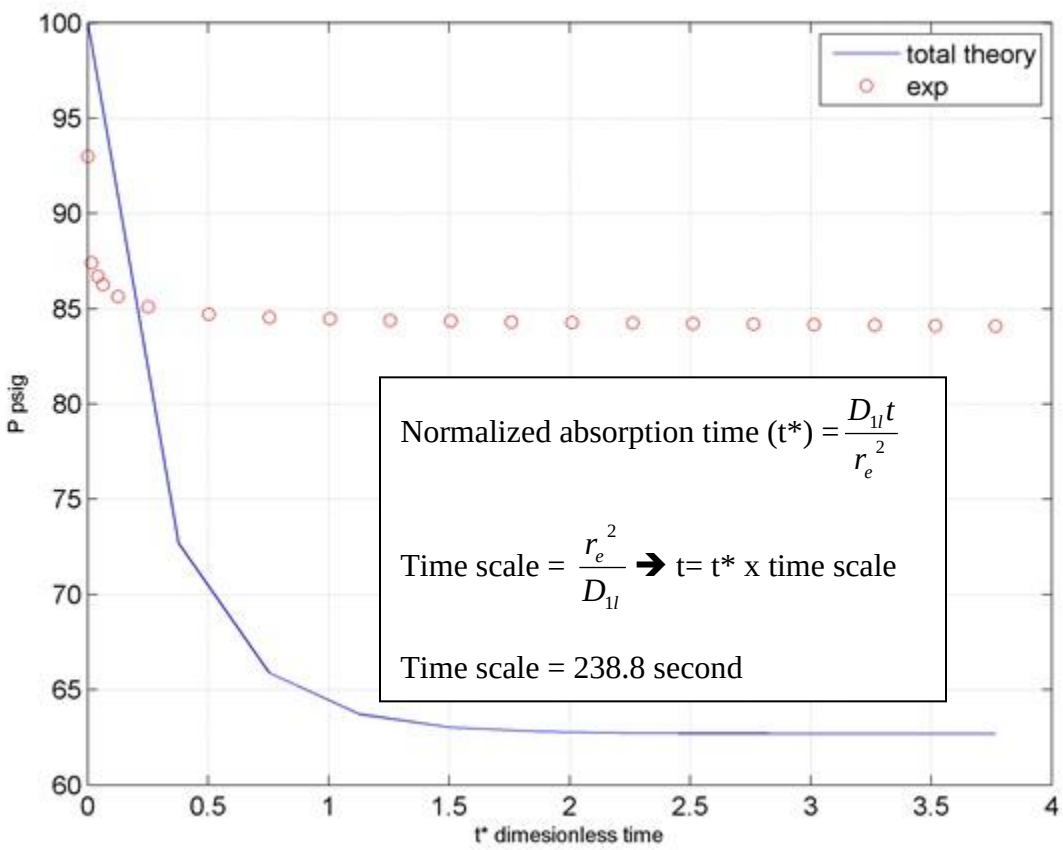

Figure 3.9 Pressure of Gas Phase as a Function of Time during the Absorption Step in a PEEK-L II Module at 23 ^{o}C, 689 kPag (100 psig), and r_e= 0.000291 m.

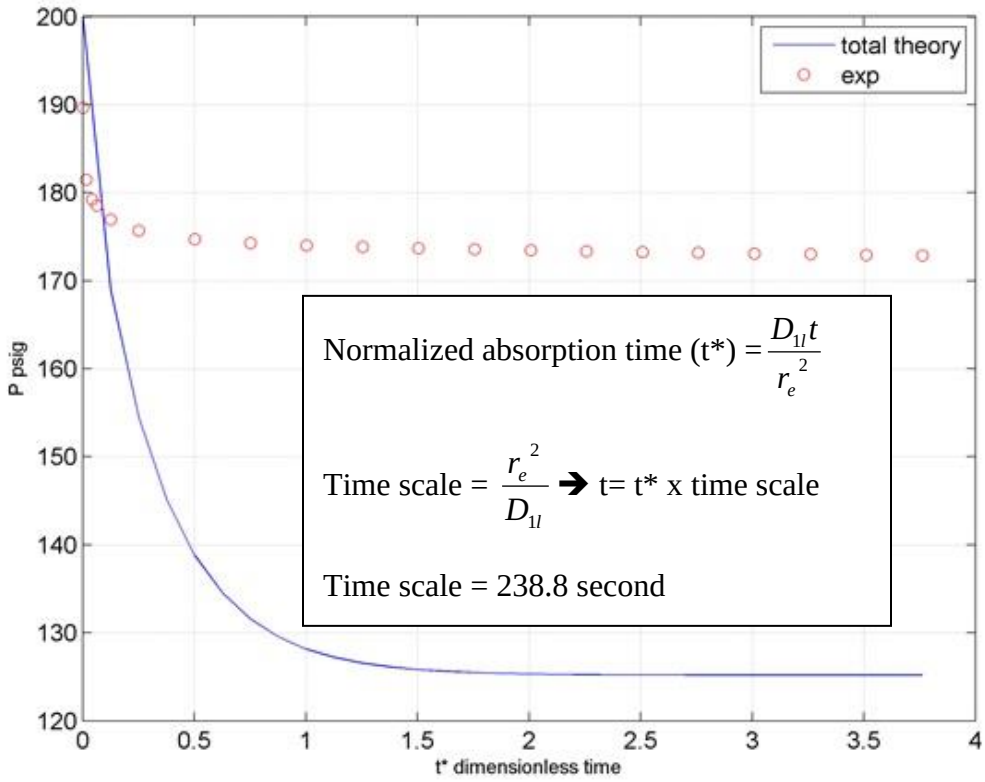

Figure 3.10 Pressure of Gas Phase as a Function of Time during the Absorption Step in a PEEK-L II Module at 23 ^{o}C, 1379 kPag (200 psig), and r_e= 0.000291 m*.
*For PEEK-L II module, ε=0.4 and r_0=0.0226 cm

$$r_e = \left(\frac{1}{1-\varepsilon}\right)^{1/2} r_0 = \left(\frac{1}{1-0.4}\right)^{1/2} 0.0226 = 0.0291\ cm$$

Unlike that in the ceramic tubule, the drops in pressure generated by the mathematical model were larger than those of the experimental runs. There are two reasons. First, the fibers in the module were wound helically in a strand with the individual fibers placed touching one another (Figure 3.11a); therefore, the calculation of r_e via Happel's approach (Equation (3.3)) will introduce some error since the fibers were artificially packed closer together. The actual r_e values should be smaller than those

calculated by Happel's approach. Ideally, a fiber should have a defined region around it without any other fibers (Figure 3.11b). When inputting a smaller value of Happel's approach-based radius into the numerical model, the theoretical curves got closer to those of the experimental results as shown in Figures 3.12 and 3.13.

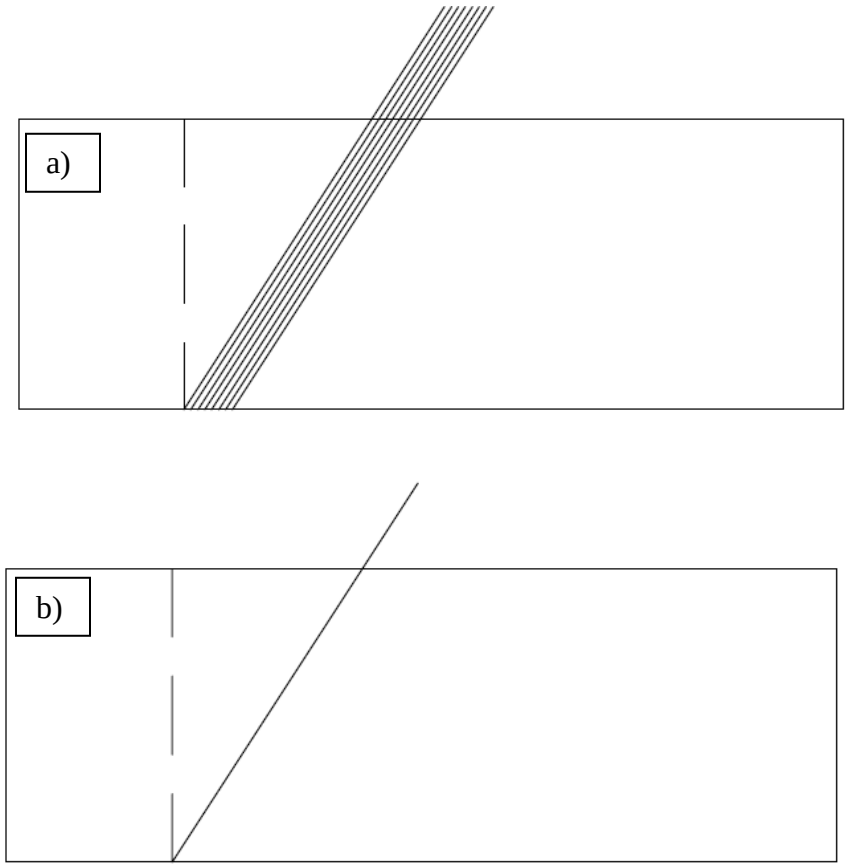

Figure 3.11 PEEK-L Module Winding.

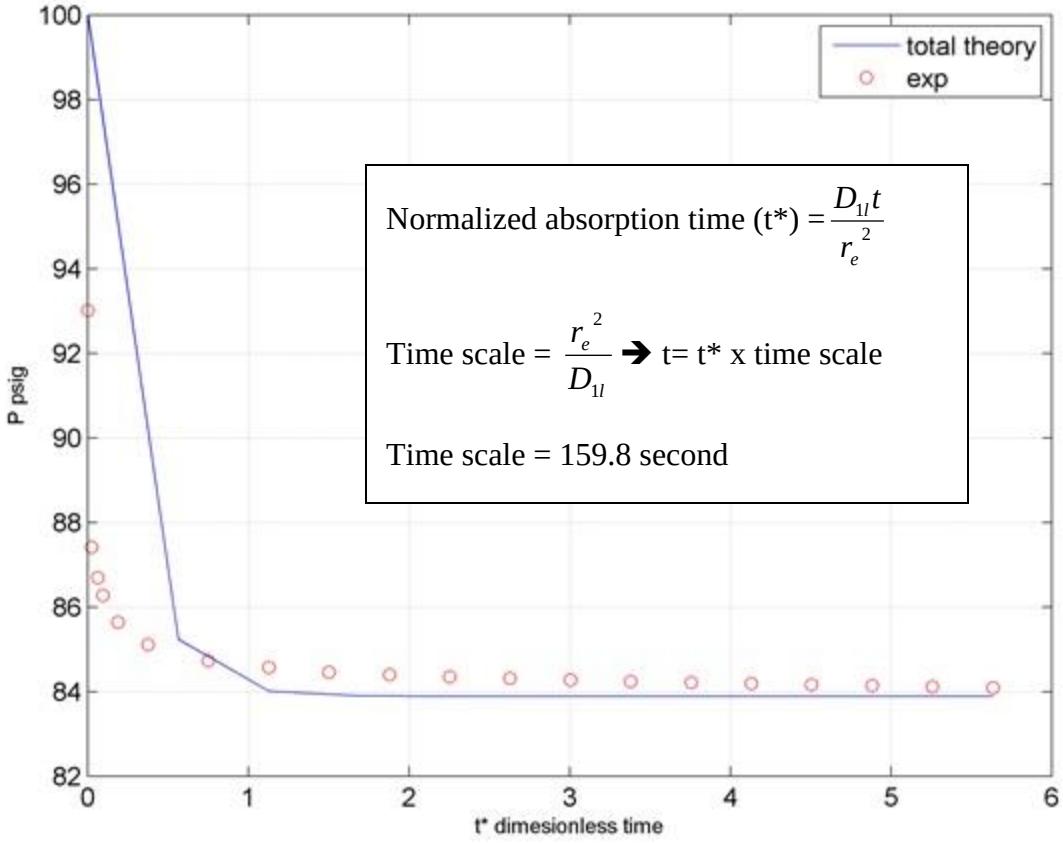

Figure 3.12 Pressure of Gas Phase as a Function of Time during the Absorption Step in a PEEK-L II Module at 23 ^{o}C, 689 kPag (100 psig), and r_e= 0.000238 m.

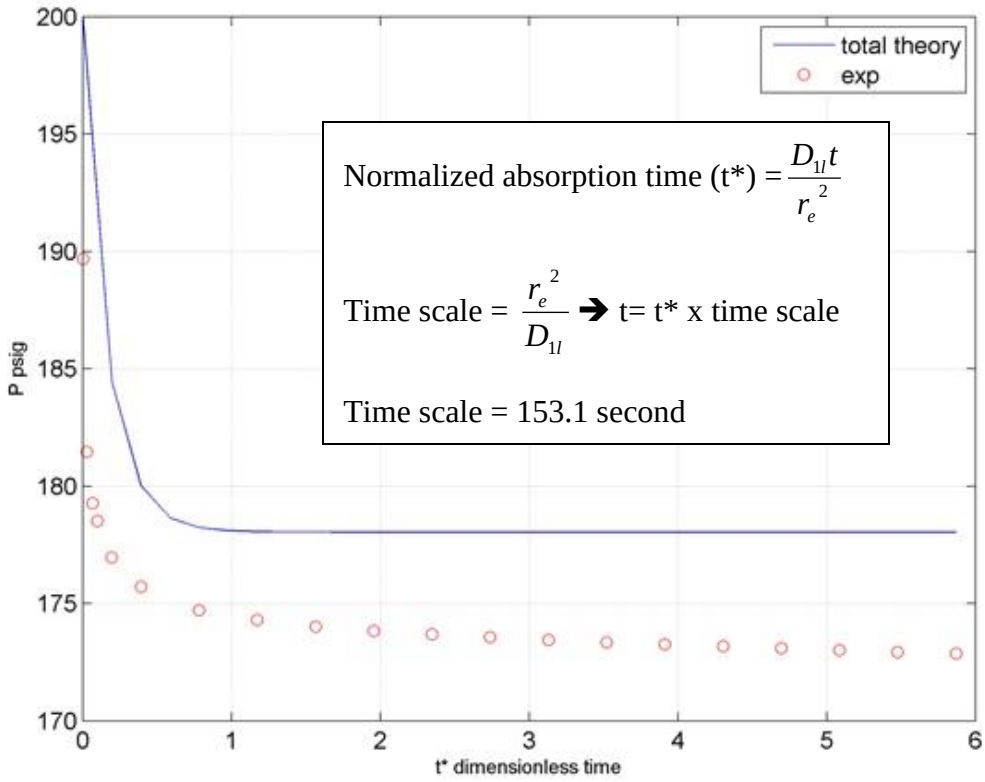

Figure 3.13 Pressure of Gas Phase as a Function of Time during the Absorption Step in a PEEK-L II Module at 23 ^{o}C, 1379 kPag (200 psig), and r_e= 0.000233 m.

Second, there was a significant amount of dead volume in the two ends of the hollow fiber module which will increase the module end pressure monitored by the pressure indicator; the gas in these large dead volumes in the PEEK membrane module will not undergo absorption. Therefore, the measured pressure drops will be lower. Dead volume is the space in one membrane module where the occupying feed gas does not come in contact with the pressurized absorbent liquid on the shell side; hence, no absorption takes place. For a membrane module, the dead volume consists of the tube-side header sections of the membrane module and related connections, and the potted

section of the module at the feed end. The total dead volume of PEEK-L II module is approximately 35.7 cm^3, which is about ~30% of the total tube side volume.

Round PTFE balls were later used to fill both ends of the tube-side headers of the PEEK-L II module to reduce the dead volume. The same absorption experiment was carried out at 689 kPag (100 psig) and room temperature. Figure 3.14 shows an improved prediction of the model with respect to the experimental run (See Figure 3.9 for the comparison between the theory and experiment when no PTFE balls were added). This shows that the dead volume strongly affects gas absorption, which also ultimately affects the quality of the products when desorption takes place.

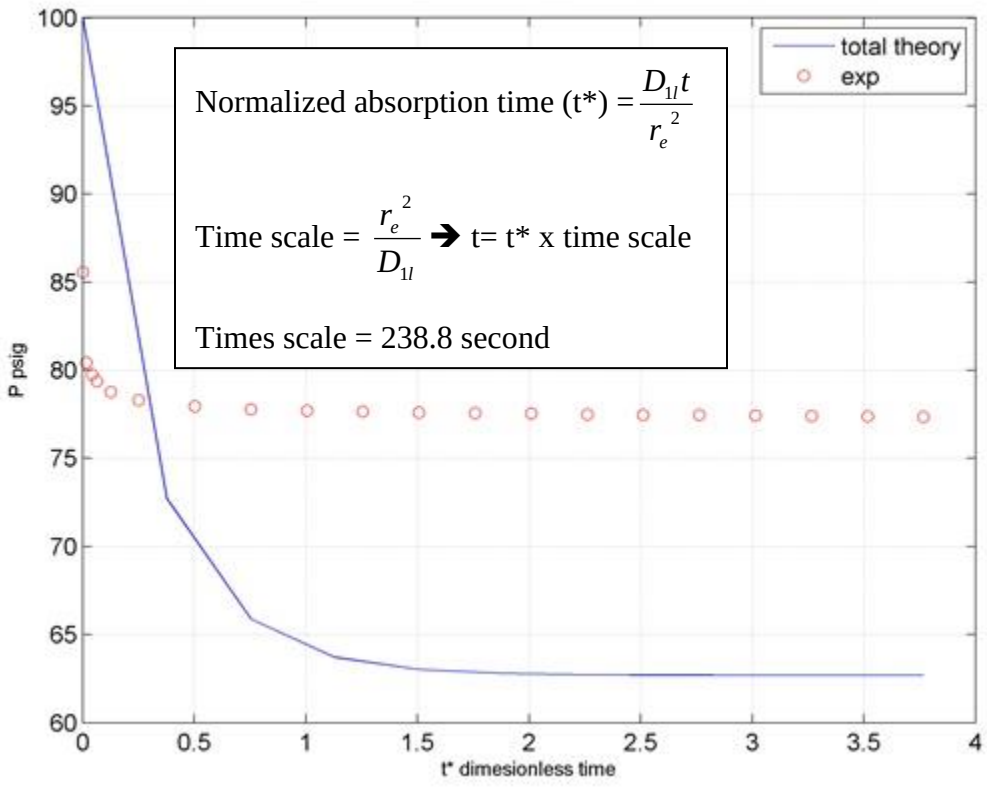

Figure 3.14 Pressure of Gas Phase as a Function of Time during the Absorption Step in a PEEK-L II Module with PTFE Balls added in the Module Tube-side Headers at 23 ^oC, 689 kPag (100 psig), and r_e= 0.000291 m.

3.3.4 Quality of Product Streams in Terms of % CO_2 Concentration in both He-rich and CO_2-rich Streams

3.3.4.1 Three Ceramic Modules in Series

The ceramic membrane module has one ceramic membrane tubule with a much larger inner diameter. In order to find out if this will have any impact, tests were carried out with three ceramic membrane modules in series at a few temperatures; the feed pressure was 689 kPag (100 psig). Figure 3.15 shows the percent carbon dioxide concentrations (%) in both product streams as the He-rich stream withdrawal and then CO_2-desorption steps were carried out.

These results show that even with three ceramic membrane modules the product qualities for both streams were poor because of its much larger tubule diameter, which results in a lot of feed gas that is required to be absorbed. However, due to limited contacting area along the tube side, only a small amount of feed gas could be absorbed. Therefore, it is more likely that the gas concentration distribution along the tube length was not fully developed for a ceramic system; the product qualities will be poor.

Figure 3.15 also shows the adverse effect of temperature on the product concentrations. As the temperature increases, less carbon dioxide and more helium would be absorbed by the ionic liquid. As a result, the % carbon dioxide in the He-rich product stream increased from 33% to 36% when temperature was increased from 23 ^{o}C to 100 ^{o}C (Figure 3.15(a)). The % carbon dioxide in the CO_2-rich product stream decreased from 52% to ~48% over the same range of temperature (Figure 3.15(b)).

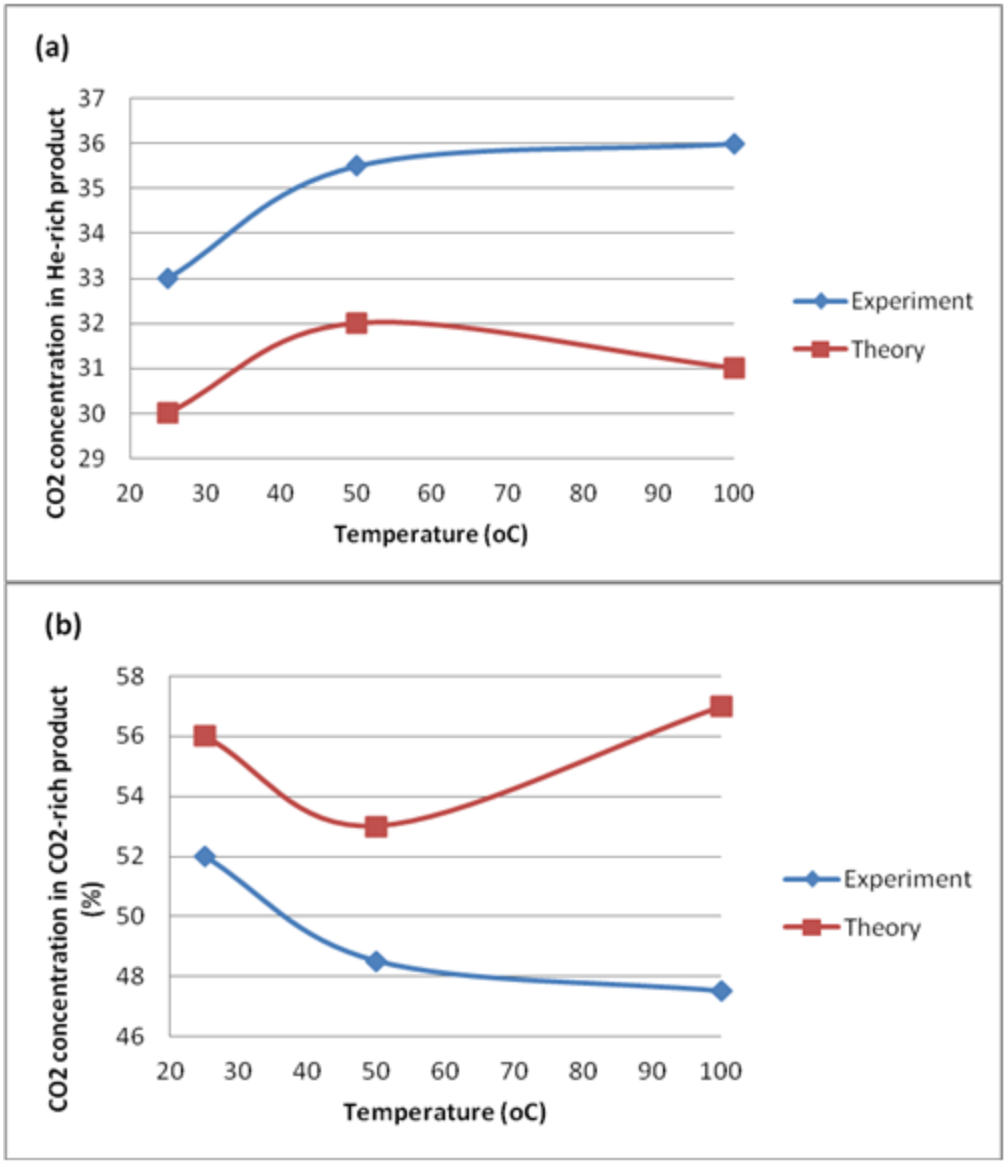

Figure 3.15 Compositions of Products at Three Different Temperatures for Three Ceramic Modules in Series at 1034 kPag (150 psig) and r_e= 0.00368 m.

3.3.4.2 One PEEK-L II Module Filled with PTFE Balls in the Module Headers

After the performance of the absorption step was studied, a set of PSMAB process tests with the PEEK-L II module having PTFE balls reducing the dead volume in the module tube-side headers was carried out at different feed pressures and temperatures. The concentrations of the two product streams are shown in Figure 3.16.

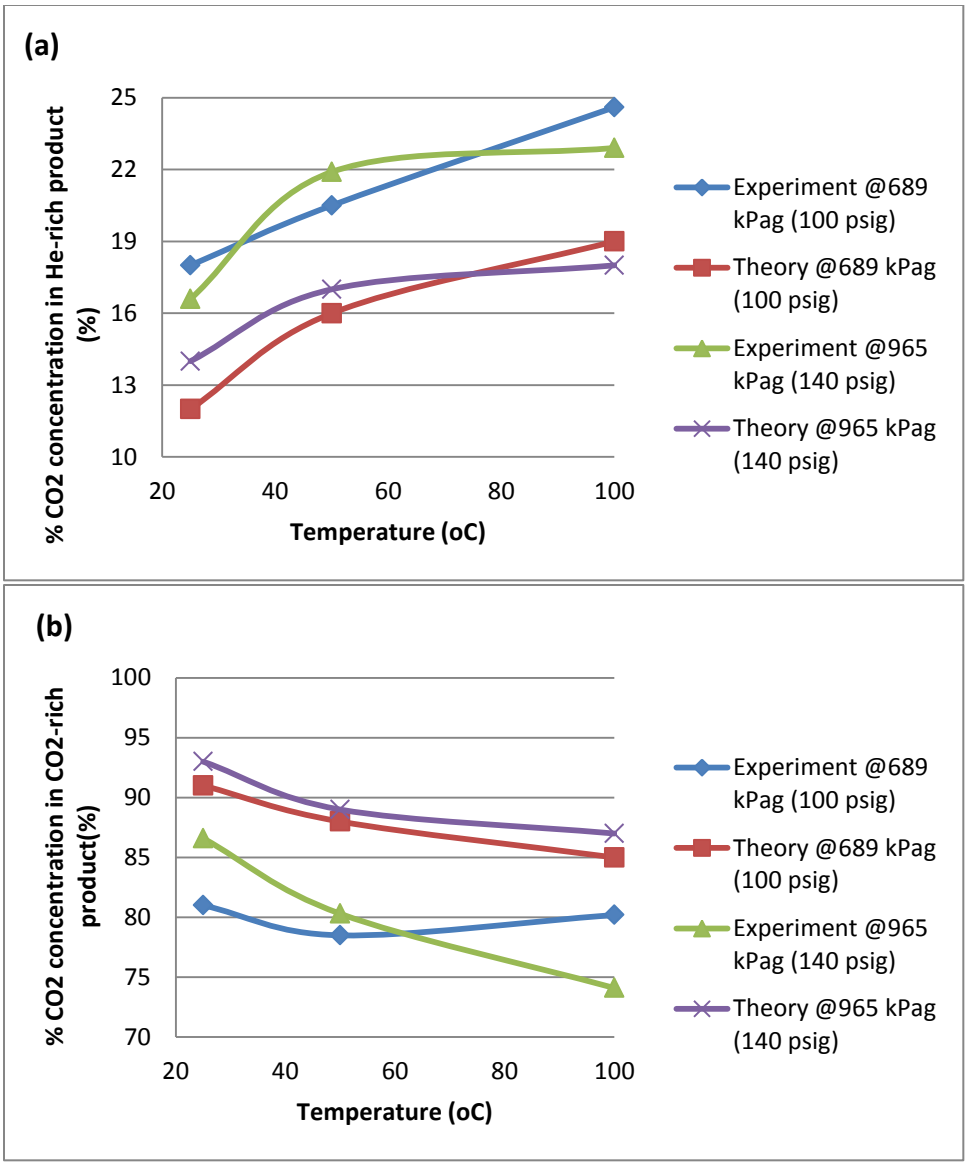

Figure 3.16 Compositions of Products for PEEK-L II Module Filled with PTFE Balls in the Module Headers at Different Feed Pressures and Temperatures (r_e= 0.000243 m).

This figure shows that an increase in feed gas pressure leads to an increase in % CO_2 concentration in the CO_2-rich product stream for the same temperature. Higher feed gas pressure means more gas would be introduced into the membrane tube side and contacted with ionic liquid (IL) to be absorbed. The % CO_2 concentration in the CO_2-rich product increased from ~81% at 689 kPag (100 psig) and 23 ^oC to 87% at 965 kPag (140

psig) and 23 ^{o}C. In the CO_2-rich product, the theoretical simulations predict significantly higher CO_2 concentrations. For example, there is a 6-10% difference in CO_2 concentration between the predictions and the measured values. The limited gas volume in the tube side of the hollow fibers undergo considerable dilution in the residual feed gas volume left in the tube-side header even after putting the PTFE balls there.

However, the PEEK-L II module provided much better results compared to the ceramic module due to it having a much larger effective gas-liquid contacting area and the correspondingly longer feed gas length. Table 3.4 shows that the effective surface area per unit volume for the ceramic module is only 4.30 cm^{-1}; it is much lower than 54.71 cm^{-1} for a PEEK-L II hollow fiber. This could directly explain why PEEK-L II module showed much higher absorption rates than the ceramic membrane module. As a result, PEEK-L II modules have much better PSMAB performance than the ceramic modules. The % CO_2 in the CO_2-rich product in PEEK-L II module was 81% compared to 56% for ceramic module system at 689 kPag (100 psig) feed and 23 ^{o}C.

Table 3.4 Estimated Dimensional Calculations for PEEK Hollow Fiber Module and Ceramic Tubule Membrane-based Modules

Module	OD; cm	ID; cm	L; cm	VVF	(V; cm^3)[1]	(A; cm^2)[2]	(A/V; cm^{-1})[3]
Ceramic	0.57	0.37	44.0	~0.4	7.33	31.5	4.30
PEEK-L II	0.0452	0.0290	41.0	~0.4	0.0356	1.95	54.7
PEEK-L III	0.0470	0.0272	41.0	~0.4	0.0426	2.45	57.5

[1] Feed gas volume in one fiber; [2] Effective contacting area for one fiber based on outer diameter; [3] Ratio between A and V

Similar observations were found for the temperature effect on the quality of both product streams and that temperature had a negative effect on the quality of the products.

3.3.5 Molar Flow Rates of Products per Cycle

The molar flow rate of the He-rich product stream per cycle can be estimated based on the change in the pressure during He-withdrawal process using Equations (3.27) and (3.28). Knowing the pressure drop during the withdrawal step at a certain temperature, one can first calculate the number of moles using the equation of state:

$$\Delta n = \frac{(\Delta P)V}{RT} = \frac{(\Delta P)\left(\pi r^2 LN\right)}{RT} \tag{3.27}$$

where r is the inner radius of one hollow fiber, L is the effective fiber length, and N is the number of fibers in a module.

Therefore, the He-rich product molar flow rate per cycle (gmol/s) is:

$$\dot{n}_{He} = \frac{\Delta n}{t} \tag{3.28}$$

where t is the cycle time.

CO_2-rich product molar flow rate per cycle, $\dot{n}_{CO2}$, can be calculated using the CO_2 species balance on the system since the compositions of product streams are known.

$$0.4(\dot{n}_{He} + \dot{n}_{CO2}) = \dot{n}_{He} x_1 + \dot{n}_{CO2} x_2 \tag{3.29}$$

where x_1 and x_2 are the CO_2 compositions in the He-rich and CO_2-rich product streams, respectively.

Table 3.5 summarizes the numerically predicted product flow rates and compositions for both CO_2-rich and He-rich streams in ceramic module and PEEK-L II module under different experimental conditions.

Table 3.5 Estimated Molar Product Flow Rates per Cycle and Compositions for all Modules* at Different Pressures and Temperatures

	P (psig)	Temperature (^oC)	He-Rich Molar Flow Rate per Cycle (gmol/s)	He-Rich Composition (% CO_2)	CO_2-Rich Molar Flow Rate per Cycle (gmol/s)	CO_2-Rich Composition (% CO_2)
Three Ceramic Modules in Series	150	23	7.00E-05	30	4.37E-05	56
		50	6.24E-05	32	3.84E-05	53
		100	5.19E-05	31	2.75E-05	57
One PEEK-L II Module	100	23	4.13E-05	12	2.27E-05	91
		50	3.71E-05	16	1.85E-05	88
		100	3.09E-05	19	1.44E-05	85
	140	23	5.80E-05	14	2.84E-05	93
		50	5.21E-05	17	2.45E-05	89
		100	4.08E-05	18	1.91E-05	87

*See Table 3.1 for number of fibers and surface area
Cycle time: 5:30:2:30; all in second

3.4 Concluding Remarks

A numerical model of a three-valve based pressure swing membrane absorption (PSMAB) process has been developed to describe the separation of low-temperature pre-combustion syngas. Absorption experiments of extended duration were implemented to understand the behavior of the absorption step for ceramic and PEEK membrane systems. Feed pressure increase improved CO_2-rich product quality and an increase in temperature adversely affected the product qualities. Ceramic system produced poor product qualities due to large tube side gas volume and small gas-liquid contacting area. The

hydrophobized PEEK hollow fiber-based system, on the other hand, provided higher product concentrations because PEEK fibers have a much larger ratio of contacting area per unit feed gas volume. Diffusion coefficients and Henry's law constants for pure carbon dioxide and helium were also determined by fitting the pressure vs. time data obtained from solubility measurements described in Chapter 2 to a MATLAB program. The diffusion coefficients values for CO_2 at different temperatures are in the same range with those reported by Camper et al. [58]. The product flow rates for CO_2-rich and He-rich streams were also estimated. Finally, the numerical model satisfactorily predicted the absorption step for both ceramic and PEEK systems. It also provided somewhat satisfactory estimates of the two product concentrations for the systems investigated.

CHAPTER 4

FIVE-VALVE PRESSURE SWING MEMBRANE ABSORPTION PROCESS AND SIMULATIONS OF TWO PEEK MODULES IN SERIES

4.1 Introduction

A pressure swing membrane absorption (PSMAB) process was originally proposed by Bhaumik et al. [27], and later developed further by Jie et al. [26]. The PSMAB process was utilized to separate a feed gas mixture containing ~40% CO_2-He balance. The process uses a microporous hydrophobic hollow fiber gas-liquid contactor with the absorbent liquid being stationary on the shell side and the feed gas mixture flowing through the tube side. The feed gas mixture was introduced into the membrane module through the tube side. There, for a short period of time the feed gas comes in contact with the stagnant and pressurized liquid absorbent on the fiber outer diameter (shown in Figure 3.1) where carbon dioxide gets absorbed. During the rest of the cycle, different product streams are withdrawn from two different ends of the tube side.

Chapter 3 provided the results of the three-valve pressure swing membrane absorption process in the ceramic and PEEK modules. Three-valve PSMAB process could not provide purified product streams (% concentration is larger than 90%). Therefore, a five-valve system for the pressure swing membrane absorption process studied by Jie et al. [26] was adopted. Jie et al. [26] could only go up to a maximum of 85% CO_2 in the CO_2-rich product stream using PEEK-L II module with PTFE balls to reduce the dead volume. Here a different approach was adopted using PEEK-L III module which has a much higher tube-side gas volume to start with. Potentially that can reduce the effect of the dead volume.

The mathematical model developed in Chapter 3 was used to predict the performance of the two PEEK-L III modules in series. The % CO_2 recovery for all modules was also calculated.

4.2 Experimental Procedure

4.2.1 Materials

The ionic liquid [bmim][DCA] was purchased from EMD Chemicals, Philadelphia, PA. Simulated pre-combustion syngas containing 40.67% CO_2- He balance was obtained from Air Gas, Piscataway, NJ.

Hydrophobized polyether ether ketone (PEEK) membrane modules were obtained from Porogen, Woburn, MA.

PAMAM dendrimer (generation 0) was purchased from Dendritech, Midland, MI.

4.2.2 Five-valve Pressure Swing Membrane Absorption (PSMAB) Process

Jie et al. [26] have illustrated a PSMAB cycle containing 5 valves in a 6 step cycle. Limited data were acquired using such a cycle. The schematic for a 5-valve PSMAB process is shown in Figure 4.1.

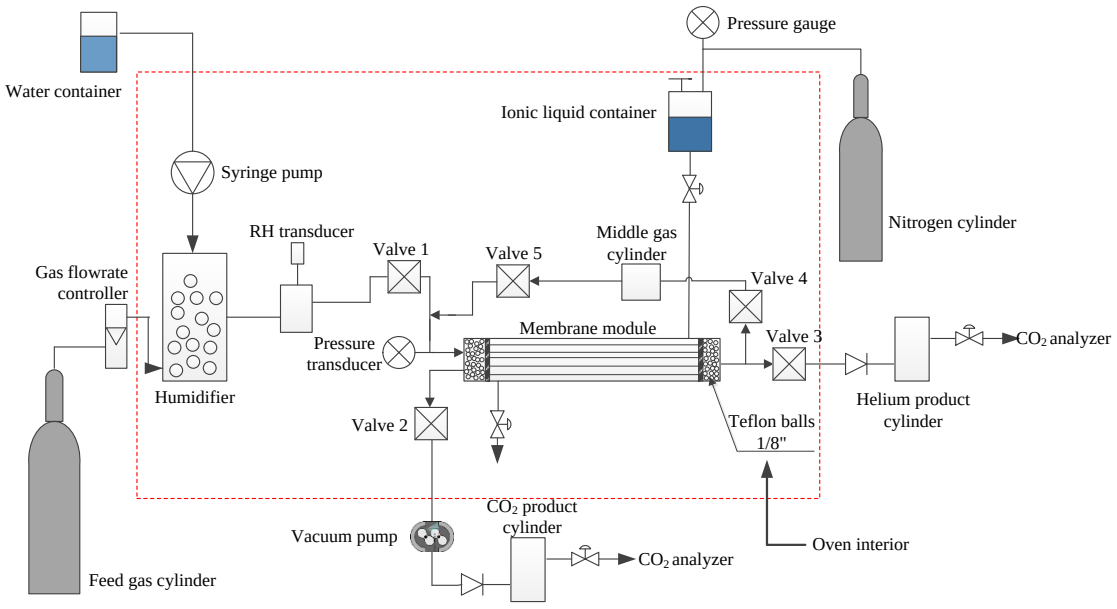

Figure 4.1 Schematic Diagram of a Five-valve Pressure Swing Membrane Absorption Apparatus.

The 6 step cycle in this process is as follows:

Feed gas introduction: Feed gas was introduced through valve 1 into the tube side of the membrane module for five seconds to develop a desired feed gas pressure (a sharp pressure increase in the tube side).

Absorption (all valves closed): Feed gas in tube side gets absorbed by the absorbent liquid in the shell side at the interface of micro-pores for 30 seconds (pressure in the tube side decreases gradually in this step due to gas absorption).

He-Product withdrawal: Valve 3 opened for two seconds to withdraw the He-rich product present in the tube side of the membrane module (a sharp pressure decrease takes place in the tube side because of He-rich product withdrawal) from the end opposite to the feed gas introduction end.

Middle-part gas withdrawal: Valve 4 opened for two seconds to withdraw the gas that occupies the middle part of the membrane module; hence, the name middle part gas.

CO_2-Product withdrawal: With all valves closed, valve 2 is opened for 30 seconds for CO_2 to desorb (pressure decreases further) and to be removed.

Middle-part gas recycle: With all valves remaining closed, valve 5 is opened for five seconds to allow the middle part gas to flow into membrane tube side as initial feed gas.

The main difference between three-valve and five-valve systems is the introduction of the middle-part gas withdrawal and middle part gas recycle in the 5-valve cycle PSMAB process. The presence of the middle-part gas withdrawal allows system to achieve better carbon dioxide concentration during CO_2-product withdrawal.

The pressure drop in the tube side of the module in each cycle is shown in Figure 4.2.

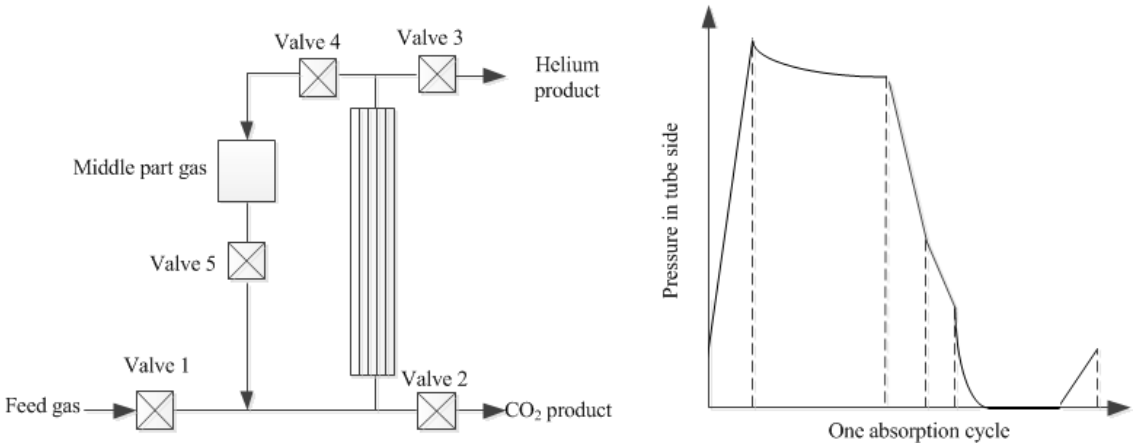

Figure 4.2 Pneumatic Valve Locations and Pressure Profile in Each Cycle of a Five-valve PSMAB Process.

4.3 Results and Discussions

4.3.1 PEEK-L III Module

The hollow fiber membrane module PEEK-L II employed did not have sufficient length or gas volume to counteract the product dilution caused by the significant volume of gas in the tube-side headers and other connections. To mitigate such dilution, a new PEEK-L III module having almost twice the membrane surface area of PEEK-L II was studied (see Table 3.1). Tables 4.1 and 4.2 summarized these results obtained using a 5-valve cycle [26].

Table 4.1 Product Qualities at Different Temperatures and Feed Pressures for PEEK-L III with [bmim][DCA] as the Liquid Absorbent for a Five-valve PSMAB System

Temperature (^{o}C)	Feed Pressure (kPag)	CO_2-Rich Product (%CO_2)	He-Rich Product (%CO_2)
23	689 (100 psig)	89.9	17.3
	1379 (200 psig)	92.5	19.2
	1724 (250 psig)	92.9	21.6
50	689 (100 psig)	87.0	19.9
	1379 (200 psig)	90.4	22.6
	1724 (250 psig)	91.0	23.6
75	689 (100 psig)	79.4	25.2
	1379 (200 psig)	87.3	27.7
	1724 (250 psig)	87.8	28.9
100	1379 (200 psig)	84.9	27.7
	1724 (250 psig)	85.5	28.8

Table 4.2 Product Qualities at Different Temperatures and Feed Pressures for PEEK-L III with 20 wt% Dendrimer in[bmim][DCA] as the Liquid Absorbent for a Five-valve PSMAB System

Pressure (psig)	Temperature (^oC)	CO_2-Rich Product (% CO_2)	He-Rich Product (% CO_2)
100	50	85.9	20.9
200		88.3	24.7
250		89.5	25.4
100	75	81.9	23.3
200		88.4	24.4
250		89.3	26.5
200	100	89.8	25.2
250		90.7	25.9

What one observes from Table 4.1 vis-à-vis the % CO_2 in the CO_2-rich product stream is that one is achieving as much as 90-92.9% CO_2 in the CO_2 product stream at pressures 689-1724 kPag (100-250 psig) and 23-50 ^oC for PEEK-L III and pure ionic liquid. This is about 7-10% higher than what was achieved with the PEEK-L II module. No attempt was made to reduce the tube-side header volume with PTFE balls. Appropriate hollow fiber lengths and tube side gas volume are therefore needed if we have to drastically reduce the dilution effect of tube-side header dead volumes.

When 20wt% dendrimer in [bmim][DCA] is used, it is seen in Table 4.2 that at 250 psig and 100 ^oC, the CO_2 level in the CO_2 product stream is as much as 90.7%.

The desired CO_2 level in this CO_2-rich product stream is 95%. It is believed that with a number of modifications in the module design and absorbent chemistry, this goal is achievable. Jie et al. [26] have already demonstrated how to achieve low CO_2 levels in the He-rich product stream.

4.3.2 Two PEEK-L III Modules in Series

Table 4.3 summarizes simulation results for two PEEK-L III modules in series for [bmim][DCA] as absorbent using the three-valve-based mathematical model developed in Chapter 3. Purified CO_2 (>90% CO_2) could be achieved for feed gas pressure of 100 psig and above at room temperature and 50 ^oC. At 200 psig, the CO_2-product stream concentration could go up to 93-97% CO_2 depending on the temperature. The He-rich stream quality was also significantly improved. CO_2 concentration in the CO_2-rich stream decreased as the temperature increased. Purified He (>90% He) could only be achieved for feed gas pressure at 100 psig and at room temperature. A 2-module/2-stage process is necessary to have both product streams achieve the desired quality.

Table 4.3 Simulation Results for Two PEEK-L III Modules in Series in [bmim][DCA]

P (psig)	T (^oC)	CO_2-Rich Product (% CO_2)	He-Rich Product (% CO_2)
100	23	95.1	7.3
	50	91.2	10.1
	100	88.1	14.6
200	23	97.3	12.1
	50	93.5	13.7
	100	90.6	18.4

4.3.3 Molar Flow Rates of Products per Cycle and % CO_2 Recovery

The molar flow rates per cycle of the product streams were calculated based on Equations (3.27) to (3.29). The % CO_2 recovery was calculated based on Equation (4.1).

$$\%CO_2 \text{ Recovery} = \frac{x_2 \dot{n}_{CO2}}{x_2 \dot{n}_{CO2} + x_1 \dot{n}_{He}} x100\% \tag{4.1}$$

where x_2 is the % CO_2 in CO_2-rich stream, x_1 is the % CO_2 in He-rich stream, $\dot{n}_{CO2}$ is the CO_2-rich product molar flow rate per cycle, and $\dot{n}_{He}$ is the He-rich product molar flow rate per cycle.

Tables 4.4 and 4.5 show complete details of the molar product flow rates per cycle, the compositions, and % CO_2 recovery for simulations of two PEEK-L III modules in series and three ceramic modules in series, respectively using [bmim][DCA] as an absorbent liquid at different feed gas pressures and temperatures.

The results shown in those tables confirmed what has observed earlier in Chapter 3. PEEK-L III module provides the best results in terms of the product quality since it has the highest feed gas volume due to the highest surface area and highest surface area per unit volume. Table 3.4 shows that the effective surface area per unit volume for the ceramic module is only 4.30 cm^{-1}; it is much lower than 57.5 cm^{-1} for a PEEK-L III hollow fiber.

Table 4.4 Estimated Molar Product Flow Rates per Cycle, Compositions, and % CO_2 Recovery for Two PEEK-L III Modules in Series

P (psig)	T(^{o}C)	He-Rich Molar Flow Rate per Cycle (gmol/s)	He-Rich Product (% CO_2)	CO_2-Rich Molar Flow Rate per Cycle (gmol/s)	CO_2-Rich Product (% CO_2)	% CO_2 Recovery (%)
100	23	9.58E-05	7.3	5.69E-05	95.1	88.55
	50	8.20E-05	10.1	4.79E-05	91.2	84.03
	100	6.17E-05	14.6	3.26E-05	88.1	76.10
200	23	2.06E-04	12.1	1.00E-04	97.3	79.65
	50	1.67E-04	13.7	8.20E-05	93.5	77.01
	100	1.34E-04	18.4	5.71E-05	90.6	67.71

Table 4.5 Estimated Molar Product Flow Rates per Cycle, Compositions, and % CO_2 Recovery for Three Ceramic Modules* in Series at 1034 kPag (150 psig) and Different Temperatures

T(^oC)	CO_2-rich Molar Flow Rate per Cycle (gmol/s)	CO_2-Rich Product (% CO_2)	He-rich Molar Flow Rate per Cycle (gmol/s)	He-Rich Product (% CO_2)	% CO_2 Recovery (%)
23	4.37E-05	56	7.00E-05	30	53.83
50	3.84E-05	53	6.24E-05	32	50.46
100	2.75E-05	57	5.19E-05	31	49.30

*See Table 3.1 for number of fibers and surface area

In addition, Tables 4.4 and 4.5 show that % CO_2 recovery is largest at room temperature since CO_2 gets absorbed the most and He gets absorbed the least. Almost 90% CO_2 was recovered at the 100 psig feed pressure and room temperature for two PEEK-L III modules in series.

4.4 Concluding Remarks

A five-valve PSMAB process was carried out to separate a feed mixture containing ~40% CO_2-He balance using [bmim][DCA] and 20wt% dendrimer in [bmim][DCA] as absorbent liquids. The five-valve PSMAB process provided better results than a three-valve process (studied in Chapter 2). The PEEK-L III module provided the best results in terms of product qualities since it has the highest feed gas volume, highest surface area, and the highest surface area per unit volume. As much as 92.9% CO_2 in the CO_2-product stream was achieved experimentally for the five-valve cycle at room temperature.

The three-valve-based simulation of two PEEK-L III modules in series using [bmim][DCA] provided the best results; as much as 97% CO_2 was achieved in the CO_2-product stream at 200 psig feed pressure and at room temperature. The CO_2 concentration in the He-rich stream for 100 psig feed gas pressure was as low as 7.3%, which results in ~93% He in the He-product stream.

The value of % CO_2 recovery was smallest for ceramic modules and highest for PEEK-L III module. The value of % CO_2 recovery is largest at room temperature. Almost 90% CO_2 was recovered in the CO_2-rich product as suggested by the simulation of two PEEK-L III modules at 100 psig feed gas pressure and at room temperature.

CHAPTER 5

GENERAL CONCLUSIONS AND RECOMMENDATIONS FOR FUTURE STUDY

A gas solubility apparatus was successfully setup to measure the solubility of pure CO_2, pure He and a CO_2-He mixture at temperatures of 50, 80, 90, and 100 ^oC and at pressures up to 1.38 MPa (~200 psig). Gas solubility measurements were made using a pressure decay method.

CO_2 solubility decreased with an increase in temperature whereas He solubility increased with an increase in temperature. The CO_2 and He solubilities increased with an increase in pressure. An increase in the PAMAM dendrimer concentration led to a substantial increase in CO_2 solubility in a liquid absorbent due to reactions with the primary amine groups in the dendrimer molecule. The presence of water in the ionic liquid containing dendrimer led to considerable increase in CO_2 absorption in the liquid absorbent due to the reactivity of the tertiary amine groups.

Among the studied absorbent liquids based on ionic liquid, 30 wt% dendrimer in [bmim][DCA] with moisture gave the highest CO_2 solubility at all temperatures studied. Higher CO_2/He solubility selectivity was observed as temperature decreased. A solution of 30 wt% dendrimer in [bmim][DCA] with moisture gave the highest CO_2/He solubility selectivity: a value of 55 at 50 ^oC and 10 at 100 ^oC. Carbon dioxide gets absorbed more in PEG 400 and in 20 wt% dendrimer in PEG 400 than in [bmim][DCA] and 20 wt% dendrimer in [bmim][DCA], respectively.

A mathematical model of a three-valve based pressure swing membrane absorption (PSMAB) process has been developed to describe the separation of ~40%

CO_2-He balance. The decreasing pressures generated by a numerical solution of the model agreed well with the experimental runs for ceramic modules during the 900 second absorption step, but were significantly lower for the PEEK hollow fiber modules due to the large dead volumes present in the PEEK modules.

The ceramic tubule system produced poor product qualities due to large tube side gas volume and small gas-liquid contacting area. The hydrophobized PEEK hollow fiber-based system, on the other hand, provided higher product concentrations because PEEK fibers have a much larger ratio of contacting area per unit feed gas volume. PEEK-L III module provided a higher CO_2 concentration in the CO_2-rich product stream as compared to PEEK-L II due to having larger tube-side gas volume vis-a-vis the dead volume and higher surface area.

The simulation results showed that purified (>90%) CO_2 and He could be obtained for two PEEK-L III modules in series using [bmim][DCA] as the absorbent. Highly purified CO_2 could also be experimentally obtained for this PEEK-L III module using the five-valve PSMAB process with [bmim][DCA] and 20wt% dendrimer in [bmim][DCA] as liquid absorbents.

Further studies on the five-valve PSMAB process utilizing PEEK modules in series for different absorbent liquids are highly recommended since PEEK modules provide the best product qualities. In addition, new PEEK modules that have less dead volumes and more surface areas are needed to increase the qualities of both product streams.

Five-valve PSMAB process for PEEK modules in a different liquid absorbent, for example, PEG 400 and 20 wt% dendrimer in PEG 400 is also of interest since carbon dioxide gets absorbed more in PEG 400 than in [bmim][DCA].

APPENDIX A

EXPERIMENTAL DATA

This appendix includes all the experimental data for solubility measurements of all absorbent liquids studied in Chapter 2.

Table A1 Experimental Data for CO_2 Solubility in [bmim][DCA] at Five Temperatures

Temperature (^oC)	Absolute P_i (bar)	Absolute P_f (bar)	Mole of Gas Absorbed (gmol)	Mole Fraction
23	7.85	3.75	3.47E-03	0.063
	14.88	856	8.86E-03	0.147
50	2.41	1.14	7.94E-04	0.015
	3.75	1.78	1.25E-03	0.024
	5.16	2.45	1.74E-03	0.033
	6.51	3.11	2.24E-03	0.042
	7.92	3.78	2.75E-03	0.051
	9.23	4.42	3.26E-03	0.060
	10.67	5.11	3.79E-03	0.069
	12.08	5.85	4.34E-03	0.078
	13.39	6.48	4.88E-03	0.087
	14.77	7.17	5.50E-03	0.097
80	2.41	1.15	5.76E-04	0.011
	4.15	1.99	1.01E-03	0.019
	5.15	2.48	1.24E-03	0.024
	6.56	3.16	1.56E-03	0.030
	7.92	3.82	1.94E-03	0.037
	9.29	4.49	2.29E-03	0.043
	10.67	5.15	2.69E-03	0.050
	12.07	5.86	3.05E-03	0.056
	13.44	6.53	3.41E-03	0.062
	14.82	7.23	3.80E-03	0.069
90	2.41	1.16	5.23E-04	0.010
	3.66	1.76	8.00E-04	0.015
	5.15	2.48	1.14E-03	0.022
	6.56	3.17	1.46E-03	0.028
	7.92	3.83	1.74E-03	0.033
	9.29	4.50	2.08E-03	0.039
	10.67	5.17	2.38E-03	0.044
	12.07	5.86	2.70E-03	0.050
	13.44	6.53	3.04E-03	0.056
	14.82	7.02	3.26E-03	0.060
100	2.33	1.12	4.46E-04	0.009
	3.80	1.83	7.32E-04	0.014
	5.15	2.49	9.97E-04	0.019
	6.54	3.16	1.28E-03	0.024
	7.91	3.83	1.55E-03	0.029
	9.33	4.53	1.86E-03	0.035
	10.73	5.22	2.15E-03	0.040
	12.07	5.89	2.42E-03	0.045
	13.45	6.56	2.71E-03	0.050
	14.74	7.21	3.01E-03	0.056

Table A2 Experimental Data for CO_2 Solubility in 20wt% Dendrimer in [bmim][DCA] at Four Temperatures

Temperature (^oC)	Absolute P_i (bar)	Absolute P_f (bar)	Mole of Gas Absorbed (gmol)	Mole Fraction
50	2.41	1.08	1.51E-03	0.038
	3.75	1.68	2.41E-03	0.059
	5.16	2.31	3.42E-03	0.081
	6.47	2.90	4.35E-03	0.101
	7.90	3.54	5.49E-03	0.125
	9.26	4.16	6.42E-03	0.143
	10.59	4.73	7.84E-03	0.169
	11.96	5.39	9.14E-03	0.191
	13.43	6.05	1.01E-02	0.208
	14.66	6.57	1.16E-02	0.231
80	2.39	1.11	9.04E-04	0.023
	3.76	1.75	1.45E-03	0.036
	5.14	2.39	2.05E-03	0.050
	6.53	3.05	2.63E-03	0.064
	7.77	3.63	3.09E-03	0.074
	9.27	4.35	3.73E-03	0.088
	10.67	4.99	4.45E-03	0.103
	12.14	5.66	5.14E-03	0.118
	13.39	6.25	5.59E-03	0.126
	14.83	6.97	6.54E-03	0.145
90	2.41	1.13	7.88E-04	0.020
	3.87	1.82	1.28E-03	0.032
	5.17	2.43	1.77E-03	0.044
	6.58	3.09	2.33E-03	0.057
	7.93	3.74	2.75E-03	0.066
	9.38	4.42	3.38E-03	0.080
	10.68	5.04	3.91E-03	0.092
	12.07	5.69	4.56E-03	0.106
	13.38	6.32	4.96E-03	0.114
	14.77	6.99	5.67E-03	0.128
100	2.47	1.17	7.43E-04	0.019
	3.76	1.72	1.10E-03	0.028
	5.16	2.43	1.58E-03	0.039
	6.52	2.99	1.94E-03	0.048
	7.91	3.74	2.44E-03	0.059
	9.27	4.39	2.91E-03	0.070
	10.61	4.87	3.31E-03	0.079
	11.99	5.70	3.86E-03	0.091
	13.43	6.39	4.30E-03	0.100
	14.47	6.91	4.84E-03	0.111

Table A3 Experimental Data for CO_2 Solubility in 20wt% Dendrimer [bmim][DCA] with Moisture at Four Temperatures

Temperature (^oC)	Absolute P_i (bar)	Absolute P_f (bar)	Mole of Gas Absorbed (gmol)	Mole Fraction
50	2.47	1.01	2.57E-03	0.038
	3.74	1.45	4.98E-03	0.071
	5.16	1.95	7.46E-03	0.102
	6.46	2.48	9.01E-03	0.121
	7.90	3.04	1.14E-02	0.148
	9.26	3.56	1.33E-02	0.169
	10.69	3.99	1.69E-02	0.205
	11.96	4.48	1.93E-02	0.227
	13.43	5.06	2.14E-02	0.247
	14.66	5.58	2.34E-02	0.263
80	2.42	1.05	1.62E-03	0.024
	3.69	1.61	2.53E-03	0.037
	5.16	2.26	3.57E-03	0.052
	6.72	2.93	4.84E-03	0.069
	7.90	3.45	5.78E-03	0.081
	9.26	4.07	6.55E-03	0.091
	10.59	4.62	7.93E-03	0.108
	11.96	5.24	9.34E-03	0.125
	13.43	5.87	1.07E-02	0.141
	14.66	6.43	1.11E-02	0.146
90	2.45	1.07	1.39E-03	0.021
	3.66	1.63	2.11E-03	0.031
	5.16	2.29	3.10E-03	0.045
	6.47	2.88	3.89E-03	0.056
	7.90	3.53	4.68E-03	0.067
	9.26	4.11	5.62E-03	0.079
	10.59	4.74	6.43E-03	0.089
	11.96	5.37	7.30E-03	0.100
	13.43	6.03	8.36E-03	0.113
	14.66	6.60	9.00E-03	0.121
100	2.41	1.08	1.21E-03	0.018
	3.78	1.70	1.96E-03	0.029
	5.16	2.32	2.69E-03	0.039
	6.41	2.89	3.33E-03	0.048
	7.90	3.57	4.16E-03	0.060
	9.26	4.19	4.93E-03	0.070
	10.59	4.77	5.80E-03	0.081
	11.96	5.41	6.54E-03	0.091
	13.43	6.07	7.56E-03	0.104
	14.66	6.65	8.22E-03	0.112

Table A4 Experimental Data for CO_2 Solubility in 30wt% Dendrimer in [bmim][DCA] at Four Temperatures

Temperature (^oC)	Absolute P_i (bar)	Absolute P_f (bar)	Mole of Gas Absorbed (gmol)	Mole Fraction
50	2.43	1.07	1.76E-03	0.047
	3.74	1.66	2.60E-03	0.070
	5.16	2.28	3.72E-03	0.097
	6.47	2.86	4.77E-03	0.121
	7.90	3.49	6.08E-03	0.149
	9.26	4.08	7.40E-03	0.176
	10.59	4.65	8.70E-03	0.201
	11.96	5.28	9.99E-03	0.224
	13.43	5.91	1.16E-02	0.250
	14.66	6.49	1.27E-02	0.268
80	2.43	1.13	9.86E-04	0.028
	3.62	1.68	1.51E-03	0.042
	5.16	2.39	2.24E-03	0.062
	6.47	3.00	2.82E-03	0.076
	7.90	3.66	3.55E-03	0.094
	9.26	4.29	4.26E-03	0.111
	10.59	4.91	4.89E-03	0.125
	11.96	5.60	5.63E-03	0.141
	13.43	6.26	6.51E-03	0.160
	14.66	6.84	7.05E-03	0.171
90	2.43	1.13	8.90E-04	0.025
	3.71	1.75	1.38E-03	0.038
	5.16	2.41	1.94E-03	0.053
	6.47	3.02	2.43E-03	0.065
	7.90	3.69	3.08E-03	0.081
	9.26	4.33	3.70E-03	0.096
	10.59	4.95	4.22E-03	0.108
	11.96	5.60	4.91E-03	0.123
	13.43	6.30	5.60E-03	0.138
	14.66	6.89	6.08E-03	0.148
100	2.43	1.15	7.37E-04	0.021
	3.72	1.75	1.15E-03	0.032
	5.16	2.43	1.61E-03	0.044
	6.47	3.06	2.03E-03	0.055
	7.90	3.73	2.53E-03	0.067
	9.26	4.38	3.03E-03	0.080
	10.59	5.01	3.45E-03	0.090
	11.96	5.67	3.92E-03	0.101
	13.43	6.37	4.55E-03	0.115
	14.66	6.96	5.04E-03	0.126

Table A5 Experimental Data for CO_2 Solubility in 30wt% Dendrimer in [bmim][DCA] with Moisture at Four Temperatures

Temperature (^oC)	Absolute P_i (bar)	Absolute P_f (bar)	Mole of Gas Absorbed (gmol)	Mole Fraction
50	2.43	1.01	3.53E-03	0.052
	3.74	1.37	5.83E-03	0.083
	5.16	1.85	8.62E-03	0.118
	6.47	2.22	1.21E-02	0.159
	7.77	2.67	1.47E-02	0.186
	9.26	3.16	1.80E-02	0.219
	10.59	3.62	2.05E-02	0.242
	11.96	4.01	2.47E-02	0.277
	13.43	4.35	2.96E-02	0.316
	14.66	5.63	3.28E-02	0.338
80	2.43	1.03	2.03E-03	0.031
	3.62	1.54	2.95E-03	0.044
	5.16	2.19	4.25E-03	0.062
	6.47	2.71	5.76E-03	0.082
	7.80	3.30	6.81E-03	0.096
	9.26	3.89	8.29E-03	0.114
	10.59	4.48	9.36E-03	0.127
	11.96	5.11	1.07E-02	0.142
	13.43	5.66	1.28E-02	0.166
	14.66	6.17	1.41E-02	0.180
90	2.43	1.04	1.82E-03	0.027
	3.71	1.60	2.83E-03	0.042
	5.16	2.21	3.89E-03	0.057
	6.47	2.77	4.99E-03	0.072
	7.90	3.38	6.16E-03	0.088
	9.26	3.94	7.65E-03	0.106
	10.59	4.55	8.37E-03	0.115
	11.96	5.17	9.36E-03	0.127
	13.43	5.80	1.08E-02	0.145
	14.66	6.32	1.21E-02	0.158
100	2.43	1.07	1.46E-03	0.022
	3.72	1.64	2.22E-03	0.033
	5.16	2.27	3.20E-03	0.047
	6.47	2.84	4.12E-03	0.060
	7.86	3.46	4.98E-03	0.072
	9.26	4.07	6.09E-03	0.087
	10.59	4.66	6.97E-03	0.098
	11.96	5.29	7.77E-03	0.108
	13.43	5.91	9.10E-03	0.124
	14.66	6.45	1.01E-02	0.136

Table A6 Experimental Data for He Solubility in [bmim][DCA] at Five Temperatures

Temperature (^{o}C)	Absolute P_i (bar)	Absolute P_f (bar)	Mole of Gas Absorbed (gmol)	Mole Fraction
23	8.68	4.35	1.22E-04	0.0023
	14.70	7.29	2.06E-04	0.0040
50	2.60	1.29	8.81E-05	0.0017
	3.79	1.88	1.28E-04	0.0025
	5.15	2.56	1.75E-04	0.0034
	6.51	3.23	2.22E-04	0.0043
	7.92	3.93	2.68E-04	0.0052
	9.29	4.61	3.14E-04	0.0061
	10.63	5.27	3.60E-04	0.0070
	12.05	5.97	4.09E-04	0.0079
	13.43	6.65	4.55E-04	0.0088
	14.79	7.32	5.04E-04	0.0098
80	2.51	1.24	1.24E-04	0.0024
	3.79	1.87	1.87E-04	0.0036
	5.15	2.55	2.51E-04	0.0049
	6.51	3.22	3.14E-04	0.0061
	7.56	3.74	3.68E-04	0.0071
	9.29	4.59	4.55E-04	0.0088
	10.63	5.26	5.16E-04	0.0100
	12.11	5.99	5.88E-04	0.0114
	13.88	6.85	6.76E-04	0.0131
	14.85	7.33	7.26E-04	0.0140
90	2.44	1.21	1.40E-04	0.0027
	3.79	1.87	2.16E-04	0.0042
	5.15	2.55	2.96E-04	0.0058
	6.52	3.22	3.75E-04	0.0073
	7.99	3.94	4.58E-04	0.0089
	9.27	4.58	5.40E-04	0.0104
	10.69	5.28	6.17E-04	0.0119
	12.09	5.97	6.93E-04	0.0134
	13.40	6.60	7.69E-04	0.0148
	14.81	7.29	8.49E-04	0.0163
100	2.30	1.14	1.59E-04	0.0031
	3.70	1.82	2.57E-04	0.0050
	5.15	2.54	3.57E-04	0.0069
	6.49	3.19	4.52E-04	0.0088
	7.92	3.89	5.50E-04	0.0107
	9.28	4.57	6.48E-04	0.0125
	10.64	5.24	7.47E-04	0.0144
	12.05	5.93	8.46E-04	0.0163
	13.41	6.59	9.37E-04	0.0180
	14.84	7.29	1.05E-03	0.0201

Table A7 Experimental Data for He Solubility in 20wt% Dendrimer in [bmim][DCA] at Four Temperatures

Temperature (^{o}C)	Absolute P_i (bar)	Absolute P_f (bar)	Mole of Gas Absorbed (gmol)	Mole Fraction
50	2.46	1.23	6.18E-05	0.0015
	3.78	1.88	9.49E-05	0.0024
	5.15	2.56	1.30E-04	0.0032
	7.03	3.49	1.76E-04	0.0044
	7.87	3.91	1.97E-04	0.0049
	9.40	4.67	2.36E-04	0.0059
	10.63	5.28	2.68E-04	0.0066
	12.05	5.98	3.04E-04	0.0075
	13.52	6.71	3.41E-04	0.0084
	14.82	7.35	3.70E-04	0.0092
80	2.51	1.24	8.51E-05	0.0022
	3.76	1.87	1.27E-04	0.0033
	5.15	2.56	1.76E-04	0.0045
	6.51	3.23	2.24E-04	0.0058
	7.86	3.90	2.71E-04	0.0070
	9.29	4.61	3.23E-04	0.0083
	10.63	5.27	3.71E-04	0.0095
	12.11	6.00	4.24E-04	0.0109
	13.49	6.68	4.71E-04	0.0121
	14.64	7.25	5.15E-04	0.0132
90	2.47	1.23	1.06E-04	0.0027
	3.87	1.92	1.63E-04	0.0042
	5.21	2.58	2.20E-04	0.0057
	6.57	3.25	2.78E-04	0.0071
	7.93	3.92	3.35E-04	0.0086
	9.29	4.60	3.95E-04	0.0101
	10.69	5.29	4.55E-04	0.0116
	12.11	5.99	5.17E-04	0.0132
	13.49	6.67	5.76E-04	0.0147
	14.75	7.29	6.29E-04	0.0160
100	2.45	1.22	1.36E-04	0.0034
	3.70	1.83	2.06E-04	0.0051
	5.14	2.54	2.88E-04	0.0071
	6.47	3.19	3.62E-04	0.0090
	7.99	3.94	4.47E-04	0.0110
	9.40	4.64	5.30E-04	0.0131
	10.76	5.31	6.01E-04	0.0148
	12.05	5.94	6.78E-04	0.0167
	13.46	6.63	7.59E-04	0.0186
	14.60	7.19	8.14E-04	0.0199

Table A8 Experimental Data for He Solubility in 20wt% Dendrimer [bmim][DCA] with Moisture at Four Temperatures

Temperature (^{o}C)	Absolute P_i (bar)	Absolute P_f (bar)	Mole of Gas Absorbed (gmol)	Mole Fraction
50	2.51	1.24	9.90E-05	0.0015
	3.76	1.86	1.50E-04	0.0023
	5.15	2.55	2.03E-04	0.0031
	6.51	3.23	2.52E-04	0.0038
	7.73	3.83	3.07E-04	0.0047
	9.29	4.60	3.65E-04	0.0055
	10.63	5.27	4.21E-04	0.0064
	12.11	5.99	4.84E-04	0.0073
	13.37	6.62	5.29E-04	0.0080
	14.77	7.31	5.81E-04	0.0088
80	2.51	1.24	1.31E-04	0.0020
	3.76	1.86	1.97E-04	0.0030
	5.15	2.57	2.80E-04	0.0043
	6.51	3.22	3.41E-04	0.0052
	7.98	3.94	4.18E-04	0.0064
	9.29	4.59	4.94E-04	0.0075
	10.63	5.25	5.68E-04	0.0086
	12.11	5.98	6.43E-04	0.0097
	13.49	6.66	7.11E-04	0.0107
	15.02	7.41	7.86E-04	0.0119
90	2.51	1.24	1.50E-04	0.0023
	3.76	1.85	2.25E-04	0.0034
	5.15	2.54	3.16E-04	0.0048
	6.51	3.21	3.99E-04	0.0061
	7.91	3.90	4.90E-04	0.0074
	9.29	4.58	5.65E-04	0.0086
	10.63	5.24	6.57E-04	0.0099
	12.11	5.96	7.39E-04	0.0112
	13.37	6.59	8.22E-04	0.0124
	14.82	7.30	9.17E-04	0.0138
100	2.51	1.23	1.76E-04	0.0027
	3.76	1.85	2.64E-04	0.0040
	5.15	2.54	3.57E-04	0.0054
	6.51	3.21	4.49E-04	0.0068
	8.09	3.98	5.57E-04	0.0084
	9.29	4.57	6.32E-04	0.0096
	10.63	5.23	7.22E-04	0.0109
	12.11	5.95	8.37E-04	0.0126
	13.37	6.57	9.17E-04	0.0138
	14.88	7.31	1.01E-03	0.0153

Table A9 Experimental Data for He Solubility in 30wt% Dendrimer in [bmim][DCA] at Four Temperatures

Temperature (^{o}C)	Absolute P_i (bar)	Absolute P_f (bar)	Mole of Gas Absorbed (gmol)	Mole Fraction
50	2.43	1.21	5.42E-05	0.0015
	3.78	1.88	8.52E-05	0.0024
	5.18	2.58	1.17E-04	0.0033
	6.52	3.24	1.44E-04	0.0041
	7.93	3.94	1.76E-04	0.0050
	9.28	4.61	2.10E-04	0.0060
	10.63	5.28	2.40E-04	0.0068
	12.11	6.01	2.68E-04	0.0076
	13.40	6.65	3.02E-04	0.0086
	14.21	7.05	3.21E-04	0.0091
80	2.43	1.21	7.39E-05	0.0021
	3.75	1.86	1.19E-04	0.0034
	5.18	2.57	1.62E-04	0.0046
	6.52	3.23	2.06E-04	0.0058
	7.93	3.93	2.48E-04	0.0070
	9.28	4.61	2.94E-04	0.0083
	10.63	5.27	3.32E-04	0.0094
	12.11	6.00	3.84E-04	0.0108
	13.92	6.90	4.44E-04	0.0125
	14.75	7.31	4.66E-04	0.0131
90	2.43	1.20	8.88E-05	0.0025
	3.75	1.86	1.38E-04	0.0039
	5.18	2.57	1.91E-04	0.0054
	6.52	3.23	2.44E-04	0.0069
	7.93	3.93	2.92E-04	0.0083
	9.28	4.60	3.46E-04	0.0098
	10.63	5.26	3.93E-04	0.0111
	12.11	5.99	4.48E-04	0.0126
	13.92	6.89	5.19E-04	0.0146
	14.45	7.15	5.46E-04	0.0153
100	2.43	1.19	1.09E-04	0.0031
	3.75	1.86	1.67E-04	0.0048
	5.18	2.56	2.31E-04	0.0065
	6.52	3.22	2.90E-04	0.0082
	7.93	3.92	3.60E-04	0.0102
	9.28	4.59	4.16E-04	0.0117
	10.63	5.26	4.89E-04	0.0138
	12.11	5.98	5.55E-04	0.0156
	13.92	6.88	6.29E-04	0.0177
	14.58	7.20	6.66E-04	0.0187

Table A10 Experimental Data for He Solubility in 30wt% Dendrimer in [bmim][DCA] with Moisture at Four Temperatures

Temperature (^{o}C)	Absolute P_i (bar)	Absolute P_f (bar)	Mole of Gas Absorbed (gmol)	Mole Fraction
50	2.44	1.21	4.92E-05	0.0014
	3.78	1.88	7.92E-05	0.0023
	5.18	2.58	1.04E-04	0.0030
	6.52	3.24	1.32E-04	0.0037
	7.93	3.94	1.63E-04	0.0046
	9.28	4.61	1.90E-04	0.0054
	10.63	5.28	2.20E-04	0.0062
	12.11	6.01	2.48E-04	0.0070
	13.40	6.65	2.76E-04	0.0078
	14.59	7.24	3.05E-04	0.0086
80	2.45	1.21	6.80E-05	0.0019
	3.75	1.86	1.01E-04	0.0029
	5.18	2.57	1.44E-04	0.0041
	6.52	3.24	1.76E-04	0.0050
	7.93	3.93	2.17E-04	0.0062
	9.28	4.61	2.52E-04	0.0071
	10.63	5.27	2.90E-04	0.0082
	12.11	6.00	3.30E-04	0.0093
	13.92	6.90	3.83E-04	0.0108
	14.71	7.29	4.08E-04	0.0115
90	2.43	1.21	7.74E-05	0.0022
	3.75	1.86	1.20E-04	0.0034
	5.18	2.57	1.68E-04	0.0048
	6.52	3.23	2.10E-04	0.0059
	7.93	3.93	2.57E-04	0.0073
	9.28	4.60	2.99E-04	0.0085
	10.63	5.27	3.46E-04	0.0098
	12.11	6.00	3.89E-04	0.0110
	13.92	6.89	4.48E-04	0.0126
	14.99	7.43	4.87E-04	0.0137
100	2.43	1.19	8.67E-05	0.0025
	3.75	1.86	1.34E-04	0.0038
	5.18	2.57	1.86E-04	0.0053
	6.52	3.23	2.40E-04	0.0068
	7.93	3.93	2.85E-04	0.0081
	9.28	4.60	3.30E-04	0.0093
	10.63	5.27	3.79E-04	0.0107
	12.11	5.99	4.29E-04	0.0121
	13.92	6.89	5.03E-04	0.0142
	14.73	7.29	5.30E-04	0.0149

Table A11 Experimental Data for CO_2 Solubility in PEG 400 at Four Temperatures

Temperature (^oC)	Absolute P_i (bar)	Absolute P_f (bar)	Mole of Gas Absorbed (gmol)	Mole Fraction
50	2.37	1.16	4.80E-04	0.017
	5.24	2.58	1.06E-03	0.037
	7.96	3.92	1.80E-03	0.062
	10.62	5.25	2.37E-03	0.080
	14.53	7.25	3.43E-03	0.111
80	2.42	1.19	3.58E-04	0.013
	5.22	2.57	8.03E-04	0.028
	7.88	3.89	1.24E-03	0.043
	10.38	5.15	1.59E-03	0.055
	14.32	7.08	2.32E-03	0.078
90	2.39	1.18	3.17E-04	0.011
	5.14	2.53	6.95E-04	0.025
	8.01	3.93	1.09E-03	0.038
	10.49	5.21	1.51E-03	0.052
	14.57	7.23	2.06E-03	0.070
100	2.46	1.22	2.87E-04	0.010
	5.16	2.55	6.57E-04	0.023
	8.13	4.02	1.01E-03	0.036
	10.68	5.33	1.36E-03	0.047
	14.43	7.18	1.82E-03	0.062

Table A12 Experimental Data for CO_2 Solubility in 20wt% Dendrimer in PEG 400 at Four Temperatures

Temperature (^oC)	Absolute P_i (bar)	Absolute P_f (bar)	Mole of Gas Absorbed (gmol)	Mole Fraction
50	2.47	1.16	1.36E-03	4.84E-02
	5.22	2.40	2.52E-03	8.61E-02
	8.25	3.79	4.66E-03	1.47E-01
	10.65	4.92	5.77E-03	1.78E-01
	14.48	6.69	8.54E-03	2.61E-01
80	2.41	1.15	7.54E-04	2.75E-02
	5.26	2.49	1.71E-03	6.02E-02
	7.72	3.63	2.60E-03	8.88E-02
	10.69	5.12	4.05E-03	1.32E-01
	14.78	7.03	5.13E-03	1.61E-01
90	2.46	1.18	6.46E-04	2.36E-02
	5.34	2.55	1.49E-03	5.28E-02
	7.84	3.72	2.23E-03	7.71E-02
	10.72	5.22	3.05E-03	1.02E-01
	14.73	7.05	4.31E-03	1.39E-01
100	2.39	1.16	5.89E-04	2.16E-02
	5.14	2.55	1.21E-03	4.33E-02
	7.97	3.79	2.02E-03	7.04E-02
	10.60	5.05	2.69E-03	9.16E-02
	14.52	7.02	3.80E-03	1.25E-01

Table A13 Experimental Data for He Solubility in PEG 400 at Four Temperatures

Temperature (^{o}C)	Absolute P_i (bar)	Absolute P_f (bar)	Mole of Gas Absorbed (gmol)	Mole Fraction
50	2.43	1.25	4.35E-05	1.58E-03
	5.25	2.71	9.36E-05	3.40E-03
	7.79	3.87	1.36E-04	4.94E-03
	10.48	5.20	1.79E-04	6.50E-03
	14.74	7.37	2.57E-04	9.28E-03
80	2.29	1.13	5.45E-05	1.98E-03
	5.14	2.56	1.25E-04	4.52E-03
	7.87	3.91	1.90E-04	6.89E-03
	10.72	5.32	2.57E-04	9.28E-03
	14.80	7.33	3.55E-04	1.28E-02
90	2.35	1.17	6.86E-05	2.49E-03
	5.15	2.56	1.47E-04	5.33E-03
	7.99	3.99	2.29E-04	8.27E-03
	10.69	5.31	3.08E-04	1.11E-02
	14.80	7.31	4.28E-04	1.54E-02
100	2.44	1.21	9.20E-05	3.34E-03
	5.13	2.55	1.93E-04	6.99E-03
	7.94	3.93	2.96E-04	1.07E-02
	10.58	5.23	4.00E-04	1.44E-02
	14.86	7.33	5.62E-04	2.01E-02

Table A14 Experimental Data for He Solubility in 20wt% Dendrimer in PEG 400 at Four Temperatures

Temperature (^{o}C)	Absolute P_i (bar)	Absolute P_f (bar)	Mole of Gas Absorbed (gmol)	Mole Fraction
50	2.51	1.24	4.05E-05	1.52E-03
	5.37	2.67	8.88E-05	3.31E-03
	8.97	4.46	1.50E-04	5.58E-03
	10.76	5.36	1.79E-04	6.48E-03
	14.81	7.36	2.41E-04	8.46E-03
80	2.44	1.21	5.61E-05	2.10E-03
	5.29	2.62	1.24E-04	4.64E-03
	8.25	4.10	1.89E-04	7.05E-03
	10.82	5.38	2.45E-04	9.10E-03
	14.63	7.27	3.47E-04	1.28E-02
90	2.39	1.19	6.29E-05	2.35E-03
	5.17	2.57	1.42E-04	5.29E-03
	7.94	3.94	2.34E-04	8.69E-03
	10.81	5.36	3.02E-04	1.12E-02
	15.02	7.45	4.24E-04	1.56E-02
100	2.48	1.23	8.56E-05	3.20E-03
	5.22	2.59	1.91E-04	7.11E-03
	8.30	4.11	2.87E-04	1.07E-02
	10.72	5.31	4.03E-04	1.49E-02
	14.91	7.38	5.31E-04	1.95E-02

Table A15 CO_2 Mole Fractions in [bmim][DCA] at Various Feed Pressures and Temperatures

Temperature (^oC)	Pressure (bar)	CO_2 mole fraction	Pressure Ratio	Mole Fraction Ratio
50	2.43	0.015	1.00	1.00
	3.75	0.024	1.54	1.56
	5.16	0.033	2.12	2.16
	6.51	0.042	2.68	2.74
	7.92	0.051	3.26	3.33
	9.23	0.060	3.80	3.92
	10.67	0.069	4.39	4.51
	12.08	0.078	4.97	5.12
	13.39	0.087	5.51	5.70
	14.77	0.097	6.08	6.35
80	2.43	0.015	1.00	1.00
	3.75	0.024	1.70	1.73
	5.16	0.033	2.12	2.13
	6.51	0.042	2.68	2.66
	7.92	0.051	3.24	3.28
	9.23	0.060	3.81	3.84
	10.67	0.069	4.38	4.48
	12.08	0.078	4.97	5.05
	13.39	0.087	5.51	5.60
	14.77	0.097	6.07	6.21
90	2.43	0.015	1.00	1.00
	3.75	0.024	1.52	1.52
	5.16	0.033	2.14	2.15
	6.51	0.042	2.72	2.74
	7.92	0.051	3.28	3.26
	9.23	0.060	3.85	3.86
	10.67	0.069	4.43	4.39
	12.08	0.078	5.01	4.95
	13.39	0.087	5.58	5.55
	14.77	0.097	6.15	5.92
100	2.43	0.015	1.00	1.00
	3.75	0.024	1.63	1.63
	5.16	0.033	2.21	2.21
	6.51	0.042	2.80	2.82
	7.92	0.051	3.39	3.39
	9.23	0.060	4.00	4.05
	10.67	0.069	4.60	4.66
	12.08	0.078	5.17	5.23
	13.39	0.087	5.76	5.81
	14.77	0.097	6.32	6.42

Table A16 Percent Theoretical Capacity of Primary Amines Consumed under Different Pressures and Its Corresponding Apparent Equilibrium Constants of Primary Amine Reaction with CO_2 for 20 wt% Dendrimer in [bmim][DCA] at Different Temperatures*

Temperature (^oC)	P_{feed} (bar)	% Saturation (%)	K_C
50	2.43	10.56	6100 L/mol
	3.74	24.23	
	5.16	31.85	
	6.47	38.89	
	7.90	47.72	
	9.26	53.89	
	10.59	66.74	
	11.96	77.54	
	13.43	75.83	
	14.66	97.69	29972 L^4/mol^4
80	2.39	5.51	2804 L/mol
	3.76	9.03	
	5.14	12.88	
	6.53	16.61	
	7.77	18.83	
	9.27	22.85	
	10.67	27.42	
	12.14	32.13	
	13.39	34.83	
	14.83	42.08	
90	2.41	4.13	2227 L/mol
	3.87	6.88	
	5.17	9.78	
	6.58	13.28	
	7.93	15.47	
	9.38	19.62	
	10.68	23.08	
	12.07	27.51	
	13.38	29.10	
	14.77	34.36	
100	2.47	3.84	1790 L/mol
	3.76	5.73	
	5.16	8.20	
	6.52	10.06	
	7.91	12.65	
	9.27	15.06	
	10.61	17.99	
	11.99	20.52	
	13.43	22.52	
	14.47	26.96	

*Dry system

Table A17 Percent Theoretical Capacity of Primary Amines Consumed under Different Pressures and Its Corresponding Apparent Equilibrium Constants of Primary Amine Reaction with CO_2 for 30wt% Dendrimer in [bmim][DCA] at Different Temperatures*

Temperature (^oC)	P_{feed} (bar)	% Saturation (%)	K_C
50	2.41	9.29	6659 L/mol
	3.75	13.18	
	5.16	19.22	
	6.47	25.06	
	7.90	32.37	
	9.26	39.53	
	10.59	47.15	
	11.96	55.09	
	13.43	64.05	
	14.66	69.58	10329 L^4/mol^4
80	2.43	4.49	3061 L/mol
	3.62	6.77	
	5.16	10.43	
	6.47	13.08	
	7.90	16.75	
	9.26	20.17	
	10.59	23.02	
	11.96	26.47	
	13.43	31.19	
	14.96	33.84	
90	2.43	3.93	2431 L/mol
	3.71	6.00	
	5.16	8.58	
	6.47	10.61	
	7.90	14.08	
	9.26	17.09	
	10.59	19.47	
	11.96	23.00	
	13.43	26.18	
	14.86	28.06	
100	2.43	2.98	1954 L/mol
	3.72	4.82	
	5.16	6.72	
	6.47	8.49	
	7.90	10.63	
	9.26	13.00	
	10.59	14.39	
	11.96	16.46	
	13.43	19.78	
	14.66	21.93	

*Dry system

Table A18 The Correction (%) for Henry's Law Constants of CO_2 Due to Physical Absorption the IL Containing Dendrimer and in Pure IL

	Temperature (^oC)	H_{He}[1]	H_{HeT}[2]	H_{CO2}[3]	H_{CO2T}[4]	Correction (%)[5]
20 wt% dendrimer in [bmim][DCA]	50	751.6	796.2	74.4	78.6	5.64
	80	522.4	558.3	104.2	111.5	7.00
	90	443.3	453.9	114.3	118.2	3.41
	100	364.6	357.4	129.8	127.3	1.93
30 wt% dendrimer in [bmim][DCA]	50	751.6	781.8	74.4	77.2	3.76
	80	522.4	557.3	104.2	111.3	6.81
	90	443.3	472.2	114.3	122.9	7.52
	100	364.6	387.6	129.8	138.0	6.32

[1] Henry's law constant of He for pure [bmim][DCA]
[2] Henry's law constant of He due to physical absorption in the [bmim][DCA] containing dendrimer
[3] Henry's law constant of CO_2 for pure [bmim][DCA]
[4] Henry's law constant of CO_2 due to physical absorption in the [bmim][DCA] containing dendrimer
[5] $Correction\ (\%) = \frac{\left|H_{CO2T} - H_{CO2}\right|}{H_{CO2}} x100\%$

Table A19 Solubilities of Pure CO_2 and Pure He in 20 wt% Dendrimer in [bmim][DCA] at Different Feed Pressures and Temperatures

Temperature (^oC)	Feed pressure (bar)	CO_2 mole fraction	He mole fraction
50	2.40	0.038	0.0015
	3.75	0.059	0.0024
	5.16	0.081	0.0032
	6.47	0.101	0.0044
	7.90	0.125	0.0049
	9.26	0.143	0.0059
	10.59	0.169	0.0066
	11.96	0.191	0.0075
	13.43	0.208	0.0084
	14.65	0.231	0.0092
80	2.39	0.023	0.0022
	3.75	0.036	0.0033
	5.14	0.050	0.0045
	6.53	0.064	0.0058
	7.77	0.074	0.0070
	9.26	0.088	0.0083
	10.67	0.103	0.0095
	12.13	0.118	0.0109
	13.39	0.126	0.0121
	14.83	0.145	0.0132
90	2.41	0.020	0.0027
	3.87	0.032	0.0042
	5.16	0.044	0.0057
	6.58	0.057	0.0071
	7.93	0.066	0.0086
	9.37	0.080	0.0101
	10.68	0.092	0.0116
	12.07	0.106	0.0132
	13.38	0.114	0.0147
	14.76	0.128	0.0160
100	2.46	0.019	0.0034
	3.75	0.028	0.0051
	5.15	0.039	0.0071
	6.51	0.048	0.0090
	7.90	0.059	0.0110
	9.26	0.070	0.0131
	10.60	0.079	0.0148
	11.98	0.091	0.0167
	13.43	0.100	0.0186
	14.46	0.111	0.0199

Table A20 Solubilities of Pure CO_2 and Pure He in 20 wt% Dendrimer in [bmim][DCA] with Moisture at Different Feed Pressures and Temperatures

Temperature (^oC)	Feed pressure (bar)	CO_2 mole fraction	He mole fraction
50	2.47	0.046	0.0015
	3.74	0.071	0.0023
	5.16	0.102	0.0031
	6.46	0.121	0.0038
	7.90	0.148	0.0047
	9.26	0.169	0.0055
	10.69	0.205	0.0064
	11.96	0.227	0.0073
	13.43	0.247	0.0080
	14.66	0.263	0.0088
80	2.41	0.029	0.0020
	3.69	0.041	0.0030
	5.16	0.057	0.0043
	6.72	0.069	0.0052
	7.90	0.081	0.0064
	9.26	0.091	0.0075
	10.59	0.108	0.0086
	11.96	0.125	0.0097
	13.43	0.141	0.0107
	14.66	0.151	0.0119
90	2.41	0.023	0.0023
	3.66	0.031	0.0034
	5.16	0.051	0.0048
	6.47	0.057	0.0061
	7.90	0.069	0.0074
	9.26	0.079	0.0086
	10.59	0.089	0.0099
	11.96	0.105	0.0112
	13.43	0.120	0.0124
	14.66	0.126	0.0138
100	2.41	0.020	0.0027
	3.78	0.033	0.0040
	5.16	0.043	0.0054
	6.41	0.054	0.0068
	7.90	0.065	0.0084
	9.26	0.078	0.0096
	10.59	0.084	0.0109
	11.96	0.096	0.0126
	13.43	0.107	0.0138
	14.66	0.115	0.0153

Table A21 Solubilities of Pure CO_2 and Pure He in 30 wt% Dendrimer in [bmim][DCA] for Different Feed Pressures and Temperatures

Temperature (^oC)	Feed pressure (bar)	CO_2 mole fraction	He mole fraction
50	2.43	0.047	0.0015
	3.74	0.07	0.0024
	5.16	0.097	0.0033
	6.47	0.121	0.0041
	7.90	0.149	0.0050
	9.26	0.176	0.0060
	10.59	0.201	0.0068
	11.96	0.224	0.0076
	13.43	0.250	0.0086
	14.66	0.268	0.0091
80	2.43	0.028	0.0021
	3.62	0.042	0.0034
	5.16	0.062	0.0046
	6.47	0.076	0.0058
	7.90	0.094	0.0070
	9.26	0.111	0.0083
	10.59	0.125	0.0094
	11.96	0.141	0.0108
	13.43	0.160	0.0125
	14.66	0.171	0.0131
90	2.43	0.025	0.0025
	3.71	0.038	0.0039
	5.16	0.053	0.0054
	6.47	0.065	0.0069
	7.90	0.081	0.0083
	9.26	0.096	0.0098
	10.59	0.108	0.0111
	11.96	0.123	0.0126
	13.43	0.138	0.0146
	14.66	0.148	0.0153
100	2.43	0.021	0.0031
	3.72	0.032	0.0048
	5.16	0.044	0.0065
	6.47	0.055	0.0082
	7.90	0.067	0.0102
	9.26	0.080	0.0117
	10.59	0.090	0.0138
	11.96	0.101	0.0156
	13.43	0.115	0.0177
	14.66	0.126	0.0187

Table A22 Solubilities of Pure CO_2 and Pure He in 30 wt% Dendrimer in [bmim][DCA] with Moisture at Different Feed Pressures and Temperatures

Temperature (^oC)	Feed pressure (bar)	CO_2 mole fraction	He mole fraction
50	2.43	0.052	0.0014
	3.74	0.083	0.0023
	5.16	0.118	0.0030
	6.47	0.159	0.0037
	7.77	0.186	0.0046
	9.26	0.219	0.0054
	10.59	0.242	0.0062
	11.96	0.277	0.0070
	13.43	0.316	0.0078
	14.66	0.338	0.0086
80	2.43	0.031	0.0019
	3.62	0.044	0.0029
	5.16	0.067	0.0041
	6.47	0.082	0.0050
	7.80	0.098	0.0062
	9.26	0.114	0.0071
	10.59	0.127	0.0082
	11.96	0.142	0.0093
	13.43	0.166	0.0108
	14.66	0.180	0.0115
90	2.43	0.027	0.0022
	3.71	0.042	0.0034
	5.16	0.057	0.0048
	6.47	0.072	0.0059
	7.90	0.088	0.0073
	9.26	0.106	0.0085
	10.59	0.115	0.0098
	11.96	0.127	0.0110
	13.43	0.145	0.0126
	14.66	0.158	0.0137
100	2.43	0.023	0.0025
	3.72	0.035	0.0038
	5.16	0.047	0.0053
	6.47	0.060	0.0068
	7.86	0.072	0.0081
	9.26	0.087	0.0093
	10.59	0.098	0.0107
	11.96	0.108	0.0121
	13.43	0.124	0.0142
	14.66	0.136	0.0149

APPENDIX B

SAMPLE CALCULATIONS

Sample calculation procedures for various reported results are provided here.

B.1 Solubility of CO_2 and He in Absorbent Liquids

A sample calculation of the number of moles of carbon dioxide and helium absorbed in the pure [bmim][DCA] is provided here.

Experimental Data:

$V_{cell} = V_{reference} = 150$ mL = 0.15 L

$V_{IL} = 10$ mL = 0.01 L

R = 0.082 L*atm*K^{-1}*mol^{-1}

1psi = 0.068 atm

1 psi= 0.0689 bar

T = 50 ^{o}C = 323.15 K

Mass of 10 mL of [bmim][DCA] = 10.5 g

MW of [bmim][DCA] = 205.26 g/mole

Number of moles of [bmim][DCA]:

$$n_{[bmim][DCA]} = \frac{10.5}{205.26} = 0.0511\, gmole$$

For CO_2:

$P_{feed} = 20.2$ psig

$P_{final} = 2.1$ psig

$Z_{feed} = 0.9912$

Z_{final} = 0.992

Using Equations (2.1) and (2.2), the number of moles of CO_2 in the feed (n_T) and in the gas phase at the equilibrium (n_1) are:

$$n_T = \frac{(20.2+14.7)*0.068*(0.15)}{0.9912*0.082*323.15} = 0.01355\ gmole$$

$$n_1 = \frac{(2.1+14.7)*0.068*(0.15+0.15-0.01+0.0035)}{0.992*0.082*323.15} = 0.01275\ gmole$$

where 3.5 cm^3 is the total volume of all the 1/8" tubing used for connection

Using Equation (2.3), the number of moles of CO_2 absorbed by pure [bmim][DCA] is:

$$n_2 = 0.01355 - 0.01275 = 8.0x10^{-4}\ gmole$$

Mole fraction of CO_2 in the IL:

$$x_{CO2} = \frac{n_2}{n_2 + n_{[bmim][DCA]}} = \frac{8.0x10^{-4}}{8.0x10^{-4} + 0.0511} = 0.0154$$

Henry's law constant for CO_2 in pure [bmim][DCA] at 50 ^oC is:

$$H_{CO2} = \frac{P_{final}}{x_{CO2}} = \frac{(2.1+14.7)*0.0689}{0.0154} = 75.2\,\text{bar}$$ (It appears in Table 2.2).

For He:

P_{feed} = 23.06 psig

P_{final} = 4.46 psig

Z_{feed} = 1.001

Z_{final} = 1.0001

Using Equations (2.1) and (2.2), the number of moles of He in the feed (n_T) and in the gas phase at the equilibrium (n_1) are:

$$n_T = \frac{(23.06+14.7)*0.068*(0.15)}{1.001*0.082*323.15} = 0.01452\ gmole$$

$$n_1 = \frac{(4.46+14.7)*0.068*(0.15+0.15-0.01+0.0035)}{1.0001*0.082*323.15} = 0.01443\ gmole$$

Using Equation (2.3), the number of moles of He absorbed by pure [bmim][DCA] is:

$$n_2 = 0.01452 - 0.01443 = 9.0\times10^{-5}\ gmole$$

Mole fraction of He in the IL:

$$x_{He} = \frac{n_2}{n_2 + n_{[bmim][DCA]}} = \frac{9.0\times10^{-5}}{9.0\times10^{-5} + 0.0511} = 1.75\times10^{-3}$$

Henry's law constant for He in pure [bmim][DCA] at 50 ^{o}C is:

$$H_{He} = \frac{P_{final}}{x_{He}} = \frac{(4.46+14.7)*0.068}{1.75\times10^{-3}} = 744.5\,\text{bar}$$ (It appears in Table 2.2).

B.2 Calculation of Percent Theoretical Capacity of Primary Amines Consumed

Theoretical capacity is the theoretical number of moles of carbon dioxide absorbed due to reaction with primary amines in the dendrimer based on the Equation (B.2.1).

$$2\ R(NH2)_4 + 4\ CO_2 \leftrightarrow R(NHCOO\text{-})_4 + R(NH_3^+)_4 \qquad \text{(B.2.1)}$$

For 20 wt% dendrimer in [bmim][DCA]:

Mass of 0.01 L of 20 wt% dendrimer in [bmim][DCA]= 10.72 g

Number of moles of dendrimer in the solution is:

$$n_{dendrimer} = \frac{mass\ dendrimer}{MW_{dendrimer}} = \frac{(0.2*10.72)g}{517g/mol} = 4.15x10^{-3}\ gmole$$

The theoretical moles of carbon dioxide absorbed due to reacting with primary amines in dendrimer based on the Equation (B.2.1) is:

$$n_{CO2absorbed} = 2 * n_{dendrimer} = 2 * 4.15x10^{-3}\, gmole = 8.3x10^{-3}\, gmole$$

At 50 ^{o}C and P_{feed}= 14.66 bar, the number of moles of CO_2 absorbed by primary amine in 20wt% dendrimer in [bmim][DCA] is: 8.10x10^{-3} gmole (see $n_{CO2,r}$ in section B3).

Therefore, % saturation (%) is:

$$\%Saturation = \frac{8.10x10^{-3}}{8.3x10^{-3}} x100\% = 97.7\%$$ (It appears in Table 2.6).

B.3 Calculation of K_C for 20 wt% Dendrimer in [bmim][DCA] Assuming all Primary Amines Consumed

At 50 ^{o}C, P_{feed} = 14.66 bar, P_{final} = 5.56 bar

Mass of 0.01 L of 20 wt% dendrimer in [bmim][DCA]= 10.724 g

$$n_{dendrimer} = \frac{0.2 * 10.724}{517} = 0.004148678\, gmole$$

$$n_{IL} = \frac{0.8 * 10.724}{205.26} = 0.041798045\, gmole$$

From experimental data, the number of moles of CO_2 absorbed in 20 wt% dendrimer in [bmim][DCA], $n_{2,}$ is:

n_2= 0.011589971 gmole

The Henry's law constant for CO_2 due to physical absorption in the IL containing dendrimer is calculated via the Equation (B.2.2)

$$H_{CO2T} = H_{CO2} \frac{H_{HeT}}{H_{He}} = \frac{P_{final}}{x} \qquad \text{(B.2.2)}$$

where H_{CO2T}: Henry's law constant of CO_2 due to physical absorption in the IL containing dendrimer

H_{CO2}: Henry's law constant of CO_2 in pure IL

H_{HeT}: Henry's law constant of He in the IL containing dendrimer

H_{He}: Henry's law constant of He in pure IL

x: mole fraction of CO_2

$$H_{CO2T} = 73.81181132 * \left(\frac{802.2076486}{749.8739584} \right) = 78.96313631 \,\text{bar}$$

From Equation (B.2.2), mole fraction , x, is:

$$x = \frac{P_{final}}{H_{CO2T}} = \frac{5.567454724}{78.96313631} = 0.070507011$$

Also,

$$x = \frac{n_{CO2,\,free}}{n_{CO2,\,free} + n_{dendrimer} + n_{IL}}$$

$$n_{CO2,\,free} = \frac{(n_{dendrimer} + n_{IL}) * x}{1 - x} = \frac{(0.004148678 + 0.041798045) * 0.070507011}{1 - 0.070507011} = 0.003485305 \; gmole$$

Now, n_{CO2r}, the moles of CO_2 reacted with primary amines present in dendrimer, is equal to:

$$n_{CO2,r} = n_2 - n_{CO2,\,free} = 0.011589971 - 0.003485305 = 0.008104666 \; gmole$$

From Equation (2.17), K_C can be calculated:

$$K_C = \frac{\left(\frac{n_{CO_2,r}}{4}\right)^2}{(n_{CO2,free})^4\left(n_{den} - \frac{n_{CO_2,r}}{2}\right)^2} V_{IL}{}^4 = \frac{\left(\frac{0.008104666}{4}\right)^2}{(0.003485305)^4\left(0.004148678 - \frac{0.008104666}{2}\right)^2}(0.01)^4$$

K_C = 29972.9 L^4/mol^4 (It appears in Table 2.6).

B.4 Calculation of Henry's Law Constants for CO_2 and He Used in the Mathematical Model

At 50 ^oC and 100 psig feed pressure,

V_{IL} = 10 mL = 1x10^{-5} m^3

$P_{CO2\ final}$ = 3.75 atm

n_{CO2} absorbed = 2.75x10^{-3} gmole

$P_{He\ final}$ = 3.89 atm

n_{He} absorbed = 2.68x10^{-4} gmole

Using Equations 3.25, and 3.26,

$$H_{CO2} = \frac{2.75x10^{-3}}{1x10^{-5} * (3.75)} = 73.33 \frac{gmol}{m^3 atm}$$ (It appears in Table 3.3).

$$H_{He} = \frac{2.68x10^{-4}}{1x10^{-5} * (3.89)} = 6.89 \frac{gmol}{m^3 atm}$$ (It appears in Table 3.3).

B.5 Molar Flow Rate of Product per Cycle Calculation

For PEEK-L II Module @ 100 psig feed gas and T=23 ^oC=296.13 K

N = 568

d_i = 0.029 cm

L = 41.0 cm

Pressure at the end of absorption= 73.3 psig

Pressure at the end of He-withdrawal step = 9 psig

ΔP = 73.3-9 = 64.3 psig =64.3*(0.068 atm) = 4.37 atm

$$V = 3.14 * \left(\frac{0.029}{2}\right)^2 * 41.0 * 568 = 15.37\, cc$$

$$\Delta n = \frac{(\Delta P)V}{RT} = \frac{4.37 * 15.37}{82.05 * 296.13} = 2.76x10^{-3}\, gmole$$

He-rich product molar flow rate per cycle ($\dot{n}_{He}$) is:

$$\dot{n}_{He} = \frac{\Delta n}{t} = \frac{2.76x10^{-3}}{67} = 4.13\text{x}10^{-5}$$ gmol/s (It appears in Table 3.5).

Using CO_2 species balance on the system, CO_2-rich product molar flow rate per cycle ($\dot{n}_{CO2}$) is:

$$0.4 * (\dot{n}_{CO_2} + 4.13x10^{-5}) = 0.12 * (4.13x10^{-5}) = 0.91 * (\dot{n}_{CO2})$$

$\dot{n}_{CO2} = 2.27x10^{-5}\, gmol/s$ (It appears in Table 3.5).

B.6 % CO_2 Recovery Calculation

For Two PEEK-L III Modules in Series @ 100 psig feed gas and T=23 ^{o}C

$\dot{n}_{He} = 9.58x10^{-5}\, gmol/s \text{ and } x_1 = 0.073$

$\dot{n}_{CO2} = 5.69x10^{-5}\, gmol/s \text{ and } x_2 = 0.951$

Using Equation (4.1),% CO_2 recovery in the CO_2-rich product is:

$$\%\, CO_2\ \text{Recovery} = \frac{\dot{n}_{CO2} * x_2}{\dot{n}_{CO2} * x_2 + \dot{n}_{He} * x_1} x100\% = \frac{5.69x10^{-5} * 0.951}{5.69x10^{-5} * 0.951 + 9.58x10^{-5} * 0.073}$$

$\%\, CO_2\ \text{Recovery} = 88.55\%$ (It appears in Table 4.4).

APPENDIX C

METHOD OF LINES TECHNIQUE IN SOLVING GOVERNING EQUATIONS OF PRESSURE SWING MEMBRANE ABSORPTION WITH GAS PRESSURE DROP IN THE FIBER LUMEN

When the gas pressure drop in the fiber lumen is not negligible, the governing balance equations and boundary conditions for any species j (He, CO_2) in a single hollow fiber can be written as:

Gas Phase:

$$\frac{\partial C_{jg}}{\partial t} = D_{jg}\frac{\partial^2 C_{jg}}{\partial z^2} - \frac{\partial}{\partial z}\left(v_g C_{jg}\right) - \frac{4K_{jg}d_0}{d_i^{\,2}}\left(C_{jg} - C_{jg}^{\,i}\right) \tag{C1}$$

where

$$v_g = -\frac{RTd_i^{\,2}}{32\mu_{mix}}\sum_{j=1}^{n}\frac{\partial C_{jg}}{\partial z} \tag{C2}$$

$$C_{jg}^{\,i} = \frac{C_{jl}\big|_{r=r_0}}{H_j RT} \tag{C3}$$

Initial condition:

$$\text{at } t = 0, C_{jg} = 0 \ (0 \le z \le L) \tag{C4}$$

Boundary conditions:

$$v_g C_{jg}\big|_u = v_g C_{jg}\big|_{z=0} - D_{jg}\frac{\partial C_{jg}}{\partial z}\bigg|_{z=0} \tag{C5}$$

$$D_{jg}\frac{\partial C_{jg}}{\partial z}\bigg|_{z=L} = 0 \tag{C6}$$

The corresponding governing balance equation and boundary conditions for the liquid phase for species j are:

$$\frac{\partial C_{jl}}{\partial t} = D_{jl}\left(\frac{\partial^2 C_{jl}}{\partial r^2} - \frac{1}{r}\frac{\partial C_{jl}}{\partial r}\right) \tag{C7}$$

Initial condition:

$$\text{at } t = 0, C_{jl} = 0 \; (0 \le z \le L \; and \; r_0 < r < r_e) \tag{C8}$$

Boundary conditions:

$$-D_{jl} \left. \frac{\partial C_{jl}}{\partial r} \right|_{r=r_0} = K_{jg} \left(C_{jg} - \frac{C_{jl}\big|_{r=r_0}}{H_j RT} \right) \tag{C9}$$

$$\left. \frac{\partial C_{jl}}{\partial r} \right|_{r=r_e} = 0 \tag{C10}$$

NORMALIZATION OF THE MODEL EQUATIONS

For normalization, the following scales are used:

$$z_s = l, \; r_s = r_e, \; t_s = \frac{{r_e}^2}{D_{1l}}, \; C_{js} = {C_{jg}}^u \text{ (inlet concentration)}$$

Let's introduce dimensionless variables: τ, x, η, U_j, and Q_j

$$\tau = \frac{D_{1l}}{{r_e}^2} t$$

$$x = \frac{z}{l}$$

$$\eta = \frac{r}{r_e}$$

$$U_j = \frac{C_{jg}}{{C_{jg}}^u}$$

$$Q_j = \frac{C_{jl}}{{C_{jg}}^u}$$

Then Equation (C1) becomes:

$$\frac{D_{1l}}{r_e^{\,2}} C_{jg}^{\,u} \frac{\partial U_j}{\partial \tau} = D_{jg} \frac{C_{jg}^{\,u}}{l^2} \frac{\partial^2 U_j}{\partial x^2} - \frac{C_{jg}^{\,u}}{l} \frac{\partial}{\partial x}(v_g U_j) - \frac{4K_{jg} d_0}{d_i^{\,2}} C_{jg}^{\,u} \left(U_j - \frac{1}{H_j RT} Q_j(\eta = a) \right) \quad \text{(C11)}$$

where $a = \frac{r_0}{r_e}$

$$v_g = -\sum_{K=1}^{2} \frac{RT d_i^{\,2}}{32\mu_g} \frac{C_{Kg}^{\,u}}{l} \frac{\partial U_K}{\partial x} = -\sum_{K=1}^{2} \rho_K \frac{\partial U_K}{\partial x} \quad \text{(C12)}$$

$$\text{where } \rho_K = \frac{RT d_i^{\,2}}{32\mu_g} \frac{C_{Kg}^{\,u}}{l} \quad \text{(C13)}$$

Simplifying one gets:

$$\frac{\partial U_j}{\partial \tau} = \frac{D_{jg}}{D_{1l}} \frac{r_e^{\,2}}{l^2} \frac{\partial^2 U_j}{\partial x^2} - \frac{r_e^{\,2}}{D_{1l} l} \frac{\partial}{\partial x}(v_g U_j) - 4 \frac{K_{jg} d_0 r_e^{\,2}}{d_i^{\,2} D_{1l}} \left(U_j - \frac{1}{H_j RT} Q_j(\eta = a) \right) \quad \text{(C14)}$$

where

$$\alpha_j = \frac{D_{jg} r_e^{\,2}}{D_{1l} l^2}; \delta = \frac{r_e^{\,2}}{D_{1l} l}; \psi = \frac{4K_{jg} d_0 r_e^{\,2}}{d_i^{\,2} D_{1l}}; \lambda_j = \frac{1}{H_j RT} \quad \text{(C15)}$$

and

$$\frac{\partial}{\partial x}(v_g U_j) = -\frac{\partial}{\partial x} \sum_K \rho_K \frac{\partial^2 U_K}{\partial x^2} U_j = -\sum_K \rho_u \frac{\partial}{\partial x} \left(\frac{\partial U_K}{\partial x} U_j \right) = -\sum_K \rho_K \left(\frac{\partial^2 U_K}{\partial x^2} U_j + \frac{\partial U_K}{\partial x} \frac{\partial U_j}{\partial x} \right) \quad \text{(C16)}$$

Equation (C11) becomes

$$\frac{\partial U_j}{\partial \tau} = \alpha_j \frac{\partial^2 U_j}{\partial x^2} + \delta \sum_K \rho_K \left(U_j \frac{\partial^2 U_K}{\partial x^2} + \frac{\partial U_K}{\partial x} \frac{\partial U_j}{\partial x} \right) - 4\psi_j \left(U_j - \lambda_j Q_j(\eta = a) \right) \quad \text{(C17)}$$

Initial condition:

$$U_j(x, \tau = 0) = 0 \quad \text{(C18)}$$

Boundary conditions:

Equation (C5) becomes

$$v_g{}^u C_{jg}{}^u = v_g C_{jg}{}^u U_j(x=0,\tau) - D_{jg}\frac{C_{jg}{}^u}{l}\frac{\partial U_j}{\partial x}(x=0,\tau) \tag{C19}$$

Dividing both sides by $C_{jg}{}^u$*, one gets*

$$v_g{}^u = v_g U_j(x=0,\tau) - \frac{D_{jg}}{l}\frac{\partial U_j}{\partial x}(x=0,\tau) \tag{C20}$$

Equation (C6) becomes:

$$\frac{\partial U_j}{\partial x}(x=1,\tau) = 0 \tag{C21}$$

LIQUID PHASES

Similarly, Equation (C7) becomes:

$$\frac{C_{jg}{}^u}{r_e{}^2} D_{1l}\frac{\partial Q_j}{\partial \tau} = D_{jl}\left(\frac{C_{jg}{}^u}{r_e{}^2}\frac{\partial^2 Q_j}{\partial \eta^2} + \frac{1}{r_e}\frac{1}{\eta}\frac{C_{jg}{}^u}{r_e}\frac{\partial Q_j}{\partial \eta}\right) \tag{C22}$$

$$\frac{\partial Q_j}{\partial \tau} = \frac{r_e{}^2 D_{jl}}{D_{1l}}\frac{1}{r_e{}^2}\left(\frac{\partial^2 Q_j}{\partial \eta^2} + \frac{1}{\eta}\frac{\partial Q_j}{\partial \eta}\right) \tag{C23}$$

$$\frac{\partial Q_j}{\partial \tau} = \gamma_j\left(\frac{\partial^2 Q_j}{\partial \eta^2} + \frac{1}{\eta}\frac{\partial Q_j}{\partial \eta}\right) \tag{C24}$$

Initial Condition:

$$Q_j(x,\eta,\tau=0) = 0 \tag{C25}$$

Boundary Conditions:

Equation (C9) becomes:

$$-D_{jl}\frac{C_{jg}{}^{u}}{r_e}\frac{\partial Q_j}{\partial \eta}(x,\eta=a,\tau)=K_{jg}C_{jg}{}^{u}\left(U_j(x)-\lambda_j Q_j(x,a,\tau)\right) \tag{C26}$$

$$-\frac{\partial Q_j}{\partial \eta}(x,a,\tau)=\frac{K_{jg}r_e}{D_{jl}}\left(U_j(x,\tau)-\lambda_j Q_j(x,a,\tau)\right) \tag{C27}$$

$$-\frac{\partial Q_j}{\partial \eta}(x,a,\tau)=Sh_j\left(U_j(x,\tau)-\lambda_j Q_j(x,a,\tau)\right) \tag{C28}$$

Equation (C10) becomes:

$$\frac{\partial Q_j}{\partial \eta}(x,1,\tau)=0 \tag{C29}$$

METHOD OF LINES

First and second derivatives can be approximated using the method of lines

$$\frac{\partial U_j{}^{m}}{\partial x}=\frac{U_j{}^{m}-U_j{}^{m-1}}{\Delta x} \tag{C30}$$

$$\frac{\partial^2 U_j{}^{m}}{\partial x^2}=\frac{U_j{}^{m+1}-2U_j{}^{m}+U_j{}^{m-1}}{\Delta x^2} \tag{C31}$$

Substituting equations, one gets:

$$\frac{\partial U_j{}^{m}}{\partial \tau}=\alpha_j\frac{1}{\Delta x^2}\left(U_j{}^{m+1}-2U_j{}^{m}+U_j{}^{m-1}\right)+$$

$$+\delta\left[\rho_1\left(U_j{}^{m}\frac{1}{\Delta x^2}(U_1{}^{m+1}-2U_1{}^{m}+U_1{}^{m-1})+\frac{1}{\Delta x}(U_j{}^{m}-U_j{}^{m-1})\frac{1}{\Delta x}(U_1{}^{m}-U_1{}^{m-1}\right)\right]+$$

$$+\delta\left[\rho_2\left(U_j{}^{m}\frac{1}{\Delta x^2}(U_2{}^{m+1}-2U_2{}^{m}+U_2{}^{m-1})+\frac{1}{\Delta x}(U_j{}^{m}-U_j{}^{m-1})\frac{1}{\Delta x}(U_2{}^{m}-U_2{}^{m-1})\right)\right]-4\psi_j\left(U_j{}^{m}-\lambda_j Q_j{}^{m,1}\right) \tag{C32}$$

Simplifying, equation becomes

$$\frac{\partial U_j^{\,m}}{\partial \tau} = \frac{\alpha_j}{\Delta x^2}\left(U_j^{\,m+1} - 2U_j^{\,m} + U_j^{\,m-1}\right) + \frac{\delta}{\Delta x^2}\left[U_j^{\,m}\left\{\rho_1(U_1^{\,m+1} - 2U_1^{\,m} + U_1^{\,m-1}) + \rho_2(U_2^{\,m+1} - 2U_2^{\,m} + U_2^{\,m-1})\right\}\right] +$$

$$+ \frac{\delta}{\Delta x^2}\left[(U_j^{\,m} - U_j^{\,m-1})\left\{\rho_1(U_1^{\,m} - U_1^{\,m-1}) + \rho_2(U_2^{\,m} - U_2^{\,m-1})\right\}\right] - 4\psi_j\left(U_j^{\,m} - \lambda_j Q^{m,1}\right) \qquad \text{(C33)}$$

For x=0, apply 5 point forward differences and Equation (C20) becomes,

$$v_g^{\,u} = v_g^{\,1}U_j^{\,1} - \frac{D_{jg}}{l}\frac{1}{12\Delta x}\left(-25U_j^{\,1} + 48U_j^{\,2} - 36U_j^{\,3} + 16U_j^{\,4} - 3U_j^{\,5}\right) \qquad \text{(C36)}$$

Assuming $v_g^{\,1} \cong v_g^{\,u}$, Equation (C36) can be simplified to:

$$U_j^{\,1} = \frac{1 + \frac{Pe_j^{-1}}{12\Delta x}\left(48U_j^{\,2} - 36U_j^{\,3} + 16U_j^{\,4} - 3U_j^{\,5}\right)}{1 + \frac{Pe_j^{-1}}{12\Delta x}2\delta} \qquad \text{(C37)}$$

Combine Equations (C21) and (C30), one gets

$$\frac{1}{\Delta x}\left(U_j^{\,Nx} - U_j^{\,Nx-1}\right) = 0 \qquad \text{(C38)}$$

Therefore,

$$U_j^{\,Nx} = U_j^{\,Nx-1} \qquad \text{(C39)}$$

Applying method of lines on Equation (C24), it becomes:

$$\frac{\partial Q_j^{\,m,n}}{\partial \tau} = \gamma_j\left[\frac{1}{\Delta\eta^2}\left(Q_j^{\,m,n+1} - 2Q_j^{\,m,n} + Q_j^{\,m,n-1}\right) + \frac{1}{\eta_n}\frac{1}{2\Delta\eta}\left(Q_j^{\,m,n+1} - Q_j^{\,m,n-1}\right)\right] \qquad \text{(C40)}$$

Applying central approximation to Equation (C28) when n=1 (η=a), it becomes:

$$-\frac{1}{2\Delta\eta}\left(Q_j^{\,m,2} - Q_j^{\,m,0}\right) = Sh_j\left(U_j^{\,m} - \lambda_j Q_j^{\,m,1}\right) \qquad \text{(C41)}$$

$$Q_j^{\,m,0} = Q_j^{\,m,2} + 2\Delta\eta Sh_j\left(U_j^{\,m} - \lambda_j Q_j^{\,m,1}\right) \qquad \text{(C42)}$$

Similarly, Equation (C29) becomes,

$$\frac{1}{2\Delta\eta}\left(Q_j^{\,m,Ne+1} - Q_j^{\,m,Ne-1}\right) = 0 \tag{C43}$$

Multiplying both sides by 2Δη,

$$Q_j^{\,m,Ne+1} = Q_j^{\,m,Ne-1} \tag{C44}$$

Therefore,

$$\frac{\partial Q_j^{\,m,Ne}}{\partial\tau} = \gamma_j \frac{2}{\Delta\eta^2}\left(Q_j^{\,m,Ne-1} - Q_j^{\,m,Ne}\right) \tag{C45}$$

Summary of ordinary differential equations for the gas and liquid phases are shown in Tables C1 and C2.

Table C1. Summary of ordinary differential equations for the gas phase

1. Equation for x=0

$$U_j^{\,1} = \frac{1 + \frac{Pe_j^{-1}}{12\Delta x}\left(48U_j^{\,2} - 36U_j^{\,3} + 16U_j^{\,4} - 3U_j^{\,5}\right)}{1 + \frac{Pe_j^{-1}}{12\Delta x}2\delta}$$

2. Equation for 0<x<1

$$\frac{\partial U_j^{\,m}}{\partial\tau} = \frac{\alpha_j}{\Delta x^2}\left(U_j^{\,m+1} - 2U_j^{\,m} + U_j^{\,m-1}\right) + \frac{\delta}{\Delta x^2}\left[U_j^{\,m}\left\{\rho_1(U_1^{\,m+1} - 2U_1^{\,m} + U_1^{\,m-1}) + \rho_2(U_2^{\,m+1} - 2U_2^{\,m} + U_2^{\,m-1})\right\}\right] +$$

$$+ \frac{\delta}{\Delta x^2}\left[(U_j^{\,m} - U_j^{\,m-1})\left\{\rho_1(U_1^{\,m} - U_1^{\,m-1}) + \rho_2(U_2^{\,m} - U_2^{\,m-1})\right\}\right] - 4\psi_j\left(U_j^{\,m} - \lambda_j Q^{m,1}\right)$$

3. Equation for x=1

$$U_j^{\,Nx} = U_j^{\,Nx-1}$$

Table C2. Summary of ordinary differential equations for the liquid phase

1. Equation for η=a

$$Q_j^{\,m,0} = Q_j^{\,m,2} + 2\Delta\eta Sh_j\left(U_j^{\,m} - \lambda_j Q_j^{\,m,1}\right)$$

2. Equation for a<η<1

$$\frac{\partial Q_j^{\,m,n}}{\partial \tau} = \gamma_j\left[\frac{1}{\Delta\eta^2}\left(Q_j^{\,m,n+1} - 2Q_j^{\,m,n} + Q_j^{\,m,n-1}\right) + \frac{1}{\eta_n}\frac{1}{2\Delta\eta}\left(Q_j^{\,m,n+1} - Q_j^{\,m,n-1}\right)\right]$$

3. Equation for η=1

$$\frac{\partial Q_j^{\,m,Ne}}{\partial \tau} = \gamma_j\frac{2}{\Delta\eta^2}\left(Q_j^{\,m,Ne-1} - Q_j^{\,m,Ne}\right)$$

APPENDIX D

PROGRAM FOR MODELING EQUATIONS CONSIDERING PRESSURE DROP IN THE FIBER LUMEN

Main function for simulation of gas absorption

```
project_path = 'run/test_18_new/';
 data_file = 'run_data_18';

sett.flag_dim      = 0;
sett.flag_vel      = 0;

rhs = @rhs_pd;

solver = @ode15s;

A_C = 1;
B_C = 1;
C_C = 0;
D_C = 0;
 %%%%%%%%%%%%%%%%%%%%%%%%%%%%%%%%%%%%%%%
 run(data_file);

disp('Simulation of gas absorption has started...');

mkdir(project_path);

copyfile([data_file '.m'], [project_path data_file '.m'], 'f');
 %%%%%%%%%%%%%%%%%%%%%%%%%%%%%%%%%%%%%%%
r_e = d_e / 2.0;
r_o = d_o / 2.0;
D_g = [D_A_gas, D_B_gas];
D_l = [D_A_liquid, D_B_liquid];
C_g = [C_A, C_B];
K_g = [K_A_g, K_B_g];
H = [H_A_liquid, H_B_liquid];
mu_g = [mu_g_A, mu_g_B];
mu_g_M = (C_g(1)*mu_g(1) + C_g(2)*mu_g(2)) / (C_g(1) + C_g(2));
%%%%%%%%%%%%%%%%%%%%%%%%%%%%%%%%%%%%%%%
global alp del rho pse lam iPe gam Sh bet;
alp = (D_g / D_l(1)) * (r_e / l)^2;
del = r_e^2 / l / D_l(1
rho = R * T_gas * d_i^2 / (32 * mu_g_M) * C_g / l;
pse = K_g * d_o * (r_e / d_i)^2 / D_l(1);
lam = 1.0 / R / T_gas ./ H;
iPe = D_g / l / Vg;
```

```
gam = D_l / D_l(1);
Sh = K_g * r_e ./ D_l;
bet = r_e^2 * Vg / D_l(1) / l;
%%%%%%%%%%%%%%%%%%%%%%%%%%%%%%%%%%%%%%%
z_scale = l;
r_scale = r_e;
t_scale = (r_e * r_e) / D_l(1);
C_scale = [C_A C_B];

fprintf(1, '\ntime scale = %f', t_scale);

z = linspace(0, l, Nz);
r = linspace(r_o, r_e, Nr);
t = linspace(0.0, tmax, Nt);

global e;
x = z / z_scale;
e = r / r_scale;
tau = t / t_scale;

global dx de;
dx = x(2)-x(1);
de = e(2)-e(1);
global Nx Ne;
Nx = Nz;
Ne = Nr;
%%%%%%%%%%%%%%%%%%%%%%%%%%%%%%%%%%%%%%%
UQ = zeros(Nt, 2*(Nx + Nx*Ne));
options = odeset('RelTol', 1e-6, 'AbsTol', 1e-6);
Cstart = zeros(2*(Nx + Nx*Ne), 1);
Cstart(:) = NaN;
Cstart(index(1, 1, 1:Nx, 1)) = 1;
Cstart(index(2, 1, 1:Nx, 1)) = 1;

for ie = 1:Ne,
   Cstart(index(1, 2, 1:Nx, ie)) = 0;
   Cstart(index(2, 2, 1:Nx, ie)) = 0; end

[tau_out, UQ] = solver(rhs, tau, Cstart, options);
%%%%%%%%%%%%%%%%%%%%%%%%%%%%%%%%%%%%%%%
save([project_path 'results.mat'], '*', '-double');
 %%%%%%%%%%%%%%%%%%%%%%%%%%%%%%%%%%%%%%%
plot_results([project_path 'results.mat'], tau(Nt), sett);
```

Simulation parameters for the code run:

```
%A: CO2, B : He, liquid : [bmim][DCA]
%P=100 psi, T=room temperature, 1 PEEK module

Nz = 30;
Nr = 30;
Nt = 101;

tmax = 9.0e2;    % time period for the simulation (s)

C_A = 128.4594124;   % Gas concentration (A) at inlet moles/m^3
C_B = 192.6891185;   % Gas concentration (B) at inlet moles/m^3
Vg  = 0;      % Linear velocity inside the fiber (m/s) at inlet

l   = 0.41;      % Length of fiber (m)
d_i = 0.029e-2;    % Inside diameter of fiber (m)
d_o = 0.0452e-2;    % Outside diameter of fiber (m)
d_e = 2*0.000291;    % Equivalent diameter of fiber, Happel's diam. (m), eps = 0.1

T_gas = 296.13;  % Gas temperature (K)

D_A_liquid = 3.54e-10; % Diffusion coefficient: species A in liquid (m^2/s)
D_B_liquid = 7.64e-10; % Diffusion coefficient: species B in liquid (m^2/s)
D_A_gas    = 0.075582479e-4; % Diffusion coefficient: species A in gas (m^2/s)
D_B_gas    = 0.075582479e-4; % Diffusion coefficient: species B in gas (m^2/s)

H_A_liquid = 93.32/101325; % Solubility coefficient: species A in liquid (mol/m^3.Pa)
H_B_liquid = 2.815/101325; % Solubility coefficient: species B in liquid (mol/m^3.Pa)

mu_g_A = 0.000149437*0.1;  % A gas viscocity (Pa.s)
mu_g_B = 0.000197358*0.1;  % B gas viscocity (Pa.s)
mu_g_M = 0.00017819*0.1;   % Gas mixture visosity (Pa.s)

K_A_g = 0.004689709e-4;  % A overall mass transfer coefficient (m/s)
K_B_g = 0.004833169e-4;  % B overall mass transfer coefficient (m/s)

R = 8.3144621;     % Universal Gas Constant (m^3.Pa/mol.K)
```

```
function res = plot_results(file, Tmax, sett)
alle = load(file);
%%%%%%%%%%%%%%%%%%%%%%%%%%%%%%%%%%%%%%%%%%%%%%%%%%%%%%%%%%%%%%%%%%%%%%%%%%%%%%%%
Nt = alle.Nt;
Nx = alle.Nx;
Ne = alle.Ne;
%%%%%%%%%%%%%%%%%%%%%%%%%%%%%%%%%%%%%%%%%%%%%%%%%%%%%%%%%%%%%%%%%%%%%%%%%%%%%%%%
UQ = calc_boundary(alle);
V = calc_velocity(alle, UQ);
if (sett.flag_vel == 0) V(:,:) = alle.Vg; end
%%%%%%%%%%%%%%%%%%%%%%%%%%%%%%%%%%%%%%%%%%%%%%%%%%%%%%%%%%%%%%%%%%%%%%%%%%%%%%%%
dim = Nx + Nx*Ne;
if (sett.flag_dim == 0)

   Z = alle.x;
   R = alle.e;
   T = alle.tau;
   V = V / alle.Vg;
   Ri = linspace(0, alle.d_i / alle.d_e, Ne);
else
   Z = alle.z;
   R = alle.r;
   T = alle.t;
   ii = 1:dim;
   UQ(:,ii) = alle.C_g(1) * UQ(:,ii);
   ii = dim+1:2*dim;
   UQ(:,ii) = alle.C_g(2) * UQ(:,ii);
   Ri = linspace(0, alle.d_i/2.0, Ne);

end

hState = figure('Name', [file ': Gas concentrations at oulet for both phases'], 'Position', scnsize);
box on;

subplot(1,2,1); box on; hold on;

plot(T(t_ind), UQ(t_ind, index2(1, 1, Nx, 1, Nx, Ne)), 'r'); % A gas
plot(T(t_ind), UQ(t_ind, index2(2, 1, Nx, 1, Nx, Ne)), 'b'); % B gas

xlabel('t* dimemsionless time');
ylabel('Ci/Cio');
title(['Concentrations in gas phase as function of time']);
legend('CO_2','He');

set(gca, 'FontSize', 12, 'Xcolor', 'k', 'Ycolor', 'k', 'Zcolor', 'k');
set(get(gca, 'Title'), 'Color', 'k');
grid on;
```

```
subplot(1,1,1); box on; hold on;
plot (T(t_ind),40*UQ(t_ind, index2(1, 1, Nx, 1, Nx, Ne)),'g'); % A gas Pressure
plot(T(t_ind), 60*UQ(t_ind, index2(2, 1, Nx, 1, Nx, Ne)), 'b'); % B Gas Pressure
plot (T(t_ind), 40*UQ(t_ind, index2(1, 1, Nx, 1, Nx, Ne))+ 60*UQ(t_ind, index2(2, 1, Nx, 1, Nx,
Ne)),'b'); % Total pressure drop

Experimental Data
plot([0 4 10 15 30 60 120 180 240 300 360 420 480 540 600 660 720 780 840 900]/alle.t_scale,
[ 97.59 96.10 94.59 93.61 91.90 90.14 88.47 87.55 86.92 86.45 86.07 85.74 85.45 85.28 85.04
84.74 84.53 84.34 84.16 83.98], 'ro');

xlabel('t* dimesionless time');
ylabel('P psig');
title(['Gas phase pressure as a function of time']);
legend( 'total theory','exp');

set(gca, 'FontSize', 12, 'Xcolor', 'k', 'Ycolor', 'k', 'Zcolor', 'k');
set(get(gca, 'Title'), 'Color', 'k');
grid on;

[pathstr, name, ext] = fileparts(file);

print('-depsc2', '-r300', [pathstr '/concen.eps']);
print(  '-dpng', '-r300', [pathstr '/concen.png']);

end


pur = UQ(t_ind, index2(1, 1, Nx, 1, Nx, Ne))./UQ(t_ind, index2(1, 1, 1, 1, Nx, Ne));
table = [T(t_ind)', CAg, CBg, CAl, CBl, pur];

save([pathstr '/table.dat'], 'table', '-ascii');
```

```
function W = calc_boundary(alle)

Nx = alle.Nx;
Ne = alle.Ne;

dx = alle.dx;
de = alle.de;

iPe = alle.iPe;

W = alle.UQ;

Nt = alle.Nt;

phas = 1;

ie = 1;

for it = 1:Nt

  for comp = 1 : 2

    ix = 1;

    I = index2(comp, phas, ix, ie, Nx, Ne);

    W(it,I) = 1/25*(48*W(it,I+1)-36*W(it,I+2)+16*W(it,I+3)-3*W(it,I+4));

    ix = Nx;

    I = index2(comp, phas, ix, ie, Nx, Ne);

        W(it,I) = W(it,I-1);

  end

end
```

```
function V = calc_velocity(alle, W)

Nx = alle.Nx;
Ne = alle.Ne;

dx = alle.dx;
de = alle.de;

Nt = alle.Nt;

rho = alle.rho;

V = zeros(Nt, Nx);
phas = 1;
ie = 1;

V(1,:) = 0.0;
V(1,1) = alle.Vg;

for it = 2:Nt
   V(it,1) = alle.Vg;

   for ix = 2:Nx

      I1 = index2(1, phas, ix, ie, Nx, Ne);
      I2 = index2(2, phas, ix, ie, Nx, Ne);


      V(it,ix) = - (1.0 / dx) * ( rho(1) * (W(it,I1) - W(it,I1-1)) + rho(2) * (W(it,I2) - W(it,I2-1)) );

   end
```

```
function ind = index(component, phase, ix, ie)


global Nx Ne;

dim = Nx + Nx*Ne;

ind = (component-1) * dim + (phase-1) * (ie*Nx) + ix;
```

```
function ind = index2(component, phase, ix, ie, Nx, Ne)

dim = Nx + Nx*Ne;

ind = (component-1) * dim + (phase-1) * (ie*Nx) + ix;
```

```
function dW = rhs(t, W)

global alp del rho pse lam iPe gam Sh;
global Nx Ne;
global dx de;
global e;

dim = 2*(Nx + Nx*Ne);
dW = zeros(dim, 1);

dW(:) = NaN;
dx2 = dx * dx;
de2 = de * de;

%%%%%%%%%%%%%%%%%%%%%%%%%%%%%%%%%%%%
phas = 1;

ie = 1;

for comp = 1 : 2

   ix = 1;
   I = index(comp, phas, ix, ie);
   W(I) = 1/25*(48*W(I+1)-36*W(I+2)+16*W(I+3)-3*W(I+4));
   dW(I) = 0.0;
   ix = Nx;
   I = index(comp, phas, ix, ie);
   W(I) = W(I-1);
    dW(I) = 0.0;

end

for comp = 1 : 2
    phas = 1;
    ie = 1;
    for ix = 2 : Nx-1
       I = index(comp, phas, ix, ie);
      first = alp(comp) / dx2 * (W(I+1) - 2 * W(I) + W(I-1));
      I1 = index(1, phas, ix, ie);
      I2 = index(2, phas, ix, ie);

      second = del / dx2 * (W(I) - W(I-1)) * (rho(1) * (W(I1) - W(I1-1)) + rho(2) * (W(I2) - W(I2-1)))
+ ...
del / dx2 * W(I) * ( rho(1) * (W(I1+1) - 2 * W(I1) + W(I1-1)) + ...
rho(2) * (W(I2+1) - 2 * W(I2) + W(I2-1)) );

      Ii = index(comp, 2, ix, 1);
      third = 4 * pse(comp) * (W(I) - lam(comp) * W(Ii));
```

```
      dW(I) = first + second - third;

    end

    phas = 2;
    for ix = 1 : Nx
      ie = 1;
      I  = index(comp, phas, ix, ie  );
      Ip = index(comp, phas, ix, ie+1);
      Ig = index(comp,    1, ix,    1);
       Wb = W(Ip) + 2 * de * Sh(comp) * (W(Ig) - lam(comp) * W(I));

      dW(I) = gam(comp) * ( (W(Ip) - 2 * W(I) + Wb) / de2 + (W(Ip) - Wb) / e(ie) / 2 / de);

      for ie = 2 : Ne-1
        Im = index(comp, phas, ix, ie-1);
        I  = index(comp, phas, ix, ie  );
        Ip = index(comp, phas, ix, ie+1);

        dW(I) = gam(comp) * ( (W(Ip) - 2 * W(I) + W(Im)) / de2 + (W(Ip) - W(Im)) / e(ie) / 2 / de );

      end
       ie = Ne;
       Im = index(comp, phas, ix, ie-1);
      I  = index(comp, phas, ix, ie  );

      dW(I) = 2 * gam(comp) * (W(Im) - W(I)) / de2;
    end


end
```

REFERENCES

[1] Berger, A. The Effect of Greenhouse Gases on Climate. *Proceedings of the Conference on the Future Energy Systems and Technology for CO_2 Abatement*, Antwerp, Belgium, **2002**, 3.

[2] Yang, H.; Xu, Z.; Fan, M.; Gupta, R.; Slimane, R. B.; Bland, A. E.; Wright, I. Progress in Carbon Dioxide Separation and Capture: A Review. *J. Envir Sci.* **2008**, 20, 14.

[3] Rubin, E. S.; Cooper, R. N.; Frosch, R. A.; Lee, T. H.; Marland, G.; Rosenfeld, A. H.; Stine, D. D. Realistic Mitigation Options for Global Warming. *Science* **1992**, 257, 148.

[4] Rao, A. B.; Rubin, E. S. A Technical, Economic, and Environmental Assessment of Amine-based CO_2 Capture Technology for Power Plant Greenhouse Gas Control. *Envir Sci. Tech.* **2002**, 36, 4467.

[5] Robertson, E. P. Analysis of CO_2 Separation from Flue Gas, Pipeline Transportation, and Sequestration in Coal. *Idaho National Laboratory*, **2007**.

[6] Wong, S.; Bioletti, R. Carbon Dioxide Separation Technologies. Carbon & Energy Management. *Alberta Research Council*, **2002**.

[7] Skinner, F. D.; McIntush, K. E.; Murff, M. C. Amine-based Gas Sweetening and Claus Sulfur Recovery Process Chemistry and Waste Stream Survey – Technical Report. *Gas Research Institute*, **1995**.

[8] Pressure Swing Adsorption Technology-XEBEC - A World Powered By Clean Energy. *Pressure Swing Adsorption Technology - XEBEC*. http://www.xebecinc.com/technology-what-is-psa.php [Accessed on July 8th, 2013].

[9] Temperature Swing Adsorption http://www.separationprocesses.com/Adsorption/AD_Fig040.htm [Accessed on July 8th, 2013].

[10] Baker, R. W. "Membrane Technology and Application" (2nd ed.). John Wiley & Sons Ltd, *Chichester*, United Kingdom, **2004**.

[11] Azar, C.; Lindgren, K.; Larson, E.; Mollersten, K. Carbon Capture and Storage from Fossil Fuels and Biomass – Costs and Potential Role in Stabilizing the Atmosphere. *Climatic Change* **2006**, 74, 47.

[12] Rubin, E. S.; Chen, C.; Rao, A. B. Cost and Performance of Fossil Fuel Power Plants with CO_2 Capture and Storage. *Energy Policy* **2007**, 35, 4444.

[13] Baltus, R. E.; Moganty, S. S. Diffusivity of Carbon Dioxide in Room-temperature Ionic Liquids. *Ind. Eng. Chem. Res.* **2010**, 49, 9370.

[14] Camper, D.; Becker, C.; Koval, C.; Noble, R. Diffusion and Solubility Measurements in Room Temperature Ionic Liquids. *Ind. Eng. Chem. Res.* **2006**, 45, 445.

[15] Yokozeki, A.; Shiflett, M. B. Hydrogen Purification using Room-temperature Ionic Liquids. *Applied Energy* **2007**, 84, 351.

[16] Myers, C.; Pennline, H.; Luebke, D.; Ilconich, J.; Dixon, J. K.; Maginn, E. J.; Brennecke, J. F. High Temperature Separation of Carbon Dioxide/Hydrogen Mixtures using Facilitated Supported Ionic Liquid Membrane. *J. Membrane Sci.* **2008**, 322, 28.

[17] Yegani, R.; Hirozawa, H.; Teramoto, M.; Himei, H.; Okada, O.; Takigawa, T.; Ohmura, N.; Matsumiya, N.; Matsuyana, H. Selective Separation of CO_2 by using Novel Facilitated Transport Membrane at Elevated Temperature and Pressures. *J. Membrane Sci.* **2007**, 291, 157.

[18] Meindersma, G. W.; Sanchez, L. M. G.; Hansmeier, A. R.; Haan, A. B. Application of Task Specific Ionic Liquids for Intensified Separations. *Monatshefte fur Chemie.* **2007**, 138, 1125.

[19] Kovvali, A. S.; Chen, H.; Sirkar, K. K. Dendrimer Membranes: A CO_2-selective Molecular Gate. *JACS* **2000**, 122, 7594.

[20] Kovvali, A. S.; Sirkar, K. K. Dendrimer Liquid Membranes: CO_2-separation from Gas Mixtures. *Ind. Eng. Chem. Res.* **2001**, 40, 2502.

[21] Duan, S.; Kouketsu, T.; Kazama, S.; Yamada, K. Development of PAMAM Dendrimer Composite Membranes for CO_2 Separation. *J. Membrane Sci.* **2006**, 283, 2.

[22] Duan, S.; Kouketsu, T.; Kai, T.; Kazama, S.; Yamada, K. PAMAM Dendrimer Composite Membrane for CO_2 Separation: Formation of a Chitosan Gutter Layer. *J. Membrane Sci.* **2007**, 287, 51.

[23] Taniguchi, I.; Duan, S.; Kazama, S.; Fujioka, Y. Facile Fabrication of a Novel High Performance CO_2 Separation Membrane: Immobilization of Poly(amidoamine) Dendrimers in Poly(ethylene glycol) Networks. *J. Membrane Sci.* **2008**, 322, 277.

[24] Kosaraju, P.; Kovvali, A. S.; Korivov, A.; Sirkar, K. K. Hollow Fiber Membrane Contactor Based CO_2 Absorption-stripping using Novel Solvents and Membranes. *Ind. Eng. Chem. Res.* **2005**, 44, 1250.

[25] Rolker, J.; Seiler, M.; Mokrushina, L.; Arlt, W. Potential of Branched Polymers in the Field of Gas Absorption: Experimental Gas Solubilities and Modeling. *Ind. Eng. Chem. Res.* **2007**, 46, 6572.

[26] Jie, X.; Chau, J.; Obuskovic, G; Sirkar, K. K. Preliminary Studies of CO_2 Removal from Precombustion Syngas through Pressure Swing Membrane Absorption Process with Ionic Liquid as Absorbent. *Ind. Eng. Chem. Res.* **2013**, 52, 8783.

[27] Bhaumik, S.; Majumdar, S.; Sirkar, K. K. Hollow-fiber Membrane-based Rapid Pressure Swing Absorption. *AIChE Journal* **1996**, 42, 409.

[28] Laan, G. P. Kinetics, Selectivity and Scale Up of the Fischer-tropsch Synthesis, Dissertation, University of Groningen. http://dissertations.ub.rug.nl/faculties/science/1999/g.p.van.der.laan/ [Accessed July 8th, 2013].

[29] Dendritech Inc., Mark Kaiser, *Personal Communication*, January 20th, **2012**.

[30] Muldoon, M. J.; Aki, S. N. V. K.; Anderson, J. L.; Dixon, J. K.; Brennecke, J. F. Improving Carbon Dioxide Solubility in Ionic Liquids. *J. Phys. Chem. B* **2007**, 111, 9001.

[31] Shiflett, M. B.; Yokozeki, A. Solubilities and Diffusivities of Carbon Dioxide in Ionic Liquids: [bmim][PF_6] and [bmim][BF_4]. *Ind. Eng. Chem. Res.* **2005**, 44, 4453.

[32] Shiflett, M. B.; Harmer, M. A.; Junk, C. R.; Yokozeki, A. Solubility and Diffusivity of 1,1,1,2-tetrafluoroethane in Room-temperature Ionic Liquids. *Fluid Phase Equilib*. **2006**, 242, 220.

[33] Shiflett, M. B.; Yokozeki, A. Solubility of CO_2 in Room Temperature Ionic Liquid [hmim][Tf_2N]. *J. Phys. Chem. B* **2007**, 111, 2070.

[34] Anthony, J. L.; Maginn, E. J.; Brennecke, J. F. Solubilities and Thermodynamic Properties of Gases in the Ionic Liquid 1-n-butyl-3-methylimidazolium Hexafluorophosphate. *J. Phys. Chem. B* **2002**, 106, 7315.

[35] Blanchard, L. A.; Gu, Z. Y.; Brennecke, J. F. High Pressure Phase Behavior of Ionic Liquid/CO_2 Systems. *J. Phys. Chem. B* **2001**, 105, 2437.

[36] Kamps, A. P. S.; Tuma, D.; Xia, J. Z.; Maurer, G. Solubility of CO_2 in the Ionic Liquid [bmim][PF_6]. *J. Chem. Eng. Data* **2003**, 48, 746.

[37] Baltus, R. E.; Culbertson, B. H.; Dai, S.; Luo, H. M.; DePaoli, D. W. Low-pressure Solubility of Carbon Dioxide in Room-temperature Ionic Liquids Measured with a Quartz Crystal Microbalance. *J. Phys. Chem. B* **2004**, 108, 721.

[38] Hou, Y.; Baltus, R. E. Experimental Measurement of the Solubility and Diffusivity of CO_2 in Room-temperature Ionic Liquids using a Transient Thin-liquid-film Method. *Ind. Eng. Chem. Res.* **2007**, 46, 8166.

[39] Hou, Y. Experimental Measurement of Solubility and Diffusivity of CO_2 in Room Temperature Ionic Liquids. M.S. Thesis, Clarkson University, Potsdam, NY, **2006**.

[40] Moganty, S. S. Thermodynamic, Transport, and Electrochemical Properties of Room Temperature Ionic Liquids. Ph.D. Thesis, Clarkson University, Potsdam, NY, **2009**.

[41] Angus, S.; Armstrong, B.; deReuck, K. M. eds. Carbon Dioxide International Thermodynamic Tables of the Fluid State-3. IUPAC Project Center, Imperial College, London, United Kingdom, **1976**.

[42] Angus, S.; deReuck, K. M. eds. International Thermodynamic Tables of the Fluid State-4. IUPAC Project Center, Imperial College, London on the Basis of Tables and Equations Published by R. D. McCarthy. National Bureau of Standards, Cryogenics Research Division, Boulder, USA, **1977**.

[43] Husson-Borg, P.; Majer, V.; Gomes, M. F. C. Solubilities of Oxygen and Carbon Dioxide in Butyl Methyl Imidazolium Tetraluoroborate as a Function of Temperature and at Pressures close to Atmospheric Pressure. *J. Chem. Eng. Data* **2003**, 48, 480.

[44] Sanchez, L. M. G. Functionalized Ionic Liquids Absorption Solvents for Carbon Dioxide and Olefin Separation. Ph.D. Thesis, Eindhoven University of Technology, Enschede, The Netherlands, **2008**.

[45] Finotello, A.; Bara, J. E.; Camper, D.; Noble, R. D. Room-temperature Ionic Liquids: Temperature Dependence of Gas Solubility Selectivity. *Ind. Eng. Chem. Res.* **2008**, 47, 3453.

[46] Park, H. S.; Jung, Y. M.; You, J. K.; Hong, W. H.; Kim, J. N. Analysis of the CO_2 and NH_3 Reaction in an Aqueous Solution by 2D IR COS: Formation of Bicarbonate and Carbamate. *J. Phys. Chem. A* **2008**, 112, 6558.

[47] Krevelen, V.; Hoftijzer, P. J.; Huntjens, F. J. Composition and Vapour Pressures of Aqueous Solutions of Ammonia, Carbon Dioxide, and Hydrogen Sulphide. *Re. Trav. Chim. Pays-bas* **1949**, 68, 191.

[48] Versteeg, G. F.; Van Dijck, L. A. J.; Van Swaaij, W. P. M. On the Kinetics between CO_2 and Alkanolamies both in Aqueous and Non-aqueous Solutions. An Overview. *Chem. Eng. Commun.* **1996**, 144, 113.

[49] Blauwhoff, P. M. M.; Versteeg, G. F.; Van Swaaij, W. P. M. A Study on the Reaction between CO_2 and Alkanolamines in Aqueous Solutions. *Chem. Eng. Sci.* **1983**, 38, 1411.

[50] Li, J.; Ye, Y.; Chen, L.; Qi, Z. Solubilities of CO_2 in Poly(ethylene glycols) from (303.15 to 333.15) K. *J. Chem. Eng. Data* **2011**, 57, 610.

[51] Yang, R. T. "Gas Separation by Adsorption Processes". World Scientific Publishing Company, London, United Kingdom, **1997**.

[52] Qi, Z.; Cussler, E. L. Microporous Hollow Fibers for Gas Absorption. I. Mass Transfer in the Liquid. *J. Membrane Sci.* **1985**, 23, 321.

[53] Spilman, R. W. *Chemical Engineering Progress* **1989**, 41.

[54] Happel, J. Viscous Flow Relative to Arrays of Cylinders. *AIChE Journal* **1959**, 5, 174.

[55] Karoor, S.; Sirkar, K. K. Gas Absorption Studies in Microporous Hollow Fiber Membrane Modules. *Ind. Eng. Chem. Res.***1993**, 32, 674.

[56] Bhaumik, S.; Majumdar, S.; Sirkar, K. K. Rapid Pressure Swing Absorption Cleanup of Post-shift Reactor Synthesis Gases. Final Report to DOE PETC, Pittsburgh, DOE Grant No. DE-FG22-90 PC 90300 **1994**.

[57] Brian III, B. F.; Zwiebel, I.; Artigue, R. S. Numerical Simulation of Fixed-bed Adsorption Dynamics by the Method of Lines. *AIChE Symp. Ser.* **1988**, 84, 57.

[58] Camper, D.; Becker, C.; Koval, C.; Noble, R. Diffusion and Solubility Measurements in Room Temperature Ionic Liquids. *Ind. Eng. Chem. Res.* **2006**, 45, 445.